Master's thesis

NTNU
Norwegian University of Science and Technology
Faculty of Information Technology and Electrical Engineering
Department of Electric Power Engineering

Ingrid Smisethjell

Investigation of PD formation on AlN Ceramic Substrates: Impact of Square Voltage Pulses and Dielectric Liquids

Master's thesis in Energy and the Environment
Supervisor: Kaveh Niayesh
Co-supervisor: Torstein Grav Aakre
June 2023

NTNU
Norwegian University of
Science and Technology

Ingrid Smisethjell

Investigation of PD formation on AlN Ceramic Substrates: Impact of Square Voltage Pulses and Dielectric Liquids

Master's thesis in Energy and the Environment
Supervisor: Kaveh Niayesh
Co-supervisor: Torstein Grav Aakre
June 2023

Norwegian University of Science and Technology
Faculty of Information Technology and Electrical Engineering
Department of Electric Power Engineering

NTNU
Norwegian University of
Science and Technology

Preface

This master's thesis was carried out for the Department of Electric Energy at the Norwegian University of Science and Technology (NTNU) in Trondheim during the spring of 2023. The thesis was carried out in cooperation with an ongoing project for SINTEF Energy Research named "FastTrans - Insulation stressed with fast rise time repetitive voltages from high voltage power electronics".

I want to thank my supervisor at NTNU, Professor Kaveh Niayesh, for always being available, helpful, and supportive throughout the semester. I would also like to thank my co-supervisor, Torstein Grav Aakre, at SINTEF Energy Research, for all his help and assistance in the laboratory. Additionally, I would like to thank him for engaging in professional conversations and helping post-processing the data. Also, I want to thank Lars Lundgaard, at SINTEF Energy Research, for his professional conversations and guidance. A huge thank you to Hans Kristian Hygen Meyer, at SINTEF Energy Research, for help implementing and using the high-speed camera.

In addition, I would like to extend my gratitude to the employees at NTNU's service and mechanical lab for their help and assistance when needed, both with the test object and laboratory equipment.

June 12th, 2023
Trondheim, Norway

Ingrid Smisethjell

Abstract

The electrical power industry is undergoing complex expansion and is experiencing rapid voltage changes caused by changes in operation patterns. These conditions significantly impact the components and equipment in the power grid, especially high-voltage power electronics such as Insulated Gate Bipolar Transistors (IGBTs). The ceramic substrate within an IGBT is one of the most critical parts of the power module and is exposed to Partial Discharge (PD) formation. Therefore, the master thesis aimed to contribute to further research on Aluminium Nitride (AlN) ceramic substrate and their exposure to PD formation. Hence, the objective of the thesis was to investigate how various parameters, such as sinusoidal and square voltage pulses, influence the PD formation on the substrate. In addition, the thesis also aimed to study the potential variations of PD formation in two dielectric liquids, Silicone oil and Nytro 10XN.

The measurements of PD formation of the AlN substrate were conducted using two experimental setups, sinusoidal and square voltage setups. The experimental sinusoidal voltage setup used electrical and optical measurements to detect PD, while the experimental square voltage setup only provided optical measurements. In addition, an ultra-fast gated intensified high-speed camera was included in some of the measurements for the square voltage setup. The electrical measurements were provided with the use of Omicron MPD600, which complies with IEC 60270. The optical measurements were provided by using a Photomultiplier Tube (PMT) with a light guide attached to the lens. The substrates were placed in a sample holder and covered with Silicone oil or Nytro 10XN. Three experimental procedures were used to detect the PD formation in the substrate. The first experimental procedure involved detecting the Partial Discharge Inception Voltage (PDIV) under sinusoidal, bipolar, and unipolar voltage pulses, where the voltage was ramped up and down, to observe how the different voltage pulses would affect the PD formation. The second experimental procedure involved detecting PD formation along the edge of the substrate using a high-speed camera at various bipolar voltage levels. The third experimental procedure involved varying the duty cycle of 5 % and 95 % for negative unipolar voltage pulses and analyzing how this parameter impacts PD formation.

The PDIV results indicate that different voltage pulses significantly impact PD formation on the surface. Regardless of the two dielectric liquids, the PD activity is notably increased when exposed to square voltage pulses, compared to sinusoidal voltage pulses. This observation suggests that the rise time of the voltage pulse plays a crucial role in PD formation. Furthermore, the results indicate that Nytro 10XN has a higher PDIV than Silicone oil when exposed to sinusoidal voltage pulses. However, this relation is reversed under square voltage pulses, indicating that Nytro 10XN is more exposed to the rise time than Silicone oil. The findings from the high-speed camera revealed that the rounded edges of the substrates are most exposed to PD formation. Moreover, the high-speed camera results indicate that PDs primarily occur during the flanks of the bipolar voltage pulses. In contrast, discharges occurring during the voltage plateau are due to space charges.

The findings of the different duty cycles reveal that the probability of PD occurrence is higher during the voltage turn-on compared with the turn-off. PDs occurring during the voltage turn-off are solely due to the space charge accumulated during the voltage turn-on. Furthermore, the results indicated that the variations of the duty cycles were not sufficient enough to result in significant changes in the PD formation in Silicone oil. However, a higher duty cycle resulted in higher PD probability and more space charge formation in Nytro 10XN, further validating that Nytro 10XN is more prone to discharges when exposed to square voltage pulses. Given that the majority of the measurements were conducted with optical measurements, further tests with the implementation of electrical measurements should be conducted to provide more reliable results.

Sammendrag

Det elektriske kraftsystemet gjennomgår en kompleks utvidelse og opplever raske spenningsendringer som skyldes endringer i driftsmønsteret. Disse forholdene har betydelig innvirkning på komponenter og utstyr i strømnettet, spesielt høyspenningskraftelektronikk som Insulated Gate Bipolar Transistors (IGBT). Det keramiske substratet inne i IGBT-ene er en av de mest kritiske delene av kraftmodulen og er utsatt for formasjonen av partielle utladninger (PD). Formålet med masteroppgaven var å bidra til videre forskning på Aluminiumnitrid (AlN) keramisk substrat og dets eksponering for PD-formasjon. Ett av formålene med oppgaven var å undersøke hvordan ulike parameter, som sinusformede og firkantformede spenningspulser, påvirker PD-formasjonen på substratet. Oppgaven inkluderte også en analyse av eventuelle variasjoner i PD-formasjon i to dielektriske væsker, Silikonolje og Nytro 10XN.

To eksperimentelle oppsett, et sinusformet og et firkantformet spenningsoppsett, ble brukt til å utføre PD-målingene av AlN-substratet. Det sinusformede spenningsoppsettet benyttet både elektriske og optiske målinger for å detektere PD, mens det firkantformede spenningsoppsett kun benytte optiske målinger. I noen av målingene i det firkantformede spenningsoppsett ble et høyhastighetskamera inkludert. De elektriske målingene ble utført ved bruk av Omicron MPD600, som er i samsvar med IEC 60270. De optiske målingene ble utført ved bruk av en fotomultiplikator, med en lys guide festet til linsen. Substratene ble plassert i en glassbeholder og dekket med enten silikonolje eller Nytro 10XN. Tre eksperimentelle prosedyrer ble brukt for å detektere PD-formasjon på substratet. Den første prosedyren involverte deteksjon av tennspenning for PD under sinusformede, bipolar og unipolar spenningspulser, der spenningen gradvis ble rampet opp og ned for å observere hvordan de ulike spenningspulsene påvirket PD-formasjonen. Den andre prosedyren innebar deteksjon av PD-formasjon langs kanten av substratet ved bruk av høyhastighetskameraet ved forskjellige bipolare spenningsnivåer. Den tredje prosedyren innebar variasjon av arbeidssyklusen til 5 % and 95 % for negativ unipolar spenningspulser og analyse av hvordan denne parameteren påvirket PD-formasjonen.

Resultatet fra tennspenningene indikerer at ulike spenningspulser har en betydelig innvirkning på PD-formasjonen på substratet. Uavhengige av de to dielektriske væskene, øker PD-formasjonen når substratet blir eksponert for firkantpulser sammenlignet med sinuspulser. Dette tyder på at stigetiden til spenningspulsen spiller en avgjørende rolle i PD-formasjonen. Videre viser resultatene at Nytro 10XN har en høyere tennspenning enn silikonolje når substratet blir eksponert for sinuspulser. I tilfelle av firkantpulser er dette forholdet omvendt, noe som tyder på at Nytro 10XN er mer følsom for stigetiden enn silikonolje. Resultatene fra høyhastighetskameraet avslørte at de avrunde kantene på substratet er mest utsatt for PD-formasjon. I tillegg viser resultatene fra høyhastighetskameraet at PD-formasjonen hovedsakelig skjer under flankene på bipolare spenningspulser, mens utladninger som oppstår under spenningsplattåene skyldes romladninger.

Funnene fra de ulike arbeidssyklusene avslørte at sannsynligheten for PD-formasjon er høyere under stigende flanker (fra null til høy spenning) sammenlignet med fallende flanker (fra høy til null spenning). PD-formasjon som oppstår under fallende flanker skyldes utelukkende romladninger som dannes under stigende flanke. Videre indikerte resultatene at variasjonen i arbeidssyklusen ikke var tilstrekkelige til å resultere i betydelige endringer i PD-formasjonen i silikonolje. Til tross for det resulterte en høyere arbeidssyklus i økt PD-formasjon og flere romladninger i Nytro 10XN, noe som ytterligere bekrefter at Nytro 10XN er mer følsom for utladninger når det utsettes for firkantpulser. Gitt at flertallet av målingene ble utført med optiske målinger, bør det gjennomføres ytterligere tester med implementering av elektriske målinger for å oppnå mer pålitelige resultater.

Table of Contents

List of Figures **xi**

List of Tables **xiii**

List of Abbreviations **xv**

1 Introduction **1**

1.1 Background 1

1.1.1 Motivation of the master's thesis 1

1.2 Objective of the master's thesis 1

1.2.1 Structure of the report 2

2 Theory **3**

2.1 Insulated Gate Bipolar Transistor (IGBT) 3

2.2 Partial discharge phenomena 4

2.2.1 Characterisation of partial discharges 5

2.2.2 Partial Discharge Inception and Extinction Voltage (PDIV and PDEV) . 5

2.3 Space charge phenomena 6

2.3.1 Needle to plane 7

2.3.2 Dielectric relaxation time 7

2.4 Parameters affecting IGBTs 9

2.4.1 Square voltage pulses parameters affecting IGBTs 9

2.4.2 Electrical field distribution at the triple point affecting IGBTs 10

3 Methodology **12**

3.1 Test object 12

3.1.1 Preparation of new test objects 13

3.2 Experimental setups: PD measurement techniques 14

3.2.1 Electrical measurements 14

3.2.2 Optical measurements 14

3.2.3 Ultra-fast gated intensified high-speed camera 15

3.3 Experimental setups: Sinusoidal and Square voltage 18

3.3.1 Experimental setup: Sinusoidal voltage . . . 18
3.3.2 Experimental setup: Square voltage . . . 20
3.3.3 Experimental setup: Light guide placement during ramping of Sinusoidal and Square voltage . . . 21
3.3.4 Experimental setup: Square voltage with the high-speed camera . . . 22
3.3.5 Experimental setup: Square voltage with varying duty cycle . . . 23
3.4 Preparation of test object before measurements . . . 24
3.4.1 Silicone oil . . . 25
3.4.2 Nytro 10XN . . . 26
3.5 Measurement procedures . . . 27
3.5.1 Measurement procedure: Sinusoidal, bipolar, negative, and positive unipolar voltage . . . 27
3.5.2 Measurement procedure: High-speed camera . . . 29
3.5.3 Measurement procedure: Duty cycle . . . 30
3.6 Post-processing of data . . . 31

4 Results **32**

4.1 Sinusoidal voltage setup: PD measurements . . . 32
4.1.1 PDIV and PDEV measurements . . . 32
4.2 Square voltage setup: PD measurements . . . 33
4.2.1 PDIV for bipolar, positive, and negative unipolar voltage . . . 33
4.2.2 PD detection with high-speed camera . . . 34
4.2.3 Impact of duty cycle . . . 39

5 Discussion **41**

5.1 Relaxation time in Silicone oil and Nytro 10XN . . . 41
5.2 Sinusoidal voltage setup: PDIV and PDEV measurements . . . 42
5.3 Square voltage setup: PD probability with bipolar, positive, and negative unipolar voltage pulses . . . 43
5.3.1 Impact of bipolar voltage pulses in Silicone oil and Nytro 10XN . . . 43
5.3.2 Impact of bipolar and unipolar voltage pulses in Silicone oil and Nytro 10XN . . . 43
5.4 Comparing the impact of sinusoidal and square voltage pulses . . . 45

5.5 High-speed camera: PD activity along the edge of the substrate 46
5.5.1 PD formation along the substrate edge in Silicone oil 47
5.5.2 PD formation along the substrate edge in Nytro 10XN 47
5.5.3 Comparing the PD activity in Silicone oil and Nytro 10XN 48
5.6 Comparing the impact of various duty cycles on PD formation 48
5.6.1 Influence of relaxation time with different duty cycles 52
5.6.2 Influence of subsequent PDs due to PDs activity in the previous flank . . 52
5.6.3 Comparison of PDIVs for negative unipolar voltage pulses 52
5.7 Possible errors and limitations 53
5.7.1 Test object 53
5.7.2 Preparation of Silicone oil and Nytro 10XN 53
5.7.3 Experimental setups and measuring procedure 54

6 Conclusion **55**

7 Further work **56**

References **58**

Appendix **I**

A Appendix - PD detected with the high-speed camera **I**

B Appendix - High-speed camera with camera frequency of 480 Hz and implementation of $n = 1$ and $n = 8$ **III**

List of Figures

1 Cross section of an IGBT power module 3

2 Layers of an IGBT power module 3

3 Accumulation of space charge around a positive and negative needle 7

4 Simplified principle of the needle to plane 8

5 Bipolar, positive and negative unipolar voltage pulses 9

6 Duty cycle principle 10

7 Rise time principle 10

8 The electric potential distribution of an IGBT power module substrate cross-section 11

9 Test object 13

10 Principle of PMT 15

11 The picture sequence principles for the high-speed camera for square voltage setup, with a camera frequency of 60 Hz 16

12 The picture sequence principles for the high-speed camera for square voltage setup, with a camera frequency of 480 Hz 17

13 Overview of the sinusoidal voltage setup, with the light guide and test object. . . 18

14 Schematic of the test circuit used for sinusoidal voltage measurements 19

15 Overview of the square voltage setup, with the light guide and test object. 20

16 Schematic of the test circuit used for square voltage measurements 21

17 Close up of the sinusoidal and square experimental setup, with the light guide and test object. When the light guide was not in use, the lens of the light guide was covered with a red hood. 22

18 Square voltage setup of light guide, high-speed camera, and test object. 23

19 Square voltage setup of PMT inside the cabinet and test object. 24

20 Desiccator used for Silicone oil 25

21 Desiccator used for Nytro 10XN 26

22 An overview of the measurement procedure of the ramping up and down of the voltage 27

23 Overview of the measuring procedure with the high-speed camera. 29

24 Overview of the measuring procedure conducted with Nytro 10XN. 30

25 Definition of voltage turn-on and turn-off for negative unipolar voltage pulses . . 31

26 Average probability PD curves of bipolar voltage pulses for Silicone oil and Nytro 10XN 33

27 Average probability PD curves of bipolar and unipolar voltage pulses for Silicone oil and Nytro 10XN 34

28 PD formation on the substrate surface with bipolar voltage at 11 kV_{peak} in Silicone oil with a camera frequency of 60 Hz 35

29 The probability of PD occurrence in the subsequent voltage periods given a prior occurrence of PD in the same location, for bipolar voltage at 11 kV_{peak} in Silicone oil with a camera frequency of 60 Hz 36

30 PD formation on the substrate surface with bipolar voltage at 11 kV_{peak} in Nytro 10XN with a camera frequency of 480 Hz 37

31 The PD activity occurrence in the subsequent plateaus and flanks, given a prior occurrence of PD in the same location, for bipolar voltage at 11 kV_{peak} in Nytro 10XN with a camera frequency of 480 Hz. 38

32 Probability of PD occurrence for negative unipolar with a duty cycle of 5 % for Silicone oil and Nytro 10XN, with a threshold set to 300 pC. Voltage is defined as peak-to-peak. 40

33 Probability of PD occurrence for negative unipolar with a duty cycle of 95 % for Silicone oil and Nytro 10XN, with a threshold set to 300 pC. Voltage is defined as peak-to-peak. 40

34 Average probability PD curves of bipolar and unipolar voltage pulses for Silicone oil and Nytro 10XN, with average PD probability at PDIV for sinusoidal voltage pulses for Silicone oil and Nytro 10XN 45

35 Illustration on how negative unipolar voltage pulses affect discharge formation at the sharp tips along the edge of the substrate, based on the needle-to-plane principle 50

36 Illustration on how high and low conductivity dielectric liquids behave in a needle-to-plane principle with a negatively charged tip 51

37 Picture of the substrate surface with bipolar voltage at 11 kV_{peak} in Silicone oil: Picture number 29 I

38 Picture of the substrate surface with bipolar voltage at 11 kV_{peak} in Nytro 10XN: Picture number 7 II

39 The picture sequence principles for the high-speed camera for square voltage setup, with a camera frequency of 480 Hz, with the implementation of $n = 1$ and $n = 8$. III

List of Tables

1 Overview of the start and maximum voltages for measurements conducted with positive and negative unipolar for Silicone oil and Nytro 10XN 29

2 PDIV and PDEV, electrical measurements, for Silicone oil and Nytro 10XN in sinusoidal voltage setup 32

List of Abbreviations

AC	Alternating Current
Al_2O_3	Aluminium Oxide
AlN	Aluminium Nitride
AlSiC	Aluminum Silicon Carbide
DC	Direct Current
HFCT	High-Frequency Current Transformer
HV	High Voltage
IGBT	Insulated-Gate Bipolar Transistor
PD	Partial Discharge
PDEV	Partial Discharge Extinction Voltage
PDIV	Partial Discharge Inception Voltage
PMT	Photomultiplier Tube
PRPD pattern	Phase Resolved Partial Discharge pattern
PWM	Pulse-Width Modulation
Si_3N_4	Silicon Nitride
UWBG	Ultra Wide Band Gap
WBG	Wide Band Gap

1 Introduction

1.1 Background

The electrical power industry is experiencing significant and complex expansion due to changes in consumer and supplier operation patterns, also considering the implementation of renewable energy sources [1, 2, 3]. To ensure a reliable energy supply, further development of existing equipment and new components and solutions must be developed [1, 3]. The increasing energy demand, driven by electrification and the trend toward all electric devices, can be met through higher voltages or currents [4]. Increasing the voltage is being considered and preferred [4], and with higher voltage comes the challenge regarding the insulation properties capabilities of the high-voltage equipment in the power grid [5]. High-voltage power electronics are central and essential elements widely used in the power grid [5]. It is expected that approximately 80 % of the total electric power will be transmitted through power electronics by 2030 [4, 6]. Therefore, developing power electronics is necessary to meet future energy demands [3].

To meet the requirements of applications operating in a wide range of voltage and current levels, power electronics such as Insulated Gate Bipolar Transistors (IGBTs) are used. Thus, IGBTs power modules are used in different parts of the electrical power industry, such as High-Voltage Direct Current (HVDC) power, smart grids, robotics, electric trains, etc. [7]. IGBTs and the material used will vary depending on the usage of the power electronic device. However, ceramic substrates are commonly preferred [8]. Ceramic substrates are regarded as one of the most critical components of the IGBT assembly when considering high-voltage power modules and their insulation failure causes [3, 5].

The rapid voltage changes from high-voltage power electronics cause stress to the components in the power network. Consequently, Partial Discharge (PD) formation may occur due to frequent switching and rapid starts and outages [1], within and on the surface of the substrates and leading to degradation the materials [3, 9]. PD formation is recognized as one of the most critical factors leading to failure and aging in insulation systems of equipment in the power grid [1, 3, 5, 10].

1.1.1 Motivation of the master's thesis

Earlier studies [9, 11, 12, 13] indicate that PD formation and insulation failures for IGBTs and ceramic substrates are dependent on the applied voltage pulse form. In comparison to sinusoidal voltage pulses, square voltage pulses, with their short rise time and high switching frequencies, are more stressful on the insulation system, leading to faster degradation of the insulation medium [3, 9]. Due to the significant influence of PD formation on the aging process of power electronic devices, there is considerable interest in conducting further analysis on this topic. Such investigations aim to improve knowledge and provide a deeper understanding of PD formation, as well as the possible detection of residual changes, such as space charges, on ceramic substrates. As the substrates used in IGBTs are quite complex, a simplified geometry substrate was used during this thesis to contribute to the research.

1.2 Objective of the master's thesis

This master's thesis aims to investigate the formation of PD on an Aluminium Nitride (AlN) ceramic substrate. The study primarily focuses on the substrate under square voltage pulses

while also evaluating its behavior under sinusoidal voltage pulses. An analysis of the PD formation in two different dielectric liquids, Silicone oil and Nytro 10XN, will also be conducted. Furthermore, the report aims to explore the occurrence of PD formation, specifically on the surface of the substrate. Moreover, the investigation seeks to evaluate the influence of different square voltage pulses on the PD formation and to examine the potential impact of varying the duty cycle of the voltage pulses. Lastly, the report seeks to understand better the space charge phenomenon and how it varies in the two dielectric liquids.

1.2.1 Structure of the report

The thesis begins with a theoretical basis of the IGBT, discharge phenomenons, and parameters affecting the IGBT. The subsequent section, methodology, includes the details on the test object, the experimental setups, and measuring procedures. Furthermore, the results from the experimental work are presented, followed by the discussion. The most significant findings are summarized in the conclusion, and the thesis ends with suggestions to further work.

Some parts and sections in the theory and methodology, Section 2 and 3, respectively, are taken directly from the specialization project [3]. A specific approach was used to differentiate between reused sections and new content in this thesis. Footnotes were used exclusively to mark sections taken directly from the specialization project. In this thesis, if a section includes a footnote, everything before the footnote in the section is directly taken from the project, while the sentences following the footnote are newly written for this thesis. If a section does not include a footnote, the section is newly written for this thesis. This system ensures clarity and helps the readers understand which parts are taken directly and which are written during this thesis. However, it should be noted that some adjustments and modifications have been implemented to the parts taken directly from the specialization project to improve and clarify the overall understanding.

2 Theory

The following section introduces the theoretical foundation to understand the research gap better. The section starts with a theoretical basis of the IGBT and ceramic substrates, a description of the PD and space charge phenomenon, and ends with parameters affecting the IGBTs.

2.1 Insulated Gate Bipolar Transistor (IGBT)

A typical Insulated Gate Bipolar Transistor (IGBT) power module consists of several components, making it a complex assembly, as illustrated in Figure 1. The assembly is typically placed in an external housing made of polymer and encapsulated with an insulation medium, often with dielectric/Silicone gel [5]. The diode and IGBT are soldered onto a copper metallization layer, which is brazed onto a ceramic substrate. Another metalized layer is brazed onto the opposite side of the ceramic substrate and soldered to a base plate. Typical materials used in the base plate are Aluminum Silicon Carbide (AlSiC) or copper [2, 5]. The different layers are illustrated in Figure 2. [1]

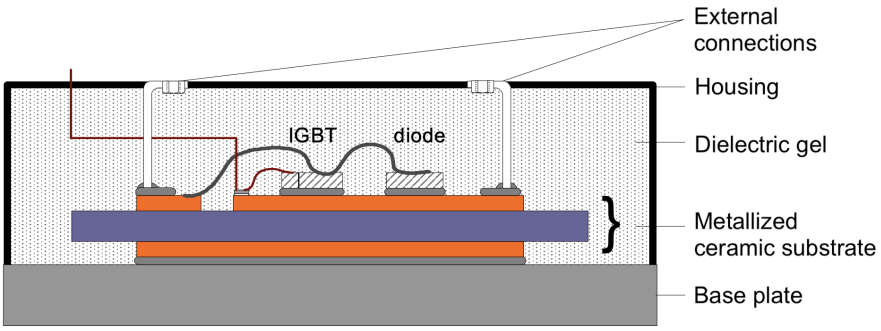

Figure 1: Schematic representation of the cross-section of an IGBT power module [3, 5].

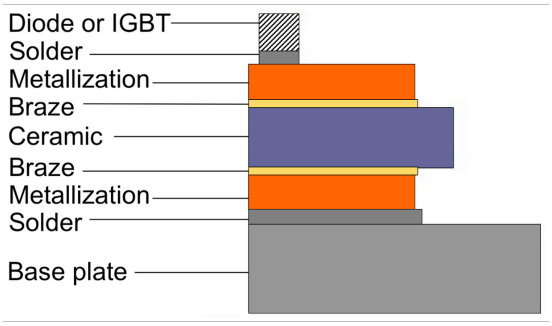

Figure 2: Schematic representation of the layers of an IGBT power module [2, 3].

The use and development of ceramic substrates have increased significantly in the past 30 years [8]. Typical ceramic substrate materials used are Aluminium Nitride (AlN), Aluminium Oxide (Al_2O_3), and Silicon Nitride (Si_3N_4) [2, 5]. The mentioned materials have different properties, and which type of material is preferred based on the needs [8]. The ceramic substrate provides electrical insulation, so choosing the best-intended material is essential. Under high voltage,

[1] Taken directly from specialization project [3]

mechanical and thermal properties must be considered when evaluating the electric insulation. Thus, based on these properties, a suitable substrate is chosen. When considering the mechanical properties, the dilatation coefficient of the ceramic should be as close to the other materials as possible. In addition, factors such as thermal conductivity and tolerating high temperatures are necessary when considering the thermal properties of the substrate [2]. AlN is preferred when considering thermal conductivity due to its high value, while the thermal conductivity for Si_3N_4 and Al_2O_3 is lower compared with the AlN [8]. Multiple materials can be used, all based on the need of the IGBTs. [1] The ceramic substrates serve two primary functions to maintain optimal and functional performance. Firstly, the ceramic is used to prevent overheating and heat dissipation generated by power loss. Secondly, the ceramic serves insulation purposes by protecting the circuit from electrical interference [3, 8].

As mentioned, the power network is exposed to a more rapid voltage change operation pattern. As a result, the local electric field distribution in the IGBTs will increase with increasing voltage. Consequently, this can potentially reduce the insulation material properties due to the formation of PD [2]. Failure analysis shows that approximately 60% of damaged high-voltage equipment results from insulation failure. Therefore, PD measurements are performed during manufacturing and operation to ensure the insulation properties of the equipment are in good condition [14]. [1]

2.2 Partial discharge phenomena

Partial discharge (PD) is an electrical breakdown phenomenon and occurs when a spark or local breakdown partially bridges the insulation between two conductors. A redistribution of charge and space charges will happen within the insulation due to the spark [15]. Two factors are necessary for a discharge to occur. The first factor is that the electrical field has to be strong enough to result in an electron avalanche. For this to happen, a free electron has to be accelerated and start the spark. The second factor is that the withstand strength has to be low enough for the local insulation to break down. The locally stored energy will be released when a discharge occurs and may be converted into various energy forms, i.e., heat, light emissions, electromagnetic radiation, chemical changes, current pulses, and acoustic waves. PD is measured in coulomb (C), and the order of magnitude is usually in pico coulomb (pC) [10]. [1]

PD is a stochastic phenomenon that varies from voltage period to voltage period in magnitude and frequency. Different PD phenomena will occur due to the various geometries and defects. PD will therefore have other behaviors based on the PD type. The different PD types can be divided into six groups [10]. [1]

Different types of PD phenomena: [1]

1. Void
2. Electrical trees
3. Surface discharge
4. Corona
5. Wedge discharge
6. Electrically floating metal

Experimental studies have shown that voids and surface discharges are critical PD formations to consider when evaluating the performance and reliability of IGBT power modules [2, 12]. Voids may occur within solid dielectric materials and consist of either trapped gases or liquids,

[1] Taken directly from specialization project [3]

usually forming during the steepest flank of the applied voltage [10, 16]. The dielectric strength of trapped gas or oil is typically lower compared with solid dielectric materials. Thus, discharges may occur when the withstand ability of the void exceeds [17]. Surface discharges may occur at the interface between solid dielectric materials and gas or liquid insulation parallel to the electric field [10, 16]. For example, sharp edges or the presence of unwanted particles in the insulation medium may distort the electrical field, resulting in surface discharges [15, 16]. [1]

PD formation will, over time, deteriorate the insulation properties and contribute to a gradual degradation of the insulation when exposed to electrical stress [10, 17]. Considering power modules, factors such as PD, electrical treeing, and water trees are the main processes affecting the aging of insulation materials [5]. The factors may occur alone or in combination. Hence, it is desirable to measure and detect PD activity, thus contributing to evaluating the condition of the insulation properties [10, 17]. [1]

2.2.1 Characterisation of partial discharges

Previous experimental work shows that multiple factors affect PD activity, such as the voltage waveform, magnitude, and frequency [18]. In high-voltage systems, the diagnostic technique of Phase Resolved Partial Discharge (PRPD) pattern is used to detect and analyze PD formation and contribute to identifying possible future failure of the insulation medium. PRPD pattern is directly related to the mechanism of the PDs [5]. The technique measures the PD activity at various phases of the applied voltage and allows the identification of the characteristics and location of the PDs. The characteristic of a void or cavity in an insulation material will be visible in a PRPD pattern. A typical pattern for voids is a symmetrical PD appearance during both voltage polarities. If PD activity is detected only during one voltage polarity, it may indicate the presence of an unsymmetrical fault, i.e., sharp edges. With the changing polarity of the applied voltage, the trapped charges inside a void or cavity will change polarity along with the applied voltage. Thus, discharges may occur in both polarities. However, with sharp edges present, the electrical field distribution and strength around the edge will vary based on the polarity of the voltage. Thus, PD may not appear for both voltage polarities. The discharges usually occur between zero crossing and the peak value of sinusoidal voltage pulses, i.e., approximately around the highest slew rate, $\frac{dU}{dt}$, of the applied voltage [5]. [1] For square voltage pulses, discharges usually occur during the flanks [19]. The rate of voltage rise varies between sinusoidal and square voltage waveforms. Consequently, the rise time of the voltage flanks plays a significant role in the formation of PD [11].

2.2.2 Partial Discharge Inception and Extinction Voltage (PDIV and PDEV)

The following section is inspired by the specialization project [3]. By progressively increasing the applied voltage, it becomes possible to reach a critical voltage across a cavity. This critical voltage initiates the formation of PDs and is commonly referred to as the Partial Discharge Inception Voltage (PDIV). If increasing the voltage further, the occurrence of PDs intensifies. These PDs mainly occur during the rising and falling flank of the sinusoidal and square voltage pulses. In the event of continued voltage elevation, PDs may appear around zero crossing for the sinusoidal voltage and during the plateaus of the square voltage pulses, which indicates the presence of space charges. Notably, the formation of PDs continues even as the voltage decreases below the ignition threshold. The extinction of PD formation indicates the attainment

[1] Taken directly from specialization project [3]

of the Partial Discharge Extinction Voltage (PDEV). By way of explanation, the PDIV typically exceeds the PDEV in magnitude. Ideally, the PDEV should be approximately half the voltage level of the PDIV inside voids [10].

2.3 Space charge phenomena

Space charges can occur in dielectric materials, as well as in liquids, gases, and gels [20]. Different voltage forms, i.e., the shape of the voltage, will result in various discharge mechanisms. The different space charge distributions are caused by the various voltage forms [15]. These charges can be either positive or negative, forming a local electric field if the applied voltage is strong enough to generate the energy needed to release the trapped charges [21]. The electric field created by the trapped space charges inside the dielectric will distort the applied electrical field. Therefore, space charges will impact the existing electric field and its distribution, thereby influencing the initiation and formation of PDs [15, 20]. [1] Hence, as mentioned, discharges may occur around zero crossing of sinusoidal voltage pulses and during the plateau of the square voltage pulses.

One of Maxwell's equations, Gauss's law, can be used to determine the distribution of electric charge by considering the relation between charge density, ρ, and permittivity, ε, [22]: [1]

$$\nabla \ \mathbf{E} = \frac{\rho}{\varepsilon} \tag{1}$$

Further, the electric field strength can be defined as the negative gradient of the potential, φ, [20]: [1]

$$\mathbf{E} = -grad \ \varphi \tag{2}$$

Furthermore, Poisson's Equation can be derived [20, 23]: [1]

$$div \ grad \ \varphi = \nabla^2 \varphi = -\frac{\rho}{\varepsilon} \tag{3}$$

The field can be calculated by application of the boundary condition (applied voltage). The field is referred to as the Laplacian field, E_L, when no space charges are present, $\rho = 0$ [20, 21]. Furthermore, if only space charges are present and no applied voltage, the space charge will generate a so-called space charge field, E_{SC}.

Depending on the polarity of the space charges, the discharges can increase or decrease the applied electrical field [20]. The dipoles are free to move in a dielectric liquid or gas and will align with the applied field relatively fast [23]. Thus, space charges can contribute to discharge but also prevent a possible discharge [20]. Multiple dielectrics are often used in high-voltage insulation systems. Thus, interfacial polarisation is a critical factor to discharges, as charges can accumulate on interfaces of a layer, or "two phase-dielectrics," under low-frequency Alternating Current (AC) voltage or Direct Current (DC) voltage [23]. The principle of the needle-to-plane can be used to understand the phenomenon better.

[1] Taken directly from specialization project [3]

2.3.1 Needle to plane

Space charges will accumulate around the tip of the needle when applying voltage [24]. The tip of a needle will create an inhomogeneous field, and the fields will be strong around the tip [23]. The accumulation of positive and negative space charges will form around the tip of the positive or negative charged needle, thus, i.e., causing electric field enhancement [17, 21, 25]. The different polarities of the space charges will have different characteristics due to the difference in the electrical field enhancement [17]. [1] Charges accumulated around the tip of the needle with the same polarity as the needle are defined as homo charges, while the discharges with the opposite polarity are defined as hetero charges [20].

Figure 3 illustrates the formation of space charges with a positive and negative needle and the corresponding field distortion due to the space charges [26]. The Poisson field (with space charge) is presented in the black, solid line, and the Laplacian field (without space charge), E_L, is presented in the black, dotted line. If the needle is negatively charged, the accumulated positive charges around the tip of the needle will increase the electrical field around the tip [21]. Even though the local field around the tip of the needle is increased, the overall electrical field will decrease. It will reduce the igniting voltage necessary for a discharge to occur [20, 21]. The opposite will happen with a positive needle [17]. [1]

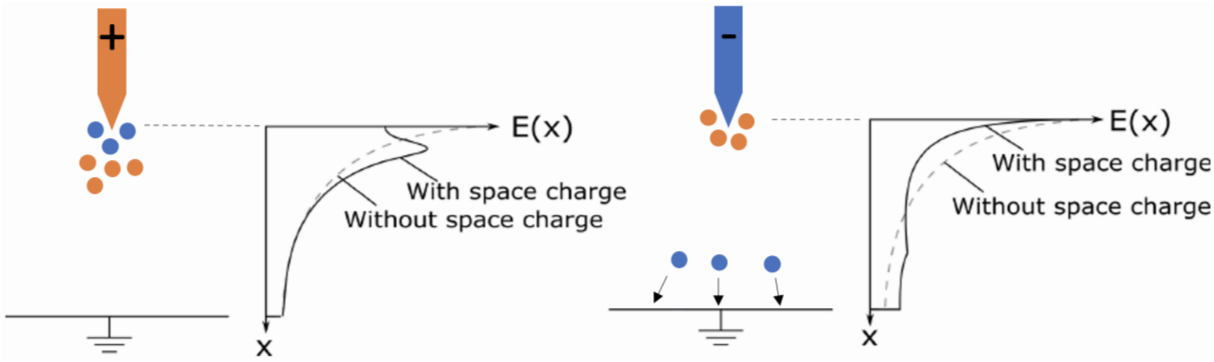

Figure 3: Accumulation of space charges around a positive and negative needle, and the corresponding field distortion due to the space charges. The color orange represents a positive charge, and blue represents a negative charge. Illustration adapted from [3, 21, 26], but with minor modifications.

2.3.2 Dielectric relaxation time

The following section is inspired by the specialization project [3]. The principle of the needle to plane can be presented through the utilization of a simplified, parallel configuration of a resistor, R, and capacitor, C. The arrangement, shown in Figure 4, can be presented as an equivalent circuit for the principle [3].

[1] Taken directly from specialization project [3]

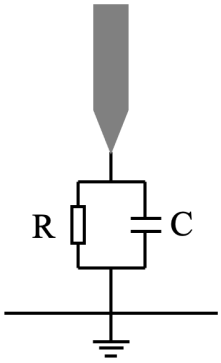

Figure 4: Simplified principle of the needle to plane [3, 27].

The time duration it takes for the electric dipoles in a dielectric material to line up with the applied electric field is known as the dielectric relaxation time [20, 21]. The relaxation time may be derived as expressed in Expression 4 [3]:

$$\tau = RC \tag{4}$$

Further, Kirchhoff's Current Law can be used to express the circuit in Figure 4. Thus, Expression 5 can be derived:

$$\frac{1}{R}v + C\frac{dv}{dt} = 0 \tag{5}$$

The two currents, conductive and displacement currents, have to be considered when evaluating the electric current density [20, 28]. Due to the moving charge through the conductor, the conductive current density has to be included and is defined in the first part of Expression 6. The time-varying electric field will result in electric charges inside the dielectric material. This effect is called displacement current and is defined in the second part of Expression 6 [20]: [1]

$$\sigma\vec{E} + \varepsilon\frac{d\vec{E}}{dt} = 0 \tag{6}$$

Based on Expression 4 - 6, the dielectric relaxation time can be expressed considering the permittivity, ε, and conductivity, σ, of the dielectric material. Thus, the dielectric relaxation time can be derived as [20]: [1]

$$\tau = \frac{\varepsilon}{\sigma} \tag{7}$$

The permittivity is defined as $\varepsilon = \varepsilon_r\varepsilon_0$. ε_r is the relative permittivity of the material. ε_0 is the permittivity in a vacuum and is considered an electric constant with the value of $8.85 \cdot 10^{-12}\frac{F}{m}$ [23]. [1] The relaxation time is temperature dependent. Accordingly, an increase in the temperature will decrease the relaxation time because the dipoles will move faster [20].

[1] Taken directly from specialization project [3]

2.4 Parameters affecting IGBTs

Wide Band Gap (WBG) semiconductors are common materials in power semiconductor devices. The creation and application of so-called ultra WBG (UWBG) materials in semiconductors is currently the subject of state-of-the-art research. Materials studied are diamond (C), Gallium oxide, and AlN, referred to as generation-after-next power electronics, and they may result in achieving higher temperatures, switching frequencies, voltage hold-offs, and reduce the energy losses [2, 3].

The Silicone gel, housing, and ceramic substrates are considered the most critical components of the IGBT assembly when considering high-voltage power modules and their insulation failure causes [5]. Previous studies have revealed that different voltage pulse types have varying effects on the degradation of the substrates. Specifically, square voltage pulses, i.e., fast transient voltage pulses, have been identified as more influential in substrate degradation compared to sinusoidal voltage pulses [12]. According to state-of-the-art, the rise time of square voltage pulses has been expressed as critical for the formation of PDs with larger magnitudes. The increased formation, in turn, contributes to faster degradation of the insulation system [13]. However, it should be noted that other parameters may affect the IGBTs. As a result, further research is necessary to understand better the IGBTs and the effect of PD formation in power modules.

2.4.1 Square voltage pulses parameters affecting IGBTs

To better understand the fast repetitive square voltage pulses and the changes made to the parameters of the voltage pulses in this thesis, it is necessary to introduce and explain the relevant parameters that affect these voltage pulses. Parameters such as bipolar and positive and negative unipolar, frequency, duty cycle, rise time, and slew rate will affect the formation of the fast repetitive square voltage pulses [21]. Therefore, a short introduction will be provided.

The signal polarity of the applied square voltage pulses can be altered as positive or negative, or both. During one signal period, bipolar pulses oscillate between positive and negative polarities, distinguishing them from unipolar pulses, where the polarity is either positive or negative. One can further categorize the latter as positive or negative unipolar [29]. The different polarities of square voltage pulses are illustrated in Figure 5.

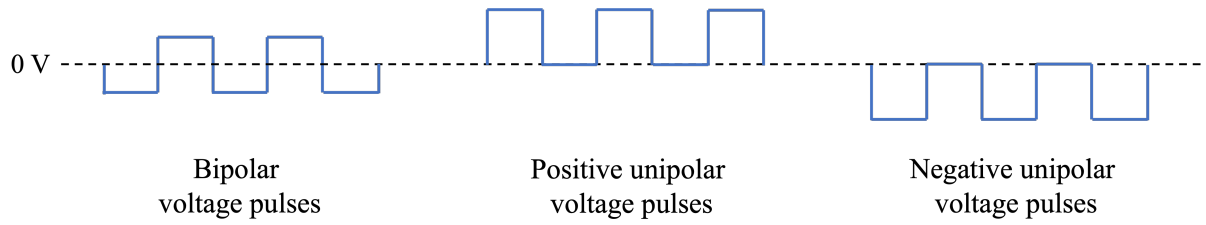

Figure 5: Bipolar, positive and negative unipolar voltage pulses

IGBTs are preferred when comparing other types of transistor devices. The main advantages of IGBTs include fast switching speeds and high-voltage capability. Hence, IGBTs are recommended for various applications, including high-voltage appliances that require Pulse-Width Modulation (PWM) [30]. The process of regulating power in converters is referred to as PWM and is widely used and recognized as the most crucial process for control implementation [31]. PWM is a technique used for generating pulses to regulate and control analog signals [32]. Frequency and the duty cycle are the primary parameters defining the signal

behavior of a PWM signal [32]. Changing the input signal's frequency and duty cycle will change the output signal's behavior. The frequency describes the rate at which the pulses occur over a particular period. While the duty cycle is the ratio of the time during which the signal is in its on-state to the total time for one complete period of the signal. The duty cycle is defined as a percentage, representing the time duration the signal value is high [32, 33]. Specifically, when the duty cycle is set to 95 %, the voltage is high, on-state, 95 % of the period, and low, off-state, for 5 % of one complete period of the signal [33]. Figure 6 illustrates the duty cycle principle for a duty cycle of 95 % and 5 %, for negative unipolar voltage pulses.

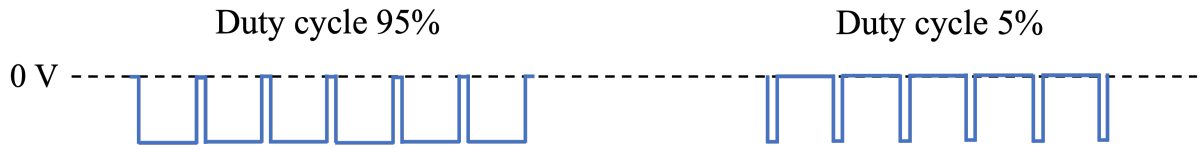

Figure 6: Duty cycle principle of a duty cycle of 95 % and 5 % for negative unipolar voltage pulses. This concept is illustrated, drawing inspiration from the work presented in [32].

Rise time and slew rate are also important parameters affecting the voltage pulses. Rise time is the duration for the voltage pulse to rise from 10 % to 90 % of its peak value [31], as presented in Figure 7. In comparison, the slew rate is defined as $\frac{dU}{dt}$, i.e., the slope of the voltage pulse. Hence, it is described as the rate of change in the voltage pulse [34].

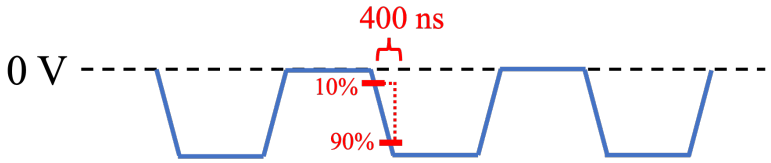

Figure 7: Principle of the rise time of a negative unipolar voltage pulse. Voltage rise time from 10 % to 90 % is presented in red with a rise time of 400 nanoseconds.

The IGBT switching frequency refers to the frequency at which the IGBTs turn on and off. Hence, an increase in the switching rate will result in a cleaner waveform as the number of pulses during each half-wave increases. IGBTs typically operate at frequencies in the kilohertz kHz range [35].

The different factors of the voltage pulses are significantly affecting the PD formation, thus affecting the insulation degradation. The PD formation is especially critical in some regions of the IGBT. The regions within a power module that experience high electric field stress and may trigger PDs are close to the sharp edges of the metallization layers and the triple points [36].

2.4.2 Electrical field distribution at the triple point affecting IGBTs

One well-known problem of the IGBT power module is the triple point on the substrate. The triple point is the point where the ceramic substrate, metallization (copper electrode), and the material encapsulating the IGBT (Silicone oil or gel) meet [9]. Field simulations performed on the cross-section of the substrate show that the triple point is most susceptible to concentrated electric potential distribution [5]. Figure 8 shows the electric potential distribution and how the field is distributed around the triple point. The color shading indicates the field distribution,

from the color blue indicating the ground potential to red indicating 10 kV [5, 37]. The triple point can be seen inside the black, dashed circle, and is exposed to the highest electrical field distribution [5, 21]. [1]

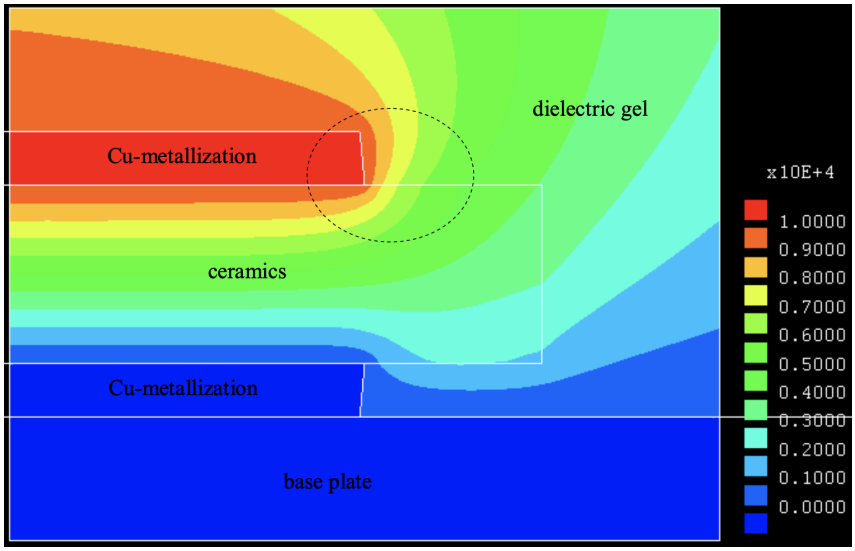

Figure 8: The electric potential distribution of an IGBT power module substrate cross-section, sourced from [5].

[1] Taken directly from specialization project [3]

3 Methodology

In the following section, the experimental work is presented. The section begins with a description of the test object, followed by an explanation of the various PD measurement techniques used in the experimental work. Subsequently, the experimental setups and preparation of the test object in the two dielectric liquids are presented. The section ends with the measurement procedures and post-processing of data.

Various experimental setups were used during the experimental work. The different setups are presented below:

- Sinusoidal voltage ramping up and down: This setup involves detecting PD activity using electrical and optical measurements, presented in Section 3.3.3.
- Square voltage ramping up and down: This setup involves detecting PD activity using optical measurements, presented in Section 3.3.3.
- Constant square voltage step: This setup involves detecting PD activity using optical measurements and an ultra-fast gated intensified high-speed camera, presented in Section 3.3.4.
- Varying the duty cycle at a constant square voltage: This setup involves detecting PD activity with different duty cycles using optical measurements, presented in Section 3.3.5.

3.1 Test object

During the PD measurements, a simplified AIN ceramic substrate was used as the test object, presented in Figure 9. As previously mentioned, the ceramic substrate is a crucial component of the IGBT, thus, making it of interest to study the ceramic substrate by itself [5]. Hence, the test object was manufactured to keep the geometric shape of the substrate simple, thus making it easier to detect PD activity. [1]

The test object can be divided into four parts: copper base, AlN substrate, copper contact, and solder lug, as seen in Figure 9. The following dimensions are presented as $length \times width \times height$. The copper base has the dimensions $55 \times 40 \times 2.0$ mm. The AlN ceramic substrate was attached to the copper base, with $50 \times 25 \times 1.0$ mm dimensions. The copper contact was then attached to the AlN, with the dimensions of $15 \times 15 \times 0.3$ mm. Further, a solder lug was attached to the copper contact, and a black wire was soldered on the solder lug. [1]

[1] Taken directly from specialization project [3]

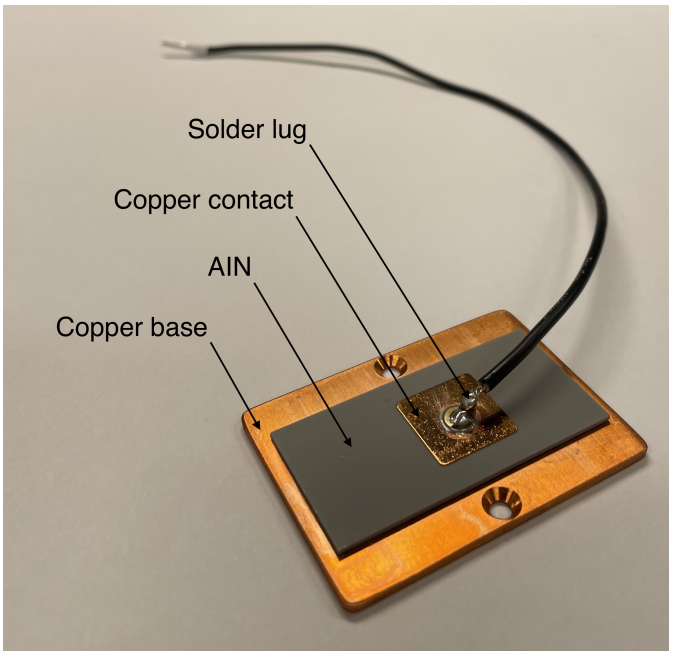

Figure 9: The test object. Illustration inspired by [21, 37].

In order to study the formation of PD along the sharp metal edge situated on the top of the substrate, it was necessary to mitigate the electrical field in other regions. The width of the copper base was therefore expanded beyond the substrate, thereby reducing the electrical field through shielding [21]. The electric potential lines are illustrated in Figure 8 [5, 21].

3.1.1 Preparation of new test objects

The majority of the experimental tests conducted during the thesis were repetitive tests. The consideration of reuse of the test object was excluded for the repetitive testing to ensure maximum similarity among the test objects and experimental tests conducted. Hence, a new substrate was used for each measurement, and many test objects were required. Therefore, new test objects had to be made during the thesis period. The manufacturer had already attached the AIN and copper contact, but the copper base had to be constructed and attached to the ceramic substrate. In addition, the solder lug and wire required attachment. The ceramic substrate was soldered to the cobber base using a solder paste to maintain the same potential on the high-voltage electrode and the test object during the measurements. A solder lug and wire were also soldered onto the copper contact on the top of the test object. After the assembly of the new substrates, they were subjected to cleaning in an ultrasonic bath. The substrates were cleaned in isopropanol alcohol for approximately two hours, followed by complete desiccation in a fume hood, after which the isopropanol was damped off.

In order to ensure equality between the substrates used during the specialization project [3] and the newly assembled substrates, identical measurements were conducted. The results revealed a considerable similarity between the substrates, thereby validating that the new test objects could be compared with the test objects used during the specialization project [3].

3.2 Experimental setups: PD measurement techniques

Two experimental setups were used to detect and measure PD activity. Sinusoidal and square voltage setups were used for the measurements. For both of the setups, the test object was placed in a metal cabinet which can be considered a Faraday cage [3, 17]. Optical measurements were obtained in both setups with the use of a Photomultiplier Tube (PMT). In order to establish a more reliable basis for comparison of the sensitivity of the measured PD activity, the same PMT was used in both experimental setups [21]. Electrical measurements were only obtained for the sinusoidal voltage setup, as it was not possible to implement in the square voltage setup.

A High-Frequency Current Transformer (HFCT) was implemented and tested for the square voltage setup. However, it did not work as intended and was therefore not further used and described.

3.2.1 Electrical measurements

The following two sections draw significant inspiration from the work undertaken in the specialization project [3].

The electrical measurements were conducted utilizing Omicron MPD600 to measure voltage and record PRPD patterns. The experimental setup conforms to the guidelines outlined in IEC 60270 *High-voltage test techniques - Partial discharge measurements*, which regulates the measurement of PDs in high-voltage insulation media [12]. The voltage drop caused by the PD was calculated by implementing a measuring impedance, and electrical measurements were subsequently determined [21]. An ABC-equivalent illustrates how the electrical signal from a discharge inside a void can be detected if the insulation is stressed by sinusoidal voltage pulses [16]. Nevertheless, it is not possible to measure the actual charge of the locally exchanged discharge directly. Hence, the apparent charge will be detected in the external circuit [10]. The details and principles regarding the ABC-equivalent are beyond the scope of this thesis and will not be further discussed [3].

The Omicron MPD600 was connected to a computer equipped with the Omicron MPD software to visualize and present the detected PD formation. The software showcases the PD activity as PRPD patterns of a 360° circuit. Before conducting the measurements, the voltage and charge were calibrated to ensure accuracy within the measurements within the OMICRON software [3, 17, 21].

3.2.2 Optical measurements

Optical measurements were provided by using a Photomultiplier Tube (PMT). PMT is a photosensitive device used to detect and measure radiant energy, which is quite versatile. Considering the electromagnetic spectrum, the PMT measures radiant energy in the range of ultraviolet, visible and near-infrared regions and converts it to electrical energy [38]. [1]

The working principle of the PMT involves radiant energy passing through an input window [39]. A semitransparent photocathode is placed on the inner surface of the input window [38]. The photoelectron, e^-, in the photocathode, will be excited due to the radiant energy [39] by the process of photoemission [38]. Due to the electrical field, the emitted photoelectrons will

[1] Taken directly from specialization project [3]

accelerate and focus onto the first dynode. There the photoelectrons will be multiplied through the process of secondary electron emission. The secondary electron emission will be repeated, and more secondary electrons will be emitted and accelerated to the next dynode. This process will be repeated at each dynode, and at the last dynode, the anode will collect the emitted photoelectrons. The collected photoelectrons will leave the PMT as the output signal [38, 39]. Thus, optical measurements can be used to detect PD activity. The working principle of the PMT is illustrated in Figure 10. [1]

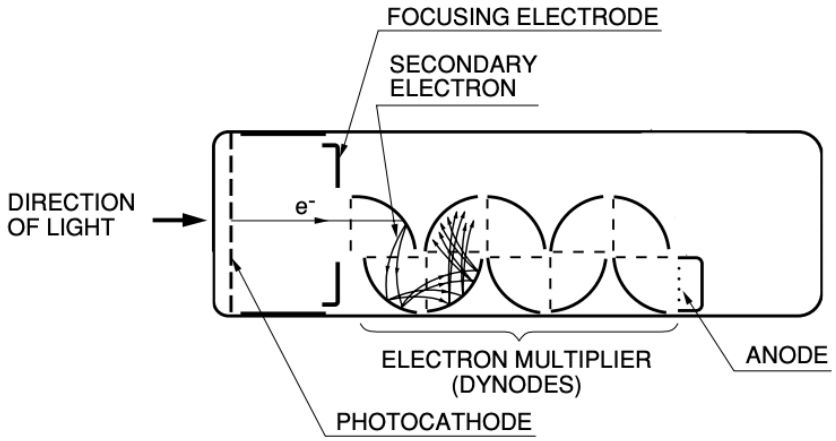

Figure 10: Working principle of a photomultiplier tube (PMT) [39].

According to experience in the laboratory, electrical measurements tend to be more reliable than optical measurements from the PMT. The optical measurements are more sensitive to noise compared with the electrical measurements [40]. If PD activity is detected with the optical measurement and not with the electrical measurement, it may be caused by external noise rather than actual PD activity. Hence, electrical measurements are preferred. The presence of dark current in optical measurements can significantly impact the reliability of the measurements. This is because dark current, caused by the thermal emission of electrons from the photocathode or dynodes, can produce false signals that can not be distinguished from actual PDs. In order to mitigate the effects of dark current, it is common to cool the PMT or to use two PMTs and compare the signals detected. By doing so, it is possible to determine with a higher degree of certainty whether the detected activity is PDs or the result of dark currents [37, 38]. Only a single PMT was utilized during the measurements conducted in this thesis. As a result, it was impossible to confirm the presence of dark currents. This limitation was taken into account during the analysis of the optical measurements. [1] Additionally, it should be noted that there was not used cooling on the PMT during the experimental work.

3.2.3 Ultra-fast gated intensified high-speed camera

In order to detect PD activity emitted as light, an ultra-fast gated intensified high-speed camera was used. At low light levels, the high-speed camera can generate picture applications [3, 41]. The HiCAM 500 high-speed camera manufactured by Lambert Instruments was used during the experimental work. The same camera was used during the experimental work in the specialization project [3].

[1] Taken directly from specialization project [3]

The high-speed camera was placed directly above the test object. The lens was adjusted to focus on the edge of the substrate, i.e., the area of interest. In order to capture clear and optimal pictures, different parameter values were configured in the programs TimeViewer and Lambert Intensifier Control Software prior to the pictures being taken [24]. The exposure time was set to 1 milliseconds, and the camera was set to take 1000 pictures. The gain level was set to 750 for all of the measurements. As all of the pictures were taken with the same gain level, the intensity of the emitted light could be directly compared [3].

The applied voltage in the system was set to 30 Hz, while the high-speed camera was set to a frequency of 60 Hz for the majority of the measurements. Thus, two pictures were taken for each voltage period. Figure 11 illustrates the picture sequence principle [3]. The voltage signal is marked in blue and illustrates one voltage period. Black and red lines denote the picture sequence principle, where the red lines describe when the camera is on (taking pictures). The axes are defined per unit (PU). The high-speed camera took one picture of the rising flank and one picture of the falling flank, illustrated with orange and green arrows, respectively. The area between the orange arrows in Figure 11 illustrates how the high-speed camera captured the PD activity for the rising flank. The same principle to the area between the green arrows and the falling flank. In other words, all PD activity occurring during the duration of one red line is captured in one picture [3]. The camera intervals were shifted to start taking pictures 10° before the rising or falling flank of the voltage, illustrated as delta, δ, in Figure 11. This angle ensured that the camera had started taking pictures before the polarity shift of the voltage, i.e., ensuring that all the PD activity at the flanks was detected. The narrow interval between the orange and green arrows is due to the dead time of the camera and occurred between each picture taken.

The high-speed camera was set to take two pictures each period and take a total of 1000 pictures in each measurement, corresponding to capturing PD activity in 500 periods. Thus, the total duration of the picture intervals was approximate $\frac{500\ periods}{30\ Hz} \approx 16.67$ seconds. [1]

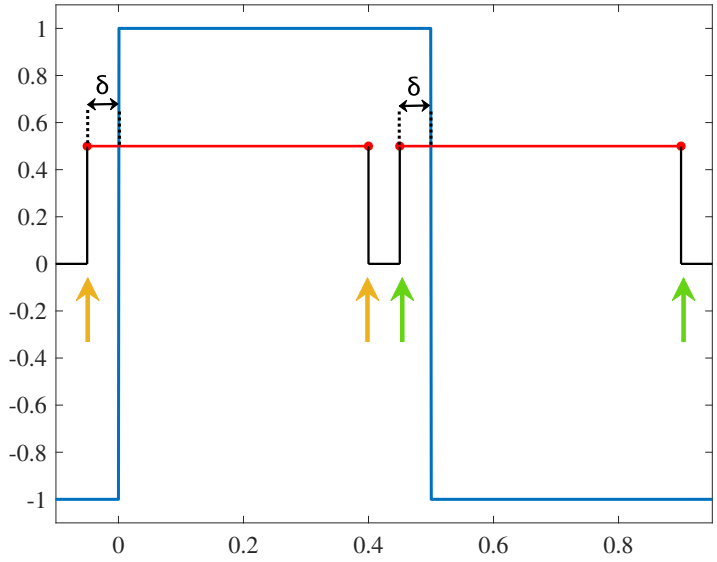

Figure 11: The picture sequence principles for the high-speed camera for square voltage setup, with a camera frequency of 60 Hz. The x- and y-axis are defined per unit (PU). The voltage signal is marked in blue.

[1] Taken directly from specialization project [3]

The program applications, TimeViewer and Lambert Intensifier Control Software, had multiple limitations whereby the duration of one picture interval had to be uniform for all picture intervals. Additionally, the program applications had a limitation of a maximum frequency of 500 Hz. In order to distinguish the PD activity on the flanks and plateaus of the voltage signal, the camera frequency was set to 480 Hz in some measurements. The frequency was chosen due to it being the highest possible value equal to or below 500 Hz and was a convenient multiple of 30, corresponding to the system frequency of 30 Hz. With this camera frequency, the camera captured 16 pictures during each voltage period. Figure 12 illustrates the picture sequence principle. Same as stated for Figure 11, the voltage signal is marked in blue, and the black and red lines describe the picture sequence principle in Figure 12. As stated earlier, all PD activity occurring during the duration of one red line is captured in one picture. Two of the 16 pictures were captured from the rising and falling flank, marked by the orange braces in Figure 12. The remaining 14 pictures were of the plateaus, marked by the green braces in Figure 12. In other words, the high-speed camera captured eight pictures in each half-period, one for the flank and the remaining seven pictures of the subsequent plateau. As stated earlier, the narrow interval between each picture is due to the dead time of the camera.

The high-speed camera was configured to capture 16 pictures each period and take a total of 1000 pictures in each measurement, corresponding to capturing PD activity in 62.5 periods. Thus, the total duration of the picture intervals was approximately $\frac{62.5\ periods}{30\ Hz} \approx 2.08$ seconds.

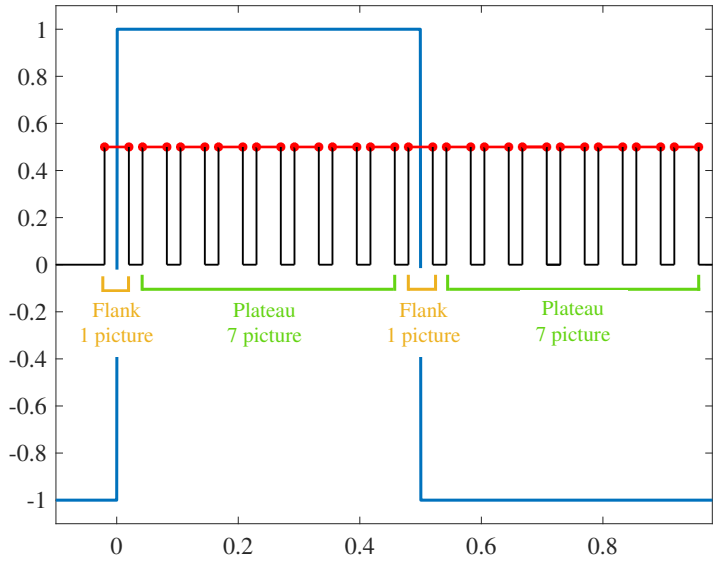

Figure 12: The picture sequence principles for the high-speed camera for square voltage setup, with a camera frequency of 480 Hz. The x- and y-axis are defined per unit (PU). The voltage signal is marked in blue.

It should be noted that Figure 11 and 12 are just illustrations of the principle of the picture sequence and not showing the correlation between the picture number and the polarity of the voltage. In other words, the illustration in Figure 12 does not indicate that the first picture is of the rising flank, positive voltage polarity, and the eighth picture is of the falling flank, negative voltage polarity. The figures are for explanation and illustration only.

3.3 Experimental setups: Sinusoidal and Square voltage

The following subsections describe the experimental setups for sinusoidal and square voltage in detail. Section 3.3.1 and 3.3.2 describe the overall experimental circuit and test circuit schematic for the sinusoidal and square voltage setups, respectively. The experimental circuit was changed due to the various measurements requiring different equipment. Consequently, the setup inside the cabinet changed throughout the different measurements. Section 3.3.3 details the experimental setup for the ramping of sinusoidal and square voltage, while Section 3.3.4 presents the experimental setup of the square voltage with the high-speed camera. Finally, Section 3.3.5 describes the experimental setup for the square voltage with varying duty cycles.

3.3.1 Experimental setup: Sinusoidal voltage

The experimental setup detects PD activity in insulation samples under sinusoidal high voltage. The experimental circuit and a test circuit schematic are presented in Figure 13 and 14, respectively. Noise induced by the power grid may affect the PD measurements. To prevent this, a resonant high-voltage circuit was used. The circuit could be run in resonance in the range of $30 - 50$ Hz. Figure 13 shows that the test object, light guide, coupling capacitor, and high-voltage transformer are placed in a metal cabinet that can be considered a Faraday cage [42]. By performing the test inside the cabinet with the door closed, light pollution and electrical noise from the surroundings are minimized [17]. [1] The light guide was attached to the PMT and serves the purpose of directing the light emitted from the source toward the light detection device. In this case, the light guide directs the detected light emitted from the surface of the substrate to the PMT placed outside the cabinet. The light guide can be seen as the grey cord in Figure 13 .

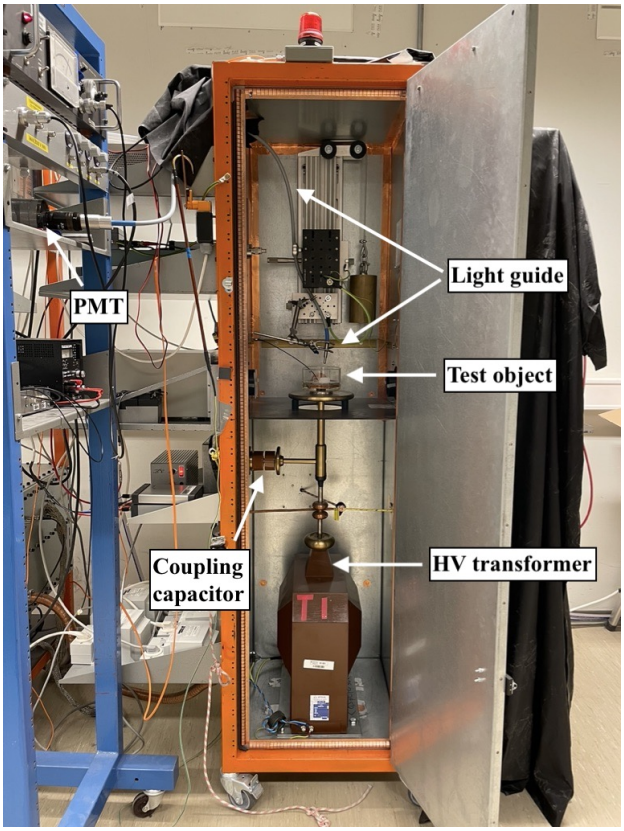

Figure 13: Overview of the sinusoidal voltage setup, with the light guide and test object.

[1] Taken directly from specialization project [3]

A schematic of the test circuit used for sinusoidal voltage measurements is presented in Figure 14. A Tektronix AFG3000 signal generator and a Cerwin-Vega! CXA-10 audio amplifier were used to feed the circuit. Parameters like the frequency and voltage could be manually adjusted using the signal generator or a Python code. To obtain resonance at a chosen frequency, a compensation inductor was connected in parallel to the output of the amplifier. Two transformers were used to obtain 50 kV_{peak}. An Arteche UCS-52 instrument transformer ($120/\sqrt{3} : 52000/\sqrt{3}, 325$ VA) was used to transform up the voltage and was connected to the amplifier output. To the instrument transformer, a Noratel SU120C isolating step-up transformer ($40 : 220, 300$ VA) was connected [42]. [1]

Electrical and optical PD measurements were received in the PD measuring system. The electrical PD measurements were provided by a measurement impedance and a coupling capacitance connected in parallel with the test object [17, 21, 37, 42]. [1] As mentioned, a PMT was used to obtain optical signals. In Figure 14, it is visible that the light guide was attached to the PMT and placed above the test object.

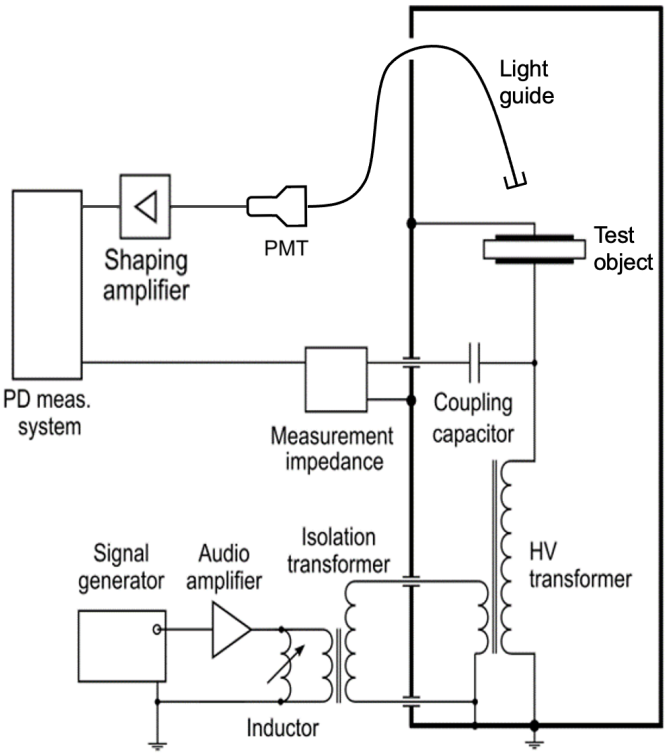

Figure 14: Schematic of the test circuit used for sinusoidal voltage measurements. The circuit presented is based on [21], but it has been subject to modifications.

The setup was connected to a primary ground to avoid the risk of ground loops [21]. Further explanation of the grounding and design of the AC resonant circuit used in the FastTrans project can be found in the project memo "*AC resonant voltage source for PD-measurements*" [42]. [1]

[1] Taken directly from specialization project [3]

3.3.2 Experimental setup: Square voltage

This experimental setup detects PD activity under square high-voltage. The experimental circuit and a test circuit schematic are presented in Figure 15 and 16, respectively. The experimental setup could only detect the PD activity optically. The optical measurement was provided with the use of a PMT for all measurements. Same as for the sinusoidal setup, the PMT was placed on the outside of the cabinet. The light guide was attached to the lens of the PMT and brought into the cabinet. The light guide can be seen as the grey wire in Figure 15. The lens of the light guide was placed above the test object with the same distance and angle as for the sinusoidal setup. The test object was placed on a small board/surface, providing an earth potential for the underside of the substrate. The high-voltage connection can be seen as the center point inside the gold circle and attached to the top side of the substrate with a black wire. As the PD activity only was detected optically, the demand for keeping the cabinet without light pollution was significant. This is especially important as the PMT is very sensitive to light. By performing the tests inside the cabinet, with the door closed, potential sources of error, such as light pollution, were reduced.

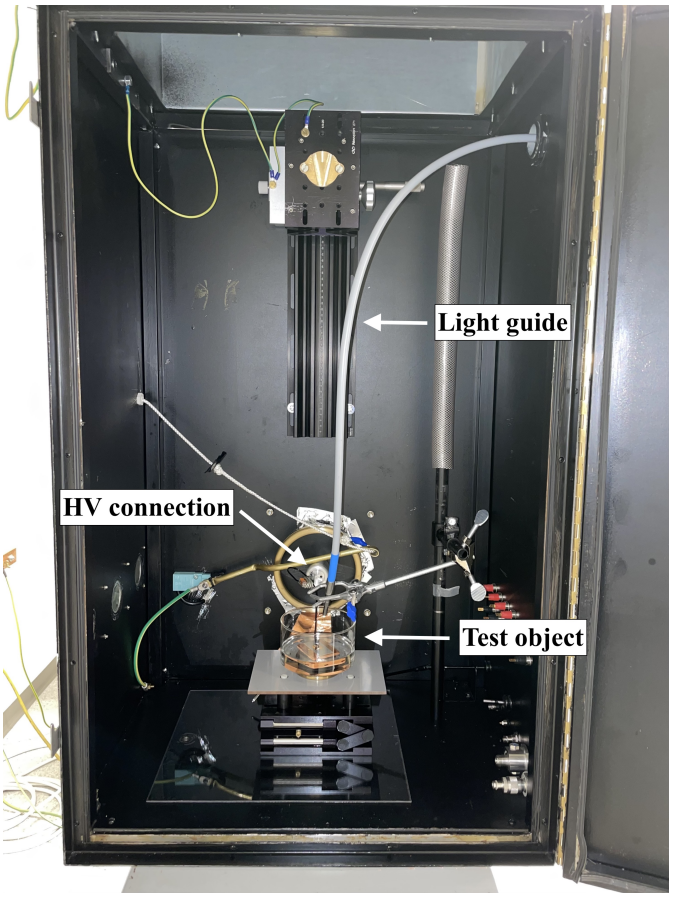

Figure 15: Overview of the square voltage setup, with the light guide and test object.

Figure 16 presents a test circuit schematic. The pulse source utilized a solid state switch to alternate between two different DC voltages. Thus, symmetrical or unsymmetrical square pulses are generated, switching between + HV and -HV with an absolute maximum permissible voltage difference of 65 kV [43]. A switch of the type Behlke HTS 651-03 GMS was used to generate the square voltage pulses. This solid-state switch is based on MOSFET technology [21, 43, 16]. The current output of the DC sources is limited to a maximum of 17 mA. To achieve this, six

capacitor banks of $C_B = 4.95\ nF$ were used to achieve a higher current, three arranged in parallel and two in series [43]. Charging resistors, R_C, in parallel, were used to charge the capacitor banks. Furthermore, the current was limited by the resistors, R_{lim}, R_H, and R_L. Based on the state of the switch, the resistors were either a series connection of R_H and R_{lim}, or R_L and R_{lim}. The resistors were split due to the thermal load [21, 43]. The values of the resistors were set to $R_{lim} = 1000\ \Omega$, $R_H = 1000\ \Omega$ and $R_L = 1000\ \Omega$. Consequently, regardless of the configuration, the total resistance, R_{tot}, of the circuit amounted to 2000 Ω [21]. In order to ensure stability in the applied voltage across the test object during the measurements, a voltmeter, V, was utilized. The PMT was connected to a shaping amplifier and connected to the PD measurement system, OMICRON MPD600 Fiber Optic MCU 502.

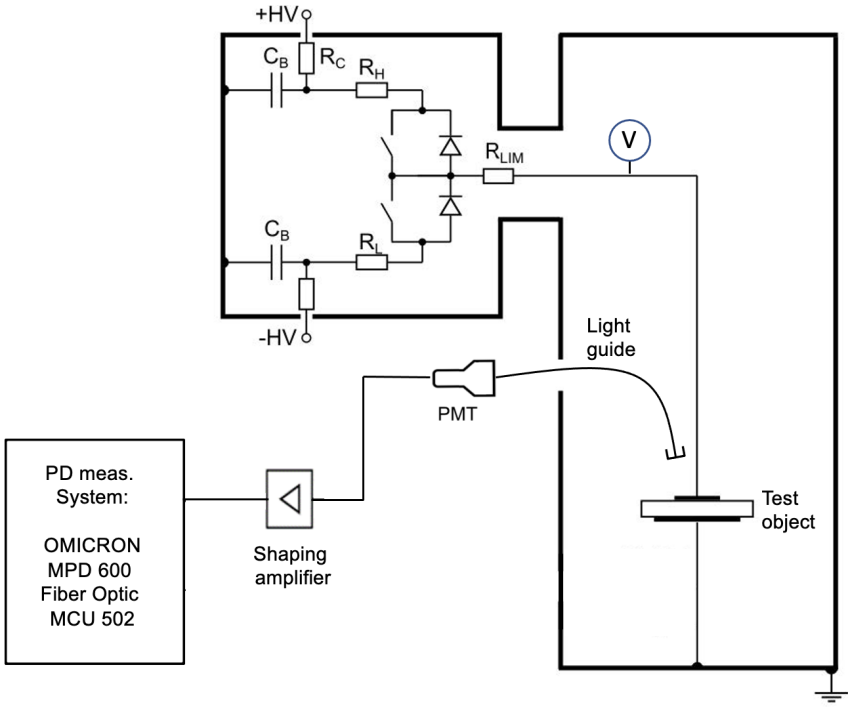

Figure 16: Schematic of the test circuit used for square voltage measurements. The circuit presented is based on [21], but it has been subject to modifications.

The master's thesis written by Folkestad, [21], used the same circuit as presented in this thesis, only with some minor changes in the PD measurement system. The results from Folkestad's thesis indicate that it was a minimal/absent difference with the different rise times of the source. Thus, only one rise time was used during the work of this thesis. The rise time of the voltage was set to 400 nanoseconds. Nevertheless, as the rise time is dependent on the applied voltage, the rise time was approximately 400 nanoseconds for all the measurements.

3.3.3 Experimental setup: Light guide placement during ramping of Sinusoidal and Square voltage

The optical measurements for both the sinusoidal and square setups were conducted the same way. For both setups, the PMT was placed outside with a light guide brought into the cabinet. This can be seen in Figure 17, showing the close up of the test object and light guide. The light guide was secured with a retort clamp, preventing movement of the light guide both prior to and

during measurements. In such a way, the light guide had the same distance and angle between the light guide and the test object throughout all measurements. The distance between the surface of the substrate and the lens was approximately 6.5 cm. Another reason for placing the PMT outside the cabinet was the limited space inside the cabinet. This decision was motivated by the desire to implement a high-speed camera for selected measurements, as the cabinet could not fit both the PMT and high-speed camera.

It should be noted that the sinusoidal voltage setup had earth potential on the top of the surface, while the square voltage setup had earth potential on the bottom of the substrate. Thus, the black wire in Figure 17a was earthed, while the black wire in Figure 17b was connected to the high-voltage side.

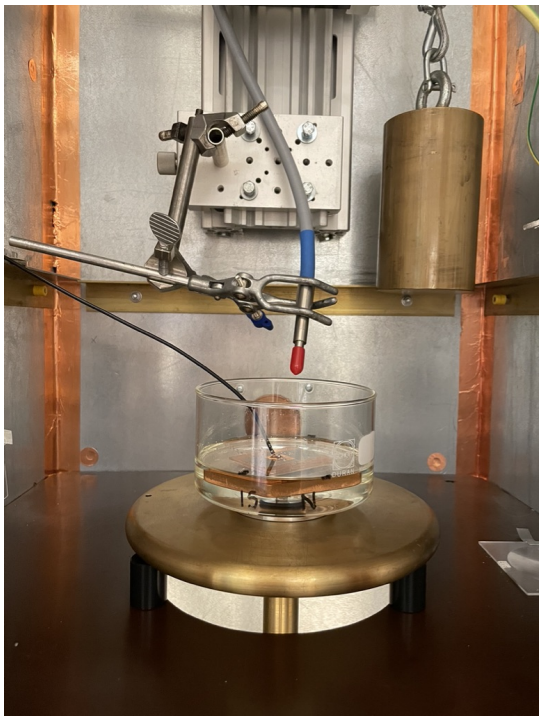

(a) Close up of the sinusoidal voltage setup, with the light guide and test object.

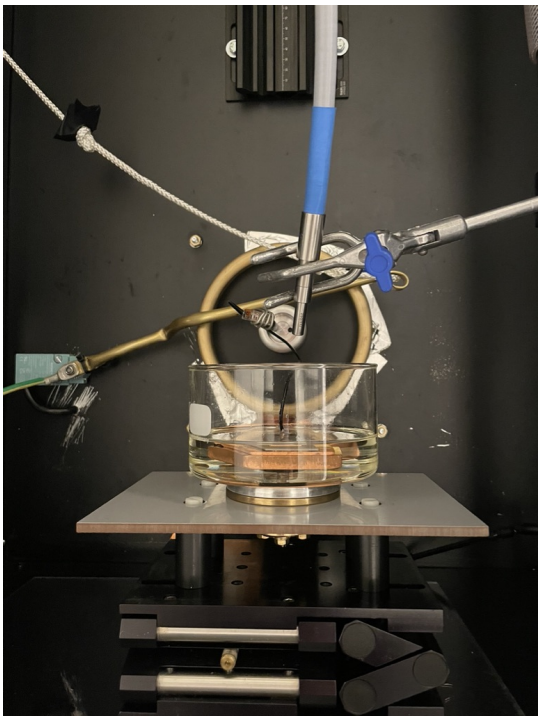

(b) Close up of the square voltage setup, with the light guide and test object.

Figure 17: Close up of the sinusoidal and square experimental setup, with the light guide and test object. When the light guide was not in use, the lens of the light guide was covered with a red hood.

3.3.4 Experimental setup: Square voltage with the high-speed camera

The measurements carried out using the high-speed camera were performed at constant square voltage levels. The optical measurements were obtained using the PMT as the primary detector. The high-speed camera was incorporated as a complementary instrument to provide additional information on the PD and space charge phenomena. Figure 18 illustrates the high-speed camera setup. Figure 18a presents an overview of the setup, while Figure 18b presents a close-up of the test object and light guide. The distance and angle between the light guide and substrate were maintained unchanged, despite including the high-speed camera in the experimental setup. The high-speed camera was placed directly above the test object, with the distance between the top of the surface of the substrate to the lens being approximately 21 cm.

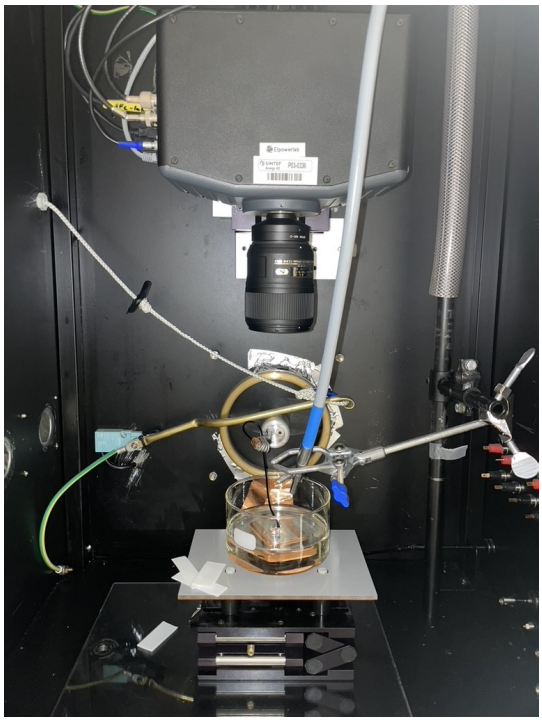

(a) Overview of the setup, with the high-speed camera, light guide, and test object.

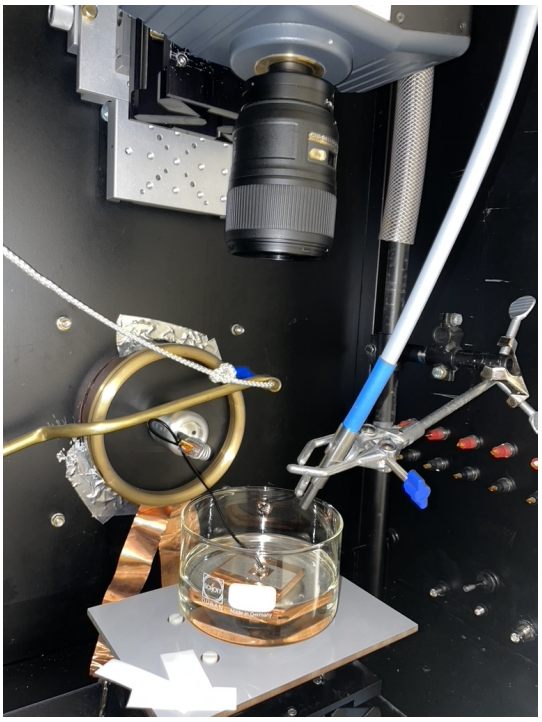

(b) Close up of the setup, with the high-speed camera lens, light guide, and test object.

Figure 18: Square voltage setup of light guide, high-speed camera, and test object.

3.3.5 Experimental setup: Square voltage with varying duty cycle

To better understand the potential effects of various parameters on the formation of PD activity and space charges, some test series were performed with varying duty cycles. The PMT was relocated inside the cabinet, as shown in Figure 19. This relocation afforded greater sensitivity for the optical measurements, as the larger PMT lens covered the test object. Figure 19a shows an overview of the setup with the PMT placed inside the cabinet, while Figure 19b provides a close-up view of the setup, with the PMT placed approximately 6.5 cm from the test object. The substrate was grounded and connected to the high-voltage side in the same manner as in the earlier square voltage setups.

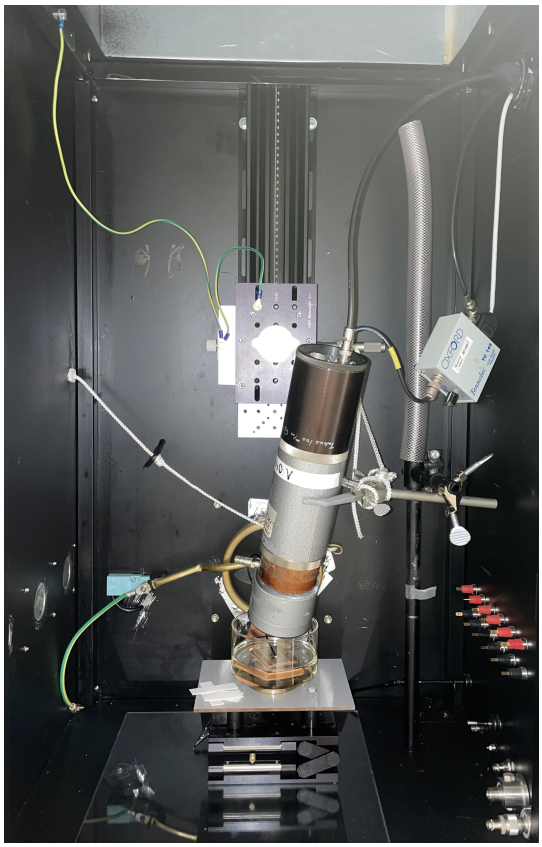

(a) Overview of the setup, with the PMT placed inside the cabinet above the test object.

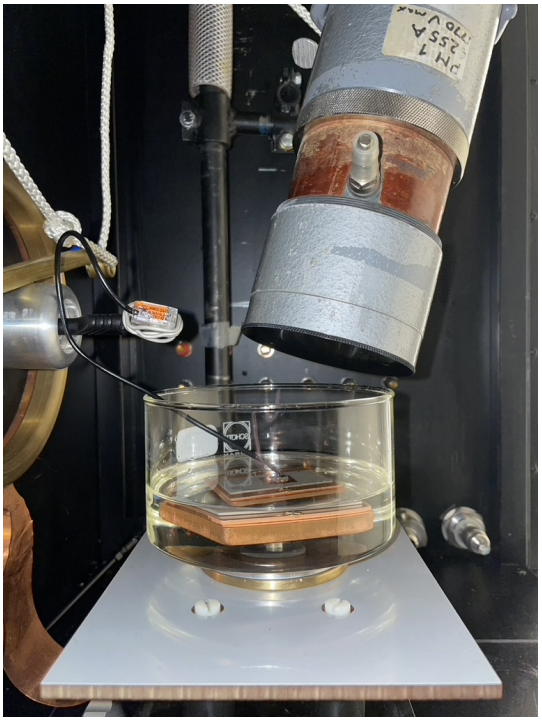

(b) Close up of the setup, with the PMT placed inside the cabinet above the test object.

Figure 19: Square voltage setup of PMT inside the cabinet and test object.

3.4 Preparation of test object before measurements

This section describes the preparation of the test objects conducted before the measurements. One part of the objective of this thesis was to see how two different dielectric liquids, Silicone oil and Nytro 10XN, would affect PD formation. As the dielectric liquids used were different and it was of interest to compare the liquids, it was essential to prepare the test objects as similarly as possible. Thus, the cleaning procedure of the substrates used in the different liquids was conducted the same way. However, the filling process of the two liquids varied due to the unavailability of the needed equipment. For both liquids, the test object was positioned in a sample holder and encapsulated by the liquid being analyzed.

The test object and sample holder were cleaned before performing measurements. They were cleaned with isopropyl alcohol, also known as isopropanol, to eliminate old oil, dust, and other unwanted particles. With special cleaning wipes, unwanted particles from the wipes were partially prevented. After the cleaning process, the test object and sample holder were degassed for approximately three minutes. The test object was placed in a sample holder and fastened with screws. The screws attached the substrate to the electrode on the bottom of the sample holder and were used to prevent the movement of the test object before and during the measurements. The two sample holders used had the same outer diameter of 115 mm and a height of 65 mm.[1]

[1]Taken directly from specialization project [3]

Two different sample holders were used to avoid any potential mixing between the dielectric liquids.

3.4.1 Silicone oil

The filling process for Silicone oil was done using a desiccator and vacuum pump. When the substrate was attached to the sample holder, the sample holder was placed inside the desiccator. Figure 20 shows the desiccator used to fill Silicone oil. The desiccator was used to prevent moisture from the atmosphere from penetrating the Silicone oil. A pipe connected to a vacuum pump was attached to one of the outlets of the desiccator while the remaining outlets were sealed. Before starting the filling process, the vacuum compressor was on for about four minutes, effectively removing the atmospheric air in the desiccator. When the vacuum was obtained inside the desiccator, the filling process of the Silicone oil started by opening the corresponding outlet. With a glass filter with a pore size of ten micrometers, any unwanted particles were prevented. The glass filter can be seen between the black strips at the top of Figure 20.

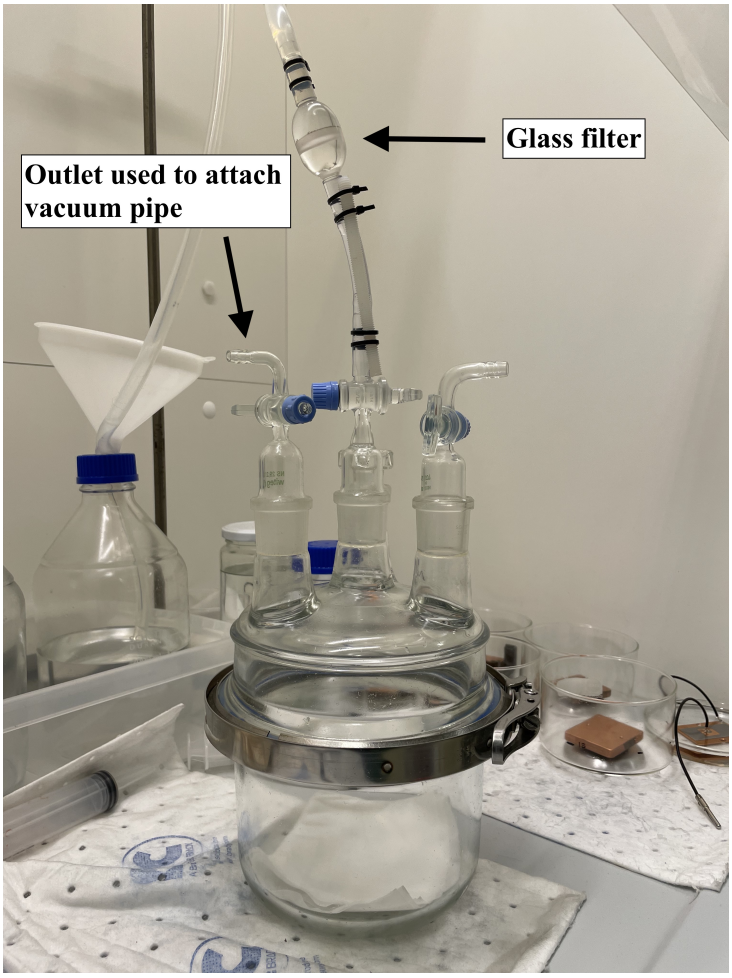

Figure 20: The desiccator was situated inside a fume hood, where a vacuum was created inside during the oil drainage process over the test object.

To provide an identical test setup as possible for each PD measurement, the distance between the top of the substrate and the surface of the oil was approximately 5 mm. Any variations here are expected to be minimal, measuring in millimeters. The filling of Silicone oil took approximately

15 minutes. The vacuum pump was on for additional ten minutes to remove air bubbles in the Silicone oil. Afterward, the Silicon oil was visually inspected to check for unwanted particles and air bubbles. If unwanted particles were observed, a syringe was used to remove the particles. [1] The Silicone oil used during the experimental measurements was of the type Wacker Silicone oil AK 10. Based on the book [44], the relative permittivity is defined to $[2.5 - 2.6]$ and the volume resistivity of Silicone oil $> 1 \cdot 10^{14}$ Ω cm.

3.4.2 Nytro 10XN

The filling process for Nytro 10XN was done by hand and not with a desiccator and pumping function as was done for Silicone oil. An effort was made to maintain a consistent repetition speed during the filling process across the substrate to ensure a relatively similar quantity of air in the oil. A desiccator was used to remove unwanted air bubbles present in the liquid. The sample holder was placed inside a desiccator, and a vacuum pump was attached to one of the desiccator outlets. Figure 21 shows the desiccator used for Nytro 10XN. After the vacuum pump had obtained vacuum inside the desiccator, the vacuum pump was on for approximately one hour to remove the air from the oil. The presence of air bubbles can be seen as a white film in Figure 21.

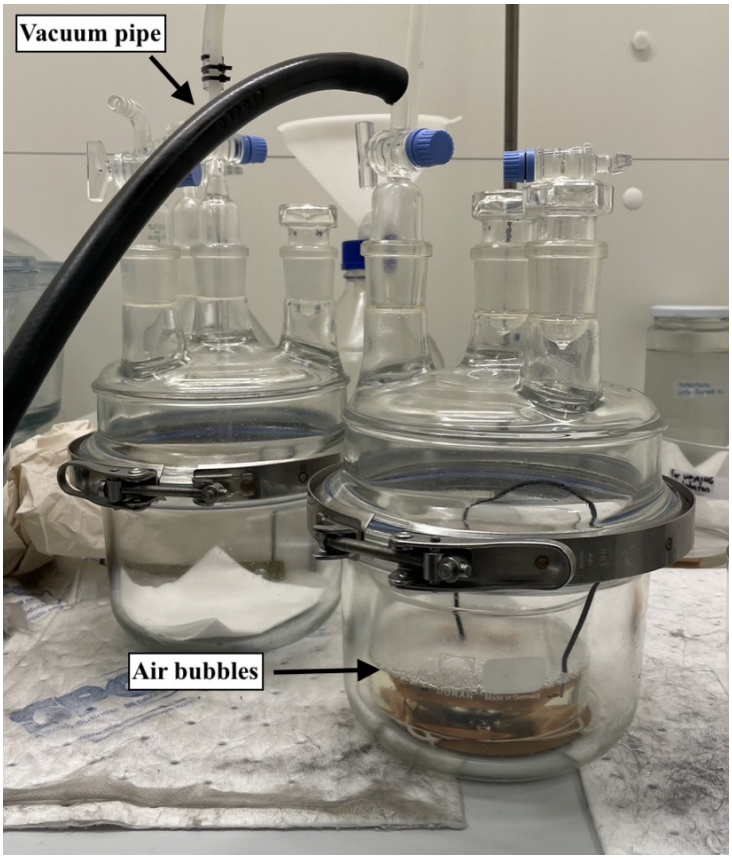

Figure 21: The desiccator was situated inside a fume hood, where a vacuum was created inside and removed the air bubbles in the Nytro 10XN.

[1] Taken directly from specialization project [3]

After vacuuming, the same visual inspection described for Silicone oil was conducted for Nytro 10XN. The experimental measurements were conducted utilizing Nytro 10XN, a mineral oil. Nytro 10XN has a conductivity value of 0.6 $\frac{pS}{m}$ and a relative permittivity of 2.17 [45].

3.5 Measurement procedures

Different measurement procedures were conducted for the various experimental setups. The following subsections present the different measuring procedures used. All measurements were performed with all lights turned off to reduce light pollution from the environment during the measurements. Additionally, a black cover was placed over the cabinet to prevent light from the outside from affecting the measurements.

3.5.1 Measurement procedure: Sinusoidal, bipolar, negative, and positive unipolar voltage

Sinusoidal voltage

The test objects were exposed to AC voltage at 30 Hz. The start voltage was set to 0.02 kV_{peak}, i.e., approximately 0 V. Ramping of the voltage was done in increments of 500 V_{peak} without any time delay, with a time step duration at each voltage level of 60 seconds. The maximum voltage level was set to 16 kV_{peak}, and was held for 60 seconds before proceeding with decrements of 500 V_{peak}. Same as for the increments, each voltage level for the decrements was held for 60 seconds. A Python code was used to control the signal generator.[1] The test was over when the start voltage was reached and held for 60 seconds. The maximum voltage was set based on initial tests, which indicated a probability of over 100 % for PD occurrence in each half-voltage period at 16 kV_{peak}, additionally without indicating the risk of breakdown.

Figure 22 is a screenshot from the OMICRON software and shows an overview of the measuring procedure of the ramping up and down the voltage for the sinusoidal measurement. The red graph presents the voltage signal, and the green graph presents the PD activity. Along the x-axis is the time duration of the test. The y-axis to the left shows the voltage level value in RMS-value, while the left y-axis presents the discharge magnitude. It should be noted that the red graph shows some indication of voltage drops during the test in Figure 22. However, when converting the values in Matlab and analyzing the voltage data, one can not see the voltage drops. Thus, the voltage drops in the red graph in Figure 22 are not real.

Five measurements, i.e., five substrates, were conducted with Silicone oil, and five measurements, i.e., five substrates, were conducted with Nytro 10XN.

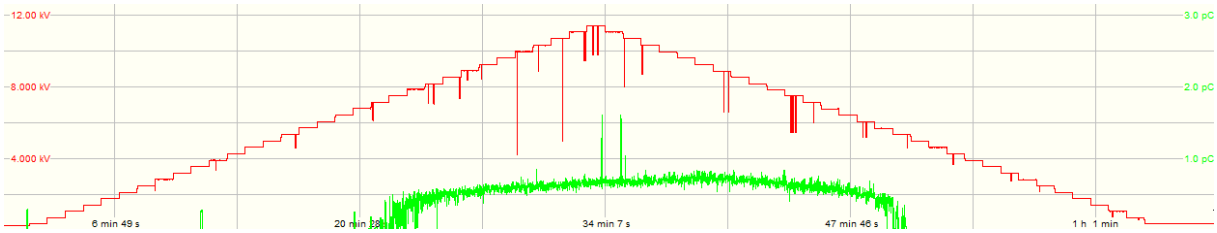

Figure 22: An overview of the measurement procedure of the ramping up and down of the voltage. Screenshot from OMICRON software [3].

[1] Taken directly from specialization project [3]

Bipolar voltage

A program in LabView was utilized to control the switch in the square voltage setup. The voltage was ramped up and down in the bipolar measurements, similarly to how it was done for the sinusoidal measurement. Ramping of the voltage was done in increments of 500 V_{peak} without any time delay, with a time step duration at each voltage level of 60 seconds. The maximum voltage, presented in the following section, was held for 60 seconds before proceeding on decrements of 500 V_{peak}. The test was over when the start voltage was reached and held for 60 seconds.

The test objects were exposed to bipolar voltage pulses at 30 Hz, with a duty cycle of 50 % and without an offset, i.e., reference at 0 V. Due to limitations in the program, the lowest possible value was 1 kV_{peak}. This was therefore used as the start voltage. The square voltage setup could reach a maximum of 20 kV_{peak}, i.e., a peak-to-peak value of 40 $kV_{peak-to-peak}$. However, none of the measurements conducted reached that voltage level for the bipolar tests. Initial measurements indicated a significant variation in PD activity at different voltage levels. Thus, unlike the sinusoidal tests, a single maximum voltage was not selected for all of the tests with bipolar. Therefore, during each test, an individual maximum voltage was set. The maximum voltage varied in the $[7-12.5]$ kV_{peak} range. This maximum voltage was chosen based on the PD activity present and set at a level that would result in a discharge in each half-voltage period, corresponding to a PD probability of 100 % in each half-period.

Five measurements, i.e., five substrates, were conducted with Silicone oil, and five measurements, i.e., five substrates, were conducted with Nytro 10XN.

Positive and negative unipolar voltage

The same LabView program used for the bipolar was also used for the positive and negative unipolar setup. The measurements were conducted by ramping up and down the voltage. The ramping of the voltage was done in increments of 1 $kV_{peak-to-peak}$ without any time delay, with a time step duration at each voltage level of 60 seconds. The test objects were exposed to positive and negative unipolar voltage pulses at 30 Hz, with a duty cycle of 50 % and without an offset, corresponding to a reference at 0 V.

The results presented in Folkestad's thesis, [21], reveal that negative unipolar voltage pulses have lower PDIV than positive unipolar voltage pulses in Silicone oil. Consequently, tests with negative unipolar for both liquids were conducted before proceeding to positive unipolar. Given that almost no PD activity above the noise level in OMICRON was detected for Silicone oil with negative unipolar, the tests for Silicone oil with positive unipolar were considered unnecessary and not further tested. However, positive and negative unipolar testing was conducted on Nytro 10XN due to detected PD activity in both polarities.

The start voltage for the Silicone oil was set at $U_{start} = 5$ $kV_{peak-to-peak}$, as the PD activity observed during the ramping was very little. The maximum voltage was set to $U_{max} = 20$ $kV_{peak-to-peak}$, representing the highest possible value for the experimental setup. Conversely, in the case of Nytro 10XN, due to the higher level of PD activity, a lower start voltage of $U_{start} = 1$ $kV_{peak-to-peak}$ was used, as the start value of 5 $kV_{peak-to-peak}$ was found to interfere with the test. The maximum voltage was set at $U_{max} = 20$ $kV_{peak-to-peak}$ for the measurements. However, during two negative unipolar tests, the maximum voltage had to be reduced due to the high level of PD activity, resulting in the risk of flashover. An overview of the start and maximum voltage for positive and negative unipolar in Silicone oil and Nytro 10XN are presented in Table 1.

Five measurements, i.e., five substrates, were used for negative unipolar voltage in Silicone oil. Five measurements, i.e., five substrates, were used for negative unipolar voltage and five substrates for positive unipolar voltage in Nytro 10XN.

Table 1: Overview of the start and maximum voltages for measurements conducted with positive and negative unipolar for Silicone oil and Nytro 10XN.

	Positive unipolar	Negative unipolar
Silicone oil	No measurements were conducted	$U_{start} = 5\ kV_{peak-to-peak}$ $U_{max} = 20\ kV_{peak-to-peak}$
Nytro 10XN	$U_{start} = 1\ kV_{peak-to-peak}$ $U_{max} = 20\ kV_{peak-to-peak}$	$U_{start} = 1\ kV_{peak-to-peak}$ $U_{max} =$ $[18.5 - 20]\ kV_{peak-to-peak}$

3.5.2 Measurement procedure: High-speed camera

The high-speed camera was used in the square voltage setup and tested on bipolar voltage pulses for Silicone oil and Nytro 10XN. However, the measuring procedure with the implementation of the high-speed camera was performed differently compared with the ramping of the bipolar voltage. The program LabView was used in the measuring procedure with the implemented high-speed camera. The voltage in the following section is referred to in peak value.

The measurement started at 7 kV_{peak}, increasing with increments of 1 kV_{peak} without any time delay, and with a time step duration of approximately two minutes at each voltage level, up to the maximum 11 kV_{peak}. The time interval between the voltage levels was chosen in order to allow sufficient time for capturing and saving the pictures. The first series of pictures was taken at 8 kV_{peak}, as the start voltage at 7 kV_{peak} was only used to stabilize the PD activity. The high-speed camera was set to 60 Hz for the majority of the picture intervals. After the picture interval with a high-speed camera frequency 60 Hz was taken at a voltage level of 11 kV_{peak}, the high-speed camera frequency was changed to 480 Hz. The reason for the frequency change was explained in Section 3.2.3. The time duration between the two picture sequence intervals at 11 kV_{peak} was approximately two minutes due to time delays regarding saving the pictures and changing the camera frequency. The measuring procedure with the high-speed camera is tried illustrated and explained in Figure 23. 1000 pictures were taken during each interval. The measuring procedure was conducted on one test object in Silicone oil and one in Nytro 10XN.

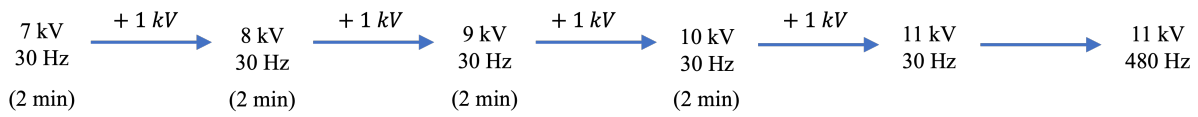

Figure 23: Overview of the measuring procedure with the high-speed camera, with time duration between the sequences. Each picture interval took 1000 pictures. The voltage level is defined in peak value. The illustration was inspired by the specialization project [3].

Figure 24, a screenshot from OMICRON Software, illustrates the measuring procedure for Nytro 10XN. The figure shows that the picture interval was taken directly after the voltage was ramped

up to the desired voltage level. The same measuring procedure was conducted for Silicone oil. The red signal presents the voltage, while the green signal corresponds to the duration of the on-time of the high-speed camera, i.e., the time at which the pictures were captured. The four green "bars" to the left are with a camera frequency of 60 Hz, while the green "bar" to the right is with a camera frequency of 480 Hz. The x-axis represents the time duration of the measurement, and the y-axis presents the voltage level in peak value.

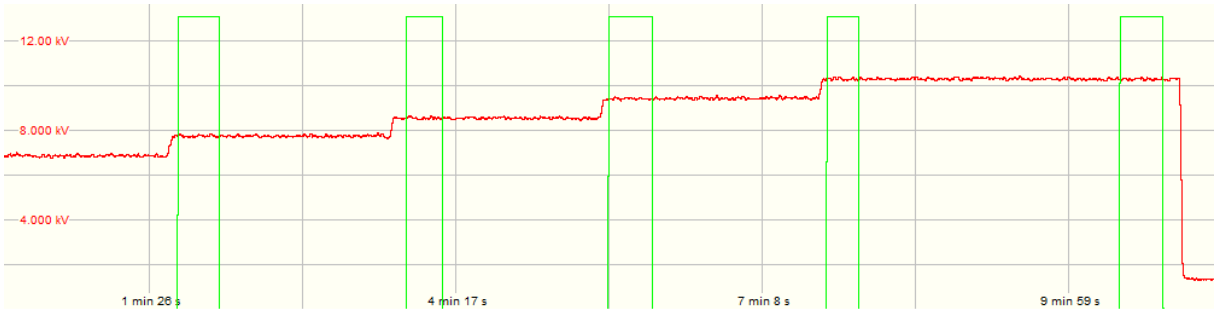

Figure 24: Overview of the measuring procedure conducted with Nytro 10XN. Screenshot from OMICRON software.

3.5.3 Measurement procedure: Duty cycle

It was also of interest to examine if the change in the duty cycle would impact PD activity. The measurement involved exposing the test object to different duty cycles and voltage levels for both liquids, Silicone oil and Nytro 10XN, under negative unipolar voltage at a frequency of 30 Hz. Initial tests were conducted to identify an optimal measuring procedure to minimize the possibility of one measurement impacting the subsequent measurement. The tests involved varying the voltage levels and time duration at each voltage level, additionally changing the time duration between the tests to identify the most suitable measuring procedure. As a result, the following measuring procedure was chosen. Measurements were conducted by starting at 2 $kV_{peak-to-peak}$ and gradually increasing the voltage in 2 $kV_{peak-to-peak}$ increments without any time delay, up to 8 $kV_{peak-to-peak}$, with a duration of 30 seconds at each voltage level. The duty cycle was changed in the following sequence: 50 % − 50 % − 20 % − 5 % − 80 % − 95 % − 50 %. Between changing the duty cycle, the voltage was turned off, and no voltage was applied over the test object for 15 minutes before proceeding to the next measurement with the changed duty cycle.

Two measurements of 50 % (numbers 1 and 2) were conducted at the start of the test to assess the condition of the liquid and detect the presence of any unwanted particles that could potentially affect the PD activity. Additionally, the identical duty cycle tests were conducted to see how the 15 minutes without voltage would affect the PD activity in the subsequent measurement. The duty cycle was then reduced to 20 % and 5 % before increasing it to 80 % and 95 %. The following order was chosen to prevent the presence of PD and potential space charges. An increase in the duty cycle would lead to greater voltage stress over the test object, potentially resulting in increased PD activity. Thus, the duty cycles 20 % and 5% were conducted prior to 80 % and 95 %. The test ended with a duty cycle of 50 % (number 3) to determine if the test object had experienced permanent damage throughout the test. By comparing PD activity during 50 % (number 3) with the PD activity in 50 % (numbers 1 and 2), it could be possible to identify permanent changes in the test object, changes in the liquid properties, or other factors.

Within the context of this thesis, the flanks of a negative unipolar voltage pulse are defined

using the voltage values of low and high. Specifically, the flank that transitions from a low to a high voltage value is defined as the voltage turn-on, while the flank that transitions from a high to a low voltage value is defined as the voltage turn-off. The principle is illustrated in Figure 25.

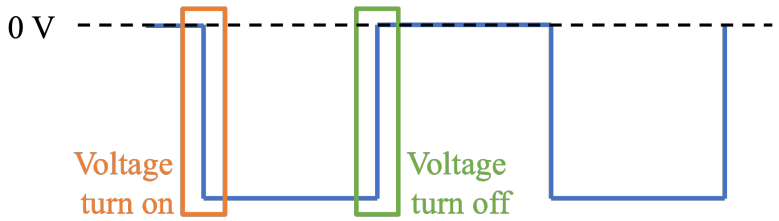

Figure 25: Definition of voltage turn-on and turn-off for negative unipolar voltage pulses.

3.6 Post-processing of data

The majority of the post-processing of data was conducted in Excel and Matlab. Additionally, the analysis of the pictures was done with the use of the software Fiji ImageJ-win64.

The pictures captured by the high-speed camera were analyzed using Fiji ImageJ-win64 software and a custom code provided by SINTEF. The software is pixel-based, and the light emission was detected by analyzing the intensity of the individual pixels in each picture. The code detected the presence of discharges by identifying light emissions crossing the edges of the copper contact electrode. If light emission was detected crossing the predetermined boundary of the electrode frame, it was identified as a PD. Although the code was a recent development, it did not function fully as intended, failing to detect some pictures containing PD formation along the electrode. Consequently, a manual review of all pictures was necessary to ensure the identification of all PDs, as the automated process was not entirely accurate.

The signal generator and high-speed camera were not triggered due to time delays in the system, resulting in a lack of automatic identification of the PD and its corresponding picture. As a result, the PD and corresponding picture had to be found manually. Furthermore, due to the dark currents in the PMT, it was challenging to manually post-process the data. As a result, it was not possible to find the PD and its corresponding picture. Therefore, it was not possible to determine the polarity of the voltage in the specific pictures.

4 Results

This section presents the findings of the experimental measurements conducted in Section 3. The section begins with the results obtained from the PDIV and PDEV measurements in the sinusoidal voltage setup. Subsequently, the obtained results from the square voltage setup are presented, including the PDIV results and the results from the high-speed camera. The section ends with the findings obtained from the duty cycle variations.

4.1 Sinusoidal voltage setup: PD measurements

4.1.1 PDIV and PDEV measurements

The PDIV and PDEV values for both Silicone oil and Nytro 10XN in the sinusoidal voltage setup are presented in Table 2. As mentioned in Section 3.5.1, five substrates were tested in Silicone oil and five in Nytro 10XN. Each table column contains the five measurement values obtained from the five substrates in each liquid. The corresponding average voltage and its 95 % confidence interval, based on the five measurement values, are presented at the bottom of the table. The peak-value voltages, kV_{peak}, were determined by identifying continuous PD activity from the electrical measurements with a threshold of 500 fC.

Table 2: PDIV and PDEV for Silicone oil and Nytro 10XN in sinusoidal voltage setup, in kV_{peak}. The average voltage and 95 % confidence interval are presented at the bottom of the table for the corresponding values. The voltage values are based on electrical measurements with a threshold of 500 fC.

Silicone oil		Nytro 10XN	
PDIV [kV]	PDEV [kV]	PDIV [kV]	PDEV [kV]
13.5	11.0	12.0	10.5
11.5	10.5	16.0	0.0
15.5	15.5	16.0	13.0
10.5	7.5	14.5	10.0
14.5	14.0	16.0	16.0
13.1 ± 1.6	11.7 ± 2.5	14.9 ± 1.4	9.9 ± 4.7

Inspection of the PDIV and PDEV from the electrical measurements was determined by visual inspection. The PD probability at that specific voltage level could be found by determining the number of PD activities detected during one minute at the PDIV level. As the PD probability is defined based on the probability of getting a PD in each half-period with a system frequency of 30 Hz, a 100 % probability corresponds to 3600 PDs in the detected one minute. Thus, the average PD appearances were found to be 5.38 % for electrical measurement in Silicone oil and 3.02 % for electrical measurement in Nytro 10XN at their corresponding PDIV level.

4.2 Square voltage setup: PD measurements

4.2.1 PDIV for bipolar, positive, and negative unipolar voltage

The experiments aimed to study the impact of various voltage pulses and polarities on the PD activity exhibited in the substrates and to compare the behavior of the two liquids. Figure 26 displays the average curves for the probability of PD for bipolar voltage pulses in Silicone oil and Nytro 10NX. The x-axis represents the peak-to-peak voltage in $kV_{peak-to-peak}$, while the y-axis represents the probability of PD in %. The 95 % confidence interval is shown for all voltage levels, highlighting the variations of the PD probability for the five substrates. The results are based on a threshold set to 500 pC.

It should be noted that the red average curve for the bipolar voltage pulse in Silicone oil pertains to only four substrates, as one substrate was excluded due to its abnormal behavior. The presence of unwanted particles or poorly manufactured substrates may have contributed to this unusual behavior.

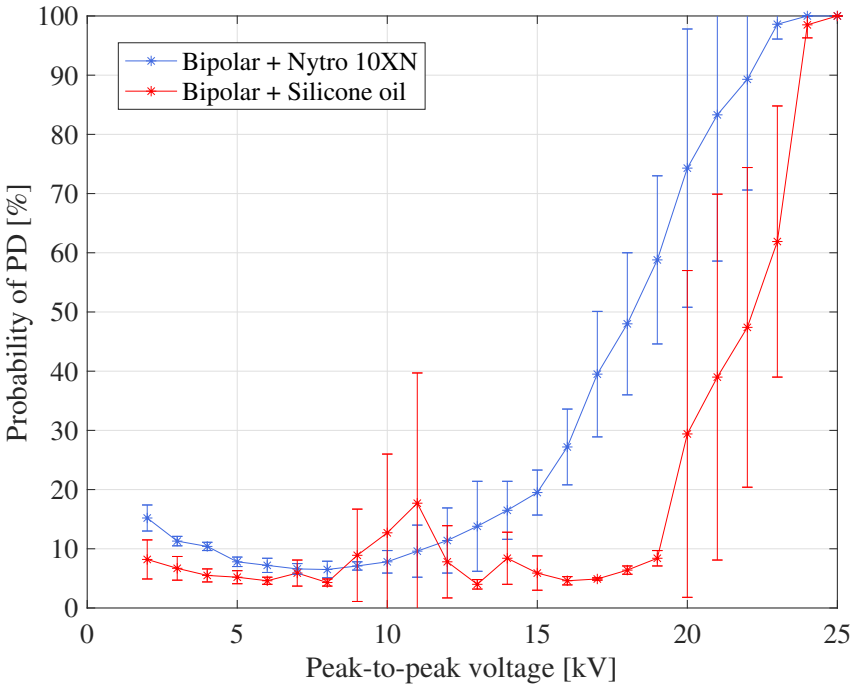

Figure 26: Average probability PD curves of bipolar voltage pulses for Silicone oil and Nytro 10XN, along with the corresponding 95 % confidence intervals at each voltage level expressed in peak-to-peak value. The threshold was set to 500 pC.

Figure 27 represents the average probability curves for the occurrence of PD in bipolar, negative unipolar, and positive unipolar voltage pulses for both Silicone oil and Nytro 10XN. The y-axis of the graph represents the probability of PD %, whereas the voltage axis is expressed in peak-to-peak value $kV_{peak-to-peak}$. The results were obtained using a 500 pC threshold.

It should be mentioned that the black curve, representing negative unipolar voltage pulses in Nytro 10XN, is based on only four substrates due to the exclusion of one substrate exhibiting abnormal behavior. The same applies to the red curve for bipolar voltage pulses in Silicone oil, as previously mentioned. Furthermore, it is relevant to note that Figure 27 does not include

any measurements for positive unipolar voltage pulses in Silicone oil due to the detection of negligible activity beyond the noise level, as explained in Section 3.5.1.

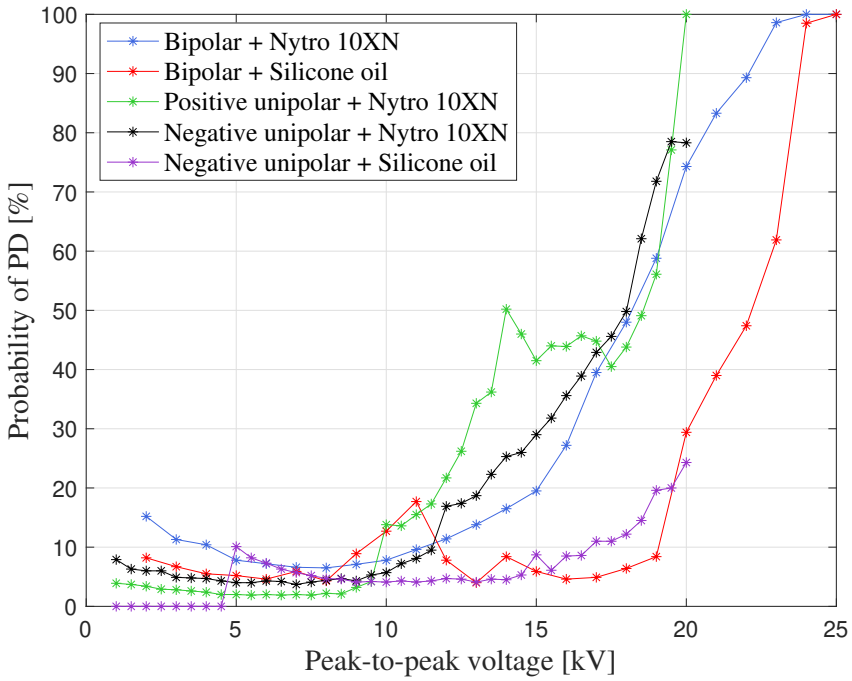

Figure 27: Average probability PD curves of bipolar, positive, and negative unipolar voltage pulses for Silicone oil and Nytro 10XN. The voltage level is expressed in peak-to-peak value. The threshold was set to 500 pC.

4.2.2 PD detection with high-speed camera

The high-speed camera was included to detect PD activity along the surface of the substrate. Additionally, it was included to identify whether PD activity occurred during the flanks or plateaus and to inspect the presence of space charges. The bipolar voltage level of 11 kV_{peak} was selected for further analysis due to its two distinct camera frequencies. An overview of the measurements conducted at bipolar voltage level of 11 kV_{peak} and which of them is further analyzed is provided below:

- Silicone oil with a camera frequency of 60 Hz: Presented.
- Silicone oil with a camera frequency of 480 Hz: Not presented.
  The findings of bipolar voltage at 11 kV_{peak} in Silicone oil with a camera frequency of 480 Hz are not included in this thesis, as the pictures showed minimal PD activity.
- Nytro 10XN with a camera frequency of 60 Hz: Not presented.
  The findings of bipolar voltage at 11 kV_{peak} in Nytro 10XN with a camera frequency of 60 Hz are not included in this thesis due to an extreme occurrence of PD activity. Specifically, the pictures revealed PD activity in all four corners and along the sides of the substrate edge in all 1000 pictures.
- Nytro 10XN with a camera frequency of 480 Hz: Presented.

The light emissions displayed a significant variation in intensity. The comparison of the light intensity was not considered during this thesis, as this had to be done manually. The detection of light intensity will not be exact as the human eye is unable to, with absolute precision, detect and compare light intensity. An example of the light intensity variations of the PDs can be seen in Appendix A. The pictures in Appendix A present more noticeable differences in the light intensity, making the variations clear. However, detecting differences in light intensity with similar light emissions proved to be more challenging.

Bipolar voltage at 11 kV_{peak} **in Silicone oil with a camera frequency of** 60 **Hz:**

Figure 28 reveals the PD activity on the surface of the substrate, i.e., the PD activity on the electrode edge, for bipolar voltage pulses, 11 kV_{peak}, with Silicone oil and a camera frequency of 60 Hz. The electrode edge is marked in green. The white dot in the figure represents the location where PD activity occurred on the edge of the substrate. Additionally, the numbers beside the white dot are used to identify the specific picture number that contains PD activity in that location. As mentioned in Section 3.2.3, a camera frequency of 60 Hz captures two pictures each voltage period, i.e., every other picture has the opposite voltage polarity. The camera was set to take 1000 pictures for all of the tests, and the picture series is defined by picture number $[0 - 999]$.

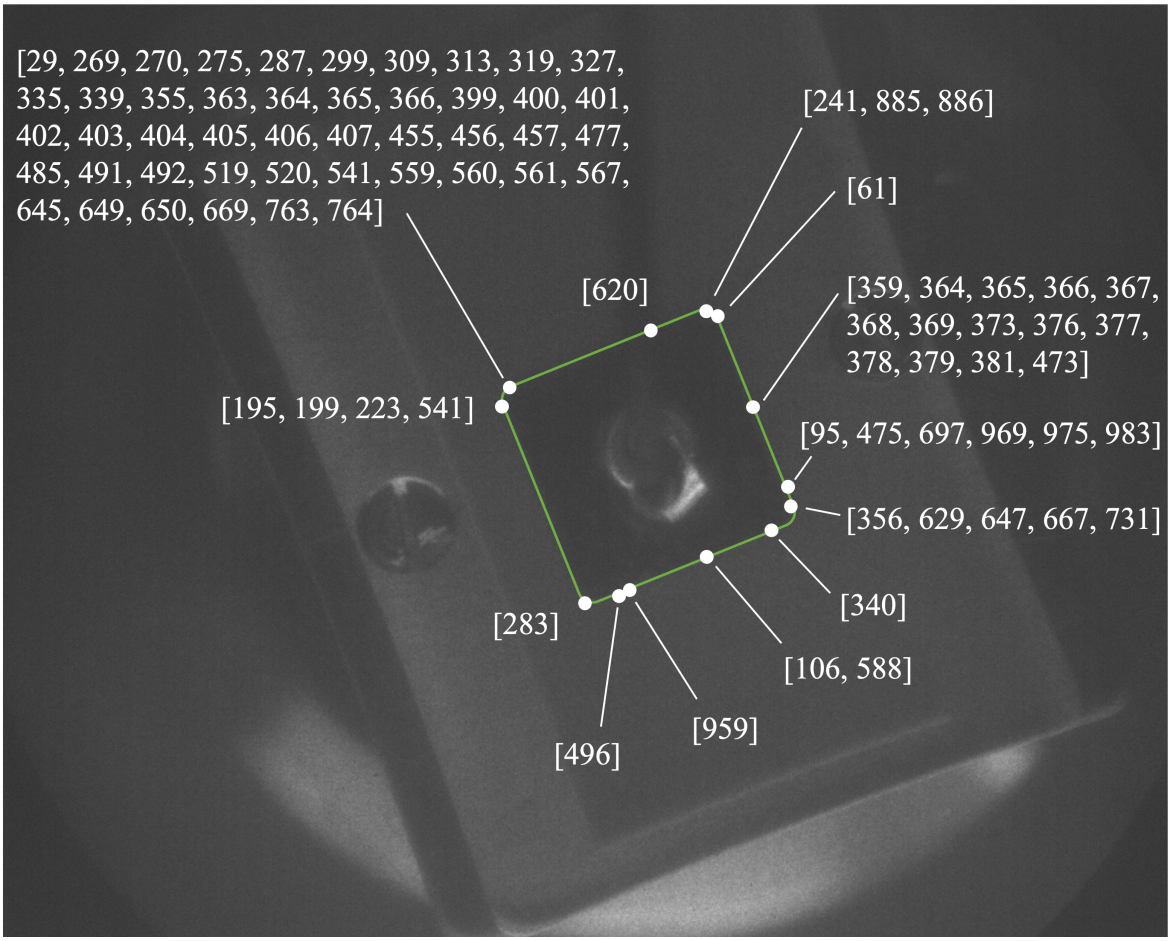

Figure 28: PD formation on the substrate surface with bipolar voltage at 11 kV_{peak} in Silicone oil with a camera frequency of 60 Hz. White dots indicate the location of the detected PD, and the corresponding picture numbers indicate which pictures the PD occurred in that specific location.

Figure 29 is a graphical representation of the findings presented in Figure 28. Figure 29 illustrates the probability of the occurrence of PD in the subsequent voltage periods if a prior PD has occurred in the same location. The left y-axis of the graph represents the number of PDs occurring in the n-half voltage periods, while the x-axis represents the number of half-voltage periods between the occurrences of PDs in the same location. As it is of interest to look at PD in subsequent voltage periods, the x-axis values are limited to the range of $[1-50]$, even though some values exceed 50. The values exceeding 50 are added with the values in the 50 bar. Thus, the 50 bar represents the combined values of 50 and > 50.

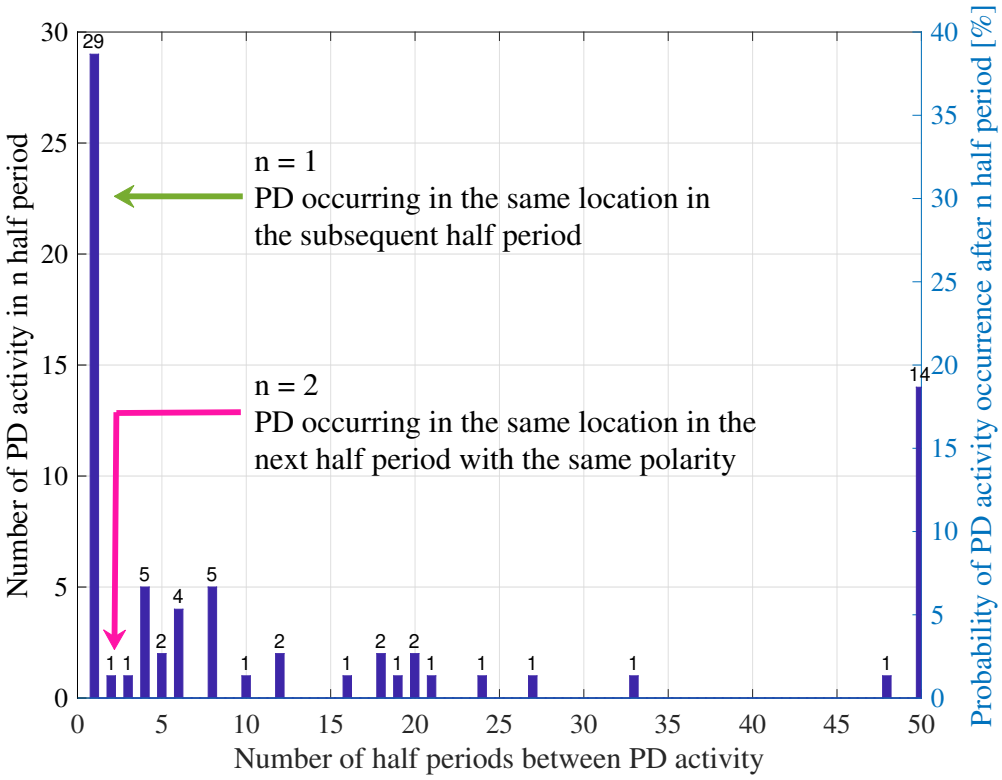

Figure 29: The probability of PD occurrence in the subsequent voltage periods given a prior occurrence of PD in the same location, for bipolar voltage at 11 kV_{peak} in Silicone oil with a camera frequency of 60 Hz.

For further explanation, given that a PD has occurred in one location, a PD occurs in the same location in the subsequent voltage period (subsequent opposite voltage polarity) 29 times.

Bipolar voltage at 11 kV_{peak} **in Nytro 10XN with a camera frequency of** 480 **Hz:**

Figure 30 illustrates the occurrence of PD on the surface of the substrate under bipolar voltage at 11 kV_{peak} in Nytro 10XN with at a camera frequency of 480 Hz. White dots indicate the location of the detected PD along the substrate edge, and the corresponding picture numbers indicate the frequency of occurrence of PDs. White picture numbers correspond to PDs detected during the voltage flanks, while yellow picture numbers indicate PDs occurring during the voltage plateaus. As stated in Section 3.2.3, a camera frequency of 480 Hz captures 16 pictures during each voltage period, i.e., eight pictures during a half-period.

It should be noted that the camera interval shifted at the end of the picture sequence, capturing only seven pictures instead of the standard eight during a single half-period. This shift only happened once, and the subsequent half-periods contain the complete set of eight pictures. The shift is marked in Figure 30 as a green "X".

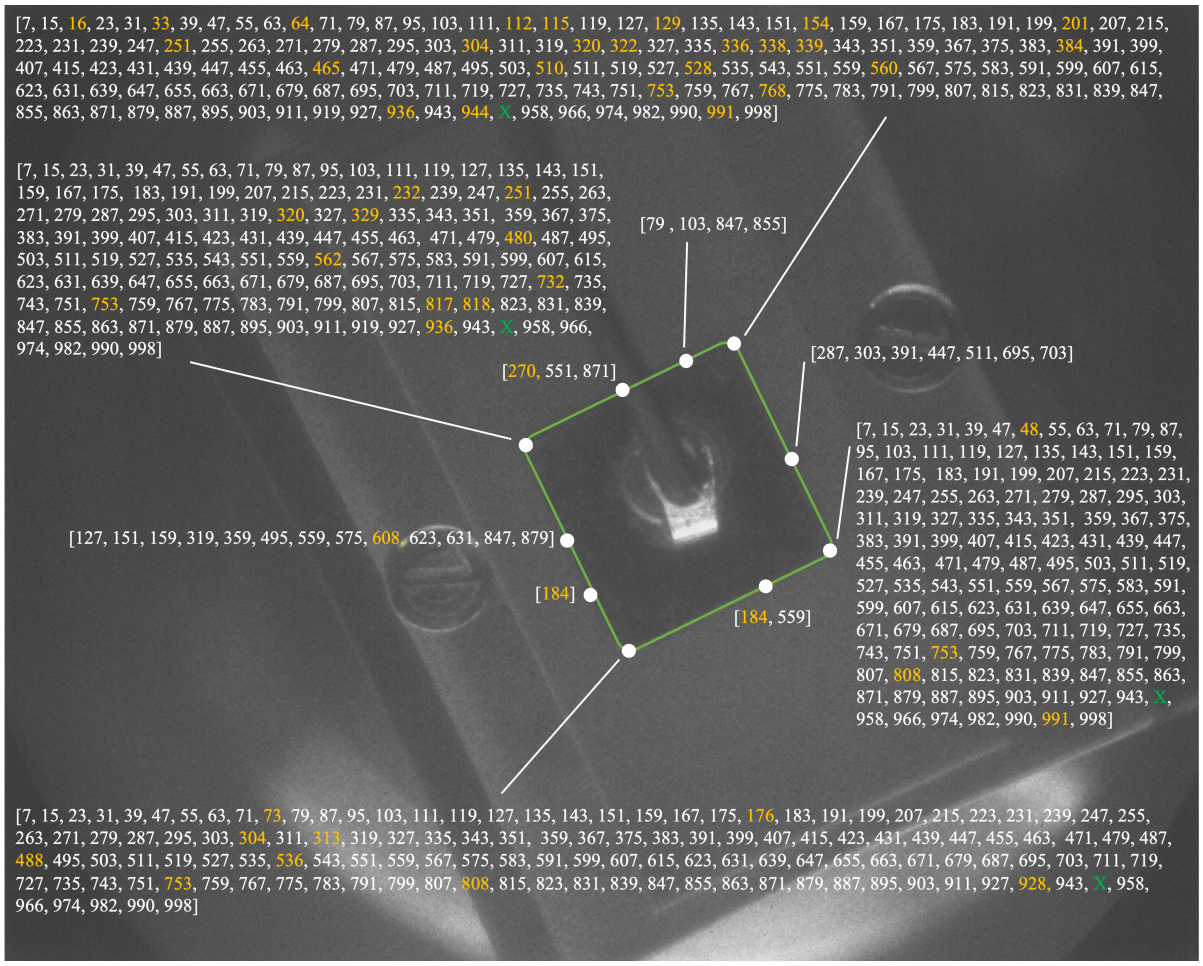

Figure 30: PD formation on the substrate surface with bipolar voltage at 11 kV_{peak} in Nytro 10XN with a camera frequency of 480 Hz. White dots indicate the location of detected PD, and the corresponding picture numbers indicate the frequency of PD occurrence. White picture numbers indicate PDs occurring during flanks, and yellow picture numbers indicate PDs occurring during the plateaus. The camera shift is marked as a green "X".

Figure 31 is a graphical representation of the findings presented in Figure 30. The x-axis in Figure 31 represents the number of pictures captured between instances of detected PD activity, assuming that a PD had occurred during a flank in the same location earlier. The y-axis indicates the number of PDs occurring in the subsequent pictures. Of the pictures captured, every eighth picture from $n = 8$ to $n = 999$ displays flanks, while the remaining pictures exhibit plateaus. In other words, the histogram bars $n = 1, n = 9, n = 17, ...$ correspond to the first picture after a flank, $n = 2, n = 10, n = 18, ...$ correspond to the second picture after a flank, and $n = 7, n = 15, n = 23, ...$ correspond to the last picture of the plateau before a flank. An illustration of the principle is shown in Appendix B.

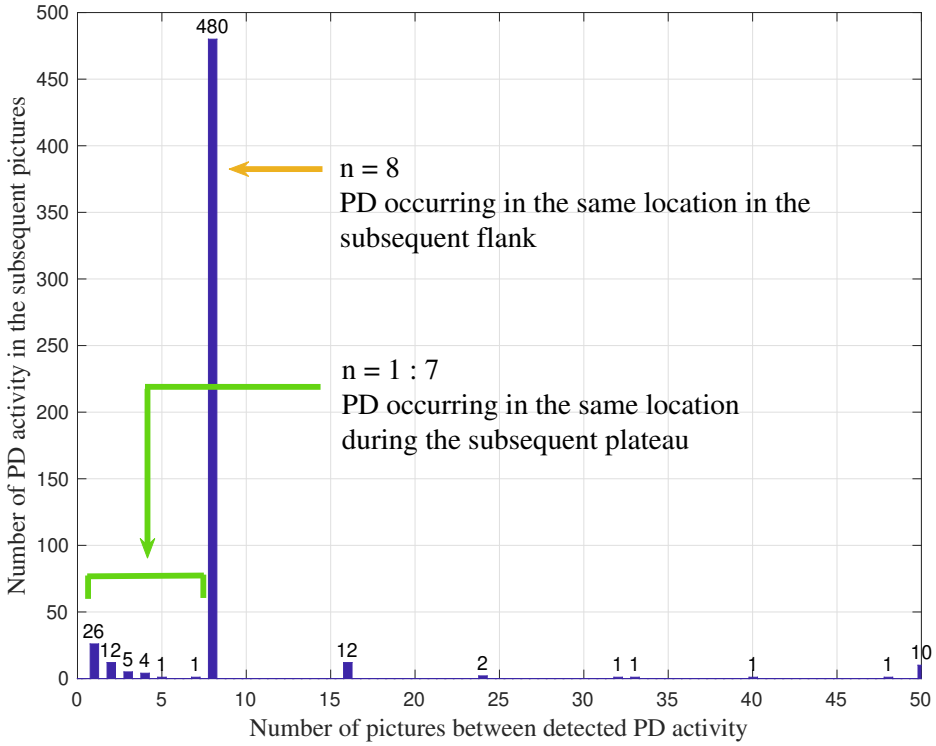

Figure 31: The PD activity occurrence in the subsequent plateaus and flanks, given a prior occurrence of PD in the same location, for bipolar voltage at 11 kV_{peak} in Nytro 10XN with a camera frequency of 480 Hz.

For further explanation, given that a PD has occurred during a flank and in one specific location on the substrate:

- A PD occurs in the same location in the subsequent picture 26 times, i.e., the PD is detected to occur in the first picture **after** the flank (bar $n = 1$), which is during the plateau.
- A PD occurs in the same location in the second picture 12 times, i.e., the PD is detected to occur in the second picture **after** the flank (bar $n = 2$), which is during the plateau.
- PD occurs in the same location during the subsequent flank (opposite polarity) 480 times, i.e., the PD is detected to occur in the eighth picture, which is the next picture of a flank (with opposite polarity), bar $n = 8$.
- A PD occurs in the same location during a flank (same polarity) 12 times, i.e., the PD is detected to occur in the sixteenth picture, which is during the flank with the same polarity as the flank where the PD was detected, bar $n = 16$. So, in this case, no PD is detected during the plateau or the opposite polarity voltage flank, but a PD occurs after one whole voltage period.

4.2.3 Impact of duty cycle

It was of interest to see how different parameters would affect the PD formation and space charge phenomenon. This was done by changing the duty cycle. The findings with the duty cycles of 20 % and 80 % have been excluded from further analysis due to their similarities to the findings with 5 % and 95 % duty cycles. Moreover, it was decided that analyzing the most "extreme" variations of duty cycles would be of greater interest. Hence, only the results from the duty cycles of 5 % and 95 % are included.

Figure 32 and 33 represent the probability of PD occurrence with duty cycles of 5 % and 95 %, respectively, for negative unipolar voltage pulses in Silicone oil and Nytro 10XN. In both figures, red corresponds to PD occurring during voltage turn-off, while blue corresponds to PD occurring during voltage turn-on. As mentioned earlier, Figure 25 illustrates the voltage turn-on and turn-off principle.

Explanation of the denotations used in Figure 32 and 33 is presented below:

- Red triangles, denoted as $P(PD+)$, indicate the probability of PD occurring during voltage turn-off.
- Blue triangles, denoted as $P(PD-)$, indicate the probability of PD occurring during voltage turn-on.
- Red circle with the black center, denoted as $P(PD+|PD-_{n-1})$, represents the probability of PD occurrence during voltage turn-off, given that a PD occurred during the prior voltage turn-on.
- Blue circle with the black center, denoted as $P(PD-|PD+_{n-1})$, represents the probability of PD occurring during voltage turn-on, given that a PD occurred during the previous voltage turn-off.

Figure 32a and 32b show the PD occurrence with a duty cycle of 5 % for Silicone oil and Nytro 10XN, respectively. The y-axis shows the probability of PD in %, and the x-axis indicates the voltage applied in peak-to-peak voltage $kV_{peak-to-peak}$. The threshold was set to 300 pC, capturing only discharge magnitudes above this level. Figure 33a and 33b show the PD occurrence with a duty cycle of 95 % for Silicone oil and Nytro 10XN, respectively.

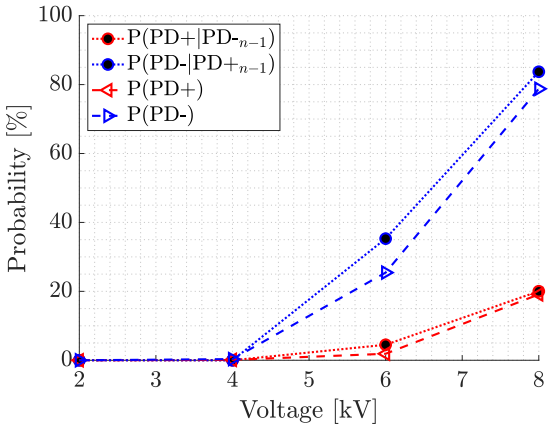

(a) With a duty cycle of 5 % in Silicone oil

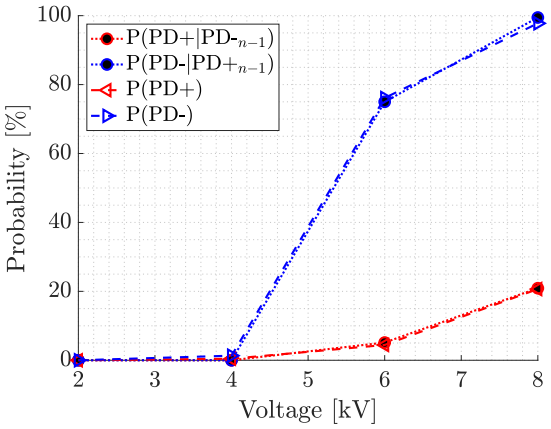

(b) With a duty cycle of 5 % in Nytro 10XN

Figure 32: Probability of PD occurrence for negative unipolar with a duty cycle of 5 % for Silicone oil and Nytro 10XN, with a threshold set to 300 pC. Voltage is defined as peak-to-peak.

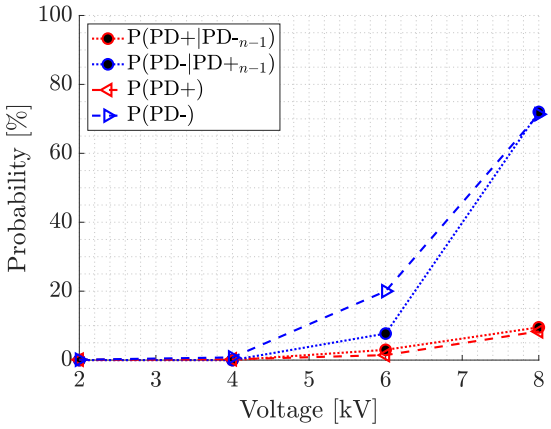

(a) With a duty cycle of 95 % in Silicone oil

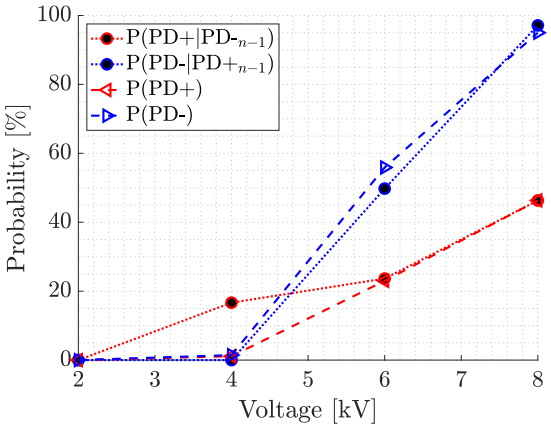

(b) With a duty cycle of 95 % in Nytro 10XN

Figure 33: Probability of PD occurrence for negative unipolar with a duty cycle of 95 % for Silicone oil and Nytro 10XN, with a threshold set to 300 pC. Voltage is defined as peak-to-peak.

5 Discussion

The following section contains a discussion of the obtained results in Section 4. Initially, the relaxation time for Silicone oil and Nytro 10XN is presented. The PDIV and PDEV measurements for the sinusoidal voltage setup in the two liquids are then discussed. Subsequently, the PD measurement results for bipolar, positive, and negative unipolar voltage pulses for both liquids are presented. Further, a comparison between the impact of sinusoidal and square voltage is presented. The results from the high-speed camera analysis are also discussed. Furthermore, the impact of the duty cycle on the experimental results is analyzed. Finally, potential errors and limitations impacting the experimental setups and the results presented in this thesis are reflected upon, concluding this section.

Findings from the specialization project [3] suggest that the substrates consist of voids within the ceramic and sharp edges/tips along the substrate surface. Consequently, discharges occurred both within the ceramic and on the surface of the substrate. For the experimental setup for sinusoidal voltage pulses, the PDs were detected within voids in the dielectric material, i.e., the AlN ceramic, and along the substrate surface. However, this was not observed for the experimental square voltage setup, as only optical measurements were utilized. Thus, only discharges along the surface of the substrate were detected. Therefore, due to limitations in the experimental square voltage setup and given that the main objective of this thesis was to examine the behavior of the substrate under square voltage pulses, further analyses of PDs inside voids will not be further discussed.

During the production process, sharp tips along the substrate edge are assumed to occur due to the metal braze. Therefore, the edge of the substrates can be assumed to consist of sharp tips. Hence, the sharp tip may resemble a needle in a dielectric liquid. Thus, the needle-to-plane principle can further explain, to some extent, the PD and space charge phenomenon on the substrate edge.

5.1 Relaxation time in Silicone oil and Nytro 10XN

The conductivity of Nytro 10XN is defined as 0.6 $\frac{pS}{m}$ as mentioned in Section 3.4.2. If calculating the conductivity of Silicone oil based on the volume resistivity defined as $> 1 \cdot 10^{14}$ Ω cm in [44], as earlier presented in Section 3.4.1, the conductivity is calculated to be 1 $\frac{pS}{m}$. As the conductivity of Nytro 10XN is usually higher than the conductivity of Silicone oil, it is reasonable to assume that the volume resistivity is a decade lower than the present value in the book [44] [46]. Additionally, it should be noted that the value of $> 1 \cdot 10^{14}$ Ω cm is the maximum limit of the volume resistivity. With the assumption of a decade lower, the volume resistivity is assumed to be $1 \cdot 10^{13}$ Ω cm. Thus, the conductivity of the Silicone oil is calculated to be approximately 0.1 $\frac{pS}{m}$, i.e., lower than the conductivity of Nytro 10XN [46].

As mentioned, the Nytro 10XN used had a conductivity value of 0.6 $\frac{pS}{m}$ and a relative permittivity of 2.17. Thus, the relaxation time can be calculated using Equation 7 and is estimated to be approximately 32 seconds. Regarding Silicone oil, the conductivity is assumed to be 0.1 $\frac{pS}{m}$ and the relative permittivity $[2.5 - 2.6]$. Thus, regarding the two relative permittivities, the relaxation time is calculated to be $[221.25 - 230.1]$ seconds, i.e., it is estimated to be somewhere between 3 minute 41 seconds and 3 minutes 50 seconds. Hence, Silicone oil is estimated to have a longer relaxation time than Nytro 10XN, regardless of relative permittivity.

The electric properties of dielectric liquids may vary based on the environment around. For instance, factors such as temperature, humidity, dust, or other particles in the air can influence the properties of the liquid. Thus, this should be taken into account when analyzing the results.

5.2 Sinusoidal voltage setup: PDIV and PDEV measurements

The voltage levels for PDIV and PDEV for the five tested substrates in Silicone oil and five substrates in Nytro 10XN in Table 2 show a distinct variation. Remarkably, the PDIV values are consistently higher for all ten substrates in both liquids compared to the PDEV values. The findings from all of the ten substrates tested validate the underlying theory. As stated in Section 2.2.2, the PDEV should be approximately half the voltage level of PDIV in voids in ideal systems. However, analyzing the PDIV and PDEV values indicate that this is not the case for the presented result in Table 2, as almost all substrates have PDEV values much higher than the half value of PDIV. Factors such as dust, air bubbles, and other particles and contamination in the liquids may affect the formation and presence of PD. Additionally, variations in the substrate's geometrical shape, such as the edge and form, may affect the result. Thus, the test object can not be determined as an ideal system as it consists of limitations and imperfections.

The PDIV was measured for Silicone oil and Nytro 10XN, resulting in average values of 13.1 $kV \pm 1.6$ and 14.9 $kV \pm 1.4$, respectively. These average values correspond to 95 % confidence intervals of 11.5 kV to 14.7 kV for Silicone oil and 13.2 kV to 16.3 kV for Nytro 10XN. Even though the PDIV values vary, the majority of the measurements for the Nytro 10XN substrates indicate much higher PDIV values compared to the measurement with Silicone oil. Due to the conductivity of Silicone oil being lower than Nytro 10XN, it is expected that present discharges in Silicone oil drift away slower. Consequently, it is assumed that the space charges did not drift away fast enough, leading to lower PDIV for Silicone oil than Nytro 10XN. However, multiple factors, such as poorly made substrates and liquid contamination, may affect PD activity. As each substrate has unique characteristics, the PD activity present will be different even at the same voltage level for different substrates. Thus, one would not expect identical PDIV or PDEV for all substrates.

The average PDEV value for Silicone oil was measured to 11.7 $kV \pm 2.5$, with a 95 % confidence interval from 9.2 kV to 14.2 kV. While, the average PDEV value for Nytro 10XN was measured to be 9.9 $kV \pm 4.7$, with a 95 % confidence interval from 5.2 kV to 14.6 kV. The 95 % confidence interval for the average PDEV of Nytro 10XN was much wider than the other measured intervals. Multiple factors may affect the wide interval. It should be noted that one of the substrates had continuous PD activity throughout the measurements with a PDEV value of 0 kV. Thus, affecting the range of the 95 % confidence interval. Additionally, another substrate showed a notably high PDEV value of 16.0 kV, affecting the wide confidence range. Although the PDEV varied a lot for the two substrates, it is observed that they have similar PDIV values. Comparing the two substrates, the substrate with a PDEV of 16.0 kV is assumed to be of high quality, and the Nytro 10XN used may not be affected by liquid contamination. However, the substrate with a PDEV of 0 kV indicates poor quality. If this is due to insufficient construction, sharp substrate edges, or just a bad batch of Nytro 10XN is not known. However, one should not disregard the potential for material degradation. For example, PD activity at the start of the measurement could have resulted in material degradation, thus permanently damaging the substrate and affecting the measurement.

To obtain more precise average PDIV and PDEV values and 95 % confidence intervals, more than five substrate measurements should be conducted for each liquid. The variation observed

in PDIV and PDEV values indicates that the presented measurements may not represent the actual PDIV and PDEV. It is not possible to determine if the presented results in Table 2 are low or high values. Thus, a more extensive set of measurements should be conducted.

5.3 Square voltage setup: PD probability with bipolar, positive, and negative unipolar voltage pulses

5.3.1 Impact of bipolar voltage pulses in Silicone oil and Nytro 10XN

The average PD probability for Nytro 10XN is higher than Silicone oil for most bipolar voltage levels in Figure 26. Both measurements started at 2 $kV_{peak-to-peak}$, the lowest start value possible, and reached a voltage level of 25 $kV_{peak-to-peak}$. For both graphs, one would assume that the start voltage was too high, as the PD activity is above the noise level of PD probability of approximately 5 %. The observed noise level is presumably due to dark currents within the PMT. Immediately following the initiation of the ramping process, it is observed that the PD probability for both liquids decreased and stabilized around the noise level before increasing around 9 $kV_{peak-to-peak}$. Around the voltage level of 9 $kV_{peak-to-peak}$ to 11.5 $kV_{peak-to-peak}$, the Silicone oil indicates having a little peak, seen in the red graph in Figure 26. In the case of one substrate, there might have been a particle or contamination in the Silicone oil. This particle/contamination caused an increase in PD activity, which subsequently disappeared as the peak probability decreased with increasing voltage levels. Therefore, it is assumed that air bubbles, dust, or other particles were the cause and have been burned away. If the discharges were caused by a sharp edge or defect on the surface substrate, one would assume such a peak would have been apparent throughout the voltage ramping.

Based on the graphs in Figure 26, it is observed that the average PDIV is higher for Silicone oil than for Nytro 10XN. Thus, more PD activity is detected at lower voltage levels in Nytro 10XN. As previously mentioned, Silicone oil has a lower conductivity than Nytro 10XN, which causes discharges to drift away faster in Nytro 10XN. The higher PD activity observed at lower voltage levels in Nytro 10XN suggests there are, most likely, more space charges present in Nytro 10XN than in Silicone oil. These findings indicate that Nytro 10XN is more exposed to the effects of bipolar voltage pulses, and more space charges are generated. Furthermore, the results suggest that Nytro 10XN is more sensitive to the shorter rise time of the voltage pulses.

Another observation is that the 95 % confidence interval ranges increase with increasing voltage for both liquids. At the start of the ramping, the majority of the substrates behave very similarly, hence no wide interval range. However, with increasing voltage levels throughout the test, it is observed that there are notable variations in the PD probability for Silicone oil and Nytro 10XN, as indicated by the wide 95 % confidence interval. As the variations are such significant, one may assume that the geometrical form of the substrate and the production quality are critical factors in PD formation in an IGBT.

5.3.2 Impact of bipolar and unipolar voltage pulses in Silicone oil and Nytro 10XN

Generally, the PD probability for Nytro 10XN is higher than Silicone oil for most bipolar and unipolar voltage levels, as seen in Figure 27. The plotted graphs in the figure consistently show that Nytro 10XN has lower PDIV values than Silicone oil for all the different voltage pulse forms. Additionally, all the graphs indicate more PD activity at the start of the measurement.

However, after starting the ramping process, the PD activity decreased and stabilized around the PD probability of approximately 5 %, i.e., stabilizing around the constant noise level, before increasing with increasing voltage.

The PD probability for bipolar, positive, and negative unipolar voltage pulses in Nytro 10XN are relatively similar. However, one observation is that the positive and negative unipolar have a higher probability for PD formation at lower voltage levels than bipolar voltage pulses. Additionally, the positive unipolar voltage pulses indicate that there are tendencies for small peaks in the PD activity throughout the graph, which is not present in the bipolar graph. Multiple factors might have influenced these results, such as differences in the quality of the substrates used for unipolar pulses, a bad batch of Nytro 10XN, and temperature or humidity changes in the environment around the test object.

In general, it is observed that PDs tend to occur easier during negative unipolar pulses compared to positive unipolar pulses [19, 46]. However, this is not the case for the findings presented for Nytro 10XN in Figure 27, as the graph for positive unipolar pulses has lower PDIV than the graph for negative unipolar pulses. Although there may be several influencing factors, one should not disregard that threshold could be an influencing factor. The findings do not include the discharge magnitudes below 500 pC, thus eliminating PDs below this threshold. Consequently, only larger PDs are detected. Therefore, it is reasonable to assume that the PDIV for negative unipolar pulses might be lower if the measurement system had greater sensitivity, indicated by a lower threshold. In other words, it is necessary to acknowledge that the threshold limit used during the measurements may have played a significant role in the results.

Considering Silicone oil alone, the PD probability graph for bipolar and negative unipolar voltage pulses are very similar if disregarding the peak around 11 $kV_{peak-to-peak}$ for bipolar. However, due to limitations in the experimental setup, it was not possible to increase the voltage to more than 20 $kV_{peak-to-peak}$ for the unipolar measurements. Hence, the PD activity above this voltage level for negative unipolar is excluded. However, if considering Nytro 10 XN with different voltage pulses, it is observed that there are similarities in the course of the graphs. One would assume that the PD activity graph above 20 $kV_{peak-to-peak}$ for negative unipolar voltage pulses in Silicone oil would resemble the graph for bipolar pulses in Silicone oil, only with a steeper PD probability graph. This assumption is based on the observation that the PD graphs of unipolar voltages in Nytro 10XN indicated higher PD activity at the same voltage levels as for bipolar voltage pulses.

It is earlier stated in [11] that there are minor changes in the PD activity with differences in the DC component of the voltage. In other words, there is not the absolute applied voltage that governs the PD formation, but the peak-to-peak voltage [11]. Thus, it indicates that there is very little difference between the PD activity if the voltage is switching from -10 $kV_{peak-to-peak}$ to 10 $kV_{peak-to-peak}$ or from 0 kV to 20 $kV_{peak-to-peak}$ [21]. However, the findings in Figure 27 indicate a difference in the graphs, i.e., the PD formation, when considering the different voltage pulses for each dielectric liquid alone. While there are similarities, notable differences can be observed. It should be noted that the graphs may be more similar if smaller PD magnitudes were considered. Nevertheless, this would only be an assumption.

5.4 Comparing the impact of sinusoidal and square voltage pulses

A comparison between the PDIV values obtained from sinusoidal voltage pulses in Table 2 and square voltage pulses in Figure 27 reveals contrasting results. For instance, Nytro 10XN displays a higher PDIV than Silicone oil with sinusoidal voltage pulses, while the opposite is shown for square voltage pulses. It should be noted that Table 2 and Figure 27 are based on electrical and optical measurements, respectively. Thus, they do not have the same sensitivity and PD detection instruments. Including electrical measurements alongside the optical measurements would provide more realistic results of the PD activity. The reason for this is that PMT solely detects light emissions from the substrate surface and does not capture PD activity within the substrate voids. Suppose the square voltage setup also included electrical measurements in addition to optical measurements, it would be reasonable to assume that the graphs in Figure 27 would have higher PD activity at lower voltage levels, as the PD formation inside the substrate would also be detected.

To better visualize the difference in the PD activity with the different voltage pulses, the PD probability for the sinusoidal and square voltage pulses is implemented in Figure 34. Figure 34 is similar to Figure 27, only with the implementations of the electrical measurements from the sinusoidal voltage pulses presented at the end of Section 4.1.1. One can not directly compare the results from sinusoidal and square voltage pulses as the sensitivity of the two measurement techniques is not identical. However, one gets an indication of how the voltage pulses affect the PD activity. The average PD probability at PDIV for electrical measurement in Silicone oil is presented in the blue circle, the average PD probability at PDIV for electrical measurement in Nytro 10XN is presented in the green diamond, and the average PD probability at PDIV for electrical measurements is presented in the pink square at each corresponding PDIV level.

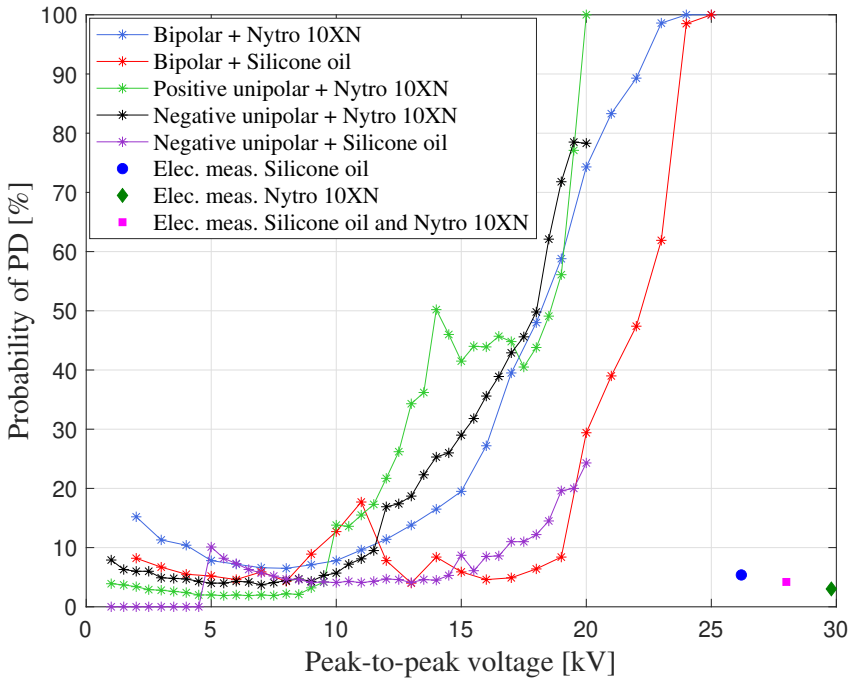

Figure 34: Average probability PD curves of bipolar, positive, and negative unipolar voltage pulses for Silicone oil and Nytro 10XN, with average PD probability at PDIV for sinusoidal voltage pulses for Silicone oil and Nytro 10XN. The voltage level is expressed in peak-to-peak value.

Figure 34 displays a significant variation of the PD activity with different voltage pulses. The rate of the rise, i.e., the rise time of the voltage, is the one parameter differing from the two voltage forms, sinusoidal and square voltage pulses. The results indicate that the fast rise and fall time in the square voltage pulses, i.e., faster voltage rise and fall, results in more PD activity [11, 21]. Considering the sharp edge of the substrate as a tip exposed to sinusoidal voltage pulses, there will be enough time for the homo charges to be accumulated, resulting in a reduction of the electric field. When the polarity of the voltage changes, the discharges will convert to hetero charges. Suppose there is a sufficient duration for the polarity change and enough time for the space charges to settle. In that case, the accumulation of hetero charges is limited, resulting in a decrease in discharge occurrences. However, this is not the case for square voltage pulses, as there is not enough time for the space charges to settle. Considering bipolar voltage pulses, there will be generated hetero charges when turning on the applied voltage. As the polarity change of the applied voltage happens fast, many hetero charges will be accumulated. The addition of the electric field, due to the voltage and the hetero charges, will result in a higher electric field. Therefore, the influence of the rise time of the voltage pulse is critical, and the PDIV for square voltage pulses is significantly lower than for sinusoidal voltage pulses.

In addition, Figure 34 also indicates that the rise time of the voltage has a more significant negative effect in Nytro 10XN than in Silicone oil. This is visual, considering that Nytro 10XN exhibits a higher PDIV than Silicone oil for sinusoidal voltage pulses, but the roles are reversed for square voltage pulses. Therefore, assuming that more charges are injected into Nytro 10XN than Silicone oil during square voltage pulses is reasonable. Thus, more homo and hetero charges are present in the volume of the liquid, resulting in more discharges.

5.5 High-speed camera: PD activity along the edge of the substrate

Figure 28 and 30 presented in Section 4.2.2 indicate that the discharges detected are observed along the whole edge of the substrate. To better understand the edge of the substrate, the edge can be divided into two parts, the edges/corners of the substrate and the straight sides of the substrate. The edge/corner of the substrate is somehow rounded and not a sharp tip [3]. Thus, the substrate edge is defined as follows: considering Figure 28, the two discharge locations occurring at the top left corner of the substrate occur at each "start" of the rounded edge. In contrast, the discharge location at the bottom left corner occurs at the "tip" of the rounded edge. The results from the high-speed camera indicate that the majority of the detected PDs occur at the rounded edge of the substrate, and some occur along the long, straight edges. In this regard, this is observed for bipolar voltage pulses at 11 kV_{peak} in both Silicone oil and Nytro 10XN, in Figure 28 and 30, respectively.

It would be of interest to find the correlation between the picture number and its corresponding voltage polarity. In such a way, one could get an indication of whether the PDs occurred during the rising or falling flank of the voltage pulses. Thus, one could observe if there is any difference in the PD activity with the different voltage polarities. However, detecting the results in the high-speed camera was difficult, as this had to be done manually, especially as the presence of dark currents in the PMT made it more challenging. Thus, the pictures and their corresponding polarities were not found for either picture interval sequence. Additionally, analyzing the intensity of the PDs would also be of interest. As mentioned in Section 4.2.2, this was not done during this thesis.

5.5.1 PD formation along the substrate edge in Silicone oil

Figure 29 shows the probability of PD occurring in the subsequent voltage period, given that a PD has occurred prior in the same location for Silicone oil with bipolar voltage pulses at 11 kV_{peak}. Given that a PD has occurred in one location, a PD occurs in the same location in the subsequent opposite voltage polarity, 29 times. Based on all of the detected PDs that occurred during the picture sequence, almost 40 % of the PDs occurred in the following half-period. This indicates that the discharge in the prior voltage polarity may affect the PD in the subsequent voltage polarity. Regarding this, one would assume the possibility of space charges affecting the PD formation. PD results in the accumulation of charge, i.e., space charge, along the metal edge or the surface of the substrate. Consequently, the presence of space charges leads to distortion of the electric field, resulting in the occurrence of discharges more likely when changing the polarity of the applied voltage [13].

Additionally, in Figure 29, it can be observed that discharges occur sporadically between the bar of $n = 2$ and $n = 49$. The bar of $n = 50$ consists of all PD activity occurring during the 50 and > 50 half-voltage periods after a PD activity. Thus, the higher height of this particular bar is likely due to the occurrence of discharges sporadically occurring during > 50 half-period. In other words, for this voltage level, the subsequent half-voltage period, $n = 1$ after a discharge, appears more prone to discharge.

With the camera frequency of 60 Hz, each picture captured a broad span of the voltage phase, as shown in Figure 11. As a result, the clear distinction between flank and plateau is not observable. Consequently, uncertainty arises regarding the specific timing of PD occurrences, such as whether they occur during the flank or plateau of the voltage pulse.

5.5.2 PD formation along the substrate edge in Nytro 10XN

Figure 30 presents the detected PD activity along the edge of the substrate for bipolar voltage pulses at 11 kV_{peak} in Nytro 10XN. As mentioned, the camera frequency was set to 480 Hz, i.e., every eighth picture was of a flank, as illustrated in Figure 12. Simultaneously, Figure 31 shows the PD activity occurrence in the subsequent plateaus and flanks, given a prior occurrence of PD in the same location during a flank.

The camera took 1000 pictures: out of them, 125 was of the flanks, while the remaining was of the plateau. Bars $n = 8$, $n = 16$, i.e., in Figure 31 are PDs occurring during the flanks. When analyzing the bar of $n = 8$, it reveals that multiple PDs are observed along the edge of the substrate in one picture, as shown by the count of 480. As the number for bar $n = 8$ is 480, one can see that multiple PDs are detected along the edge of the substrate in the same picture. The relation $\frac{480}{125} = 3.84$ indicates that in every picture of a flank after a PD in the prior flank, it was, on average, 3.84 PDs detected in different locations around the substrate. So in some flank pictures, less than three PDs were detected at different locations around the edge, while in some flank pictures, more than three PDs were detected. In other words, there is much more activity during the flanks compared with the plateaus. This is observable in Figure 30, as most picture numbers are white, i.e., flank pictures, and only a few are marked yellow, i.e., plateau pictures. Considering the PDs detected at the top left rounded edge of the substrate in Figure 30, a total of 134 PDs are detected, whereas 123 are during the flanks and 11 during the plateaus. Additionally, as seen in the histogram in Figure 31, the majority of the PDs occur during the voltage flanks.

In Figure 31, it is noticeable that in the first picture captured of the plateau following a prior PD occurrence during the flank, a total of 26 discharges were detected. Consequently, space charges are present due to the prior PD formation during the flank. The bars from $n = 1$ to $n = 7$ show an apparent decrease in the discharge occurrence as further "away" the picture taken is from the flank with the PD. This is most likely due to space charges drifting away. However, it is assumed that not all the charge drifts away. This is because when the voltage shifts polarity, the PD activity increases extremely, as seen in bar $n = 8$. Thus, space charges must be present to ignite PDs during the change of the electrical field.

Nevertheless, there are exceptions to this trend, as seen in bar $n = 16$. The histogram reveals that when a PD occurred during a flank, there were 12 cases where the next PD occurred in the same location, with a delay of a whole voltage period. If the discharges here are due to space charges, it would be assumed that the space charges shielded during the bar $n = 8$, thus preventing discharges at that specific flank, as the electrical field is dependent on the polarity of the space charges [20]. Once the voltage polarity was the same as when the first PD occurred, the electric fields aligned, leading to discharges.

5.5.3 Comparing the PD activity in Silicone oil and Nytro 10XN

Considering Figure 26, it is observed a significant difference in the average probability of PD with bipolar voltage pulses in Silicone oil and Nytro 10XN. At the voltage level of 22 $kV_{peak-to-peak}$ in Figure 26, corresponding to the voltage level used with the high-speed camera at 11 kV_{peak}, a considerable variation gap in the PD activity for Silicone oil and Nytro 10XN is observed. Nytro 10XN indicates much more PD activity than Silicone oil. The results from the high-speed camera correspond with the activity for PDs in the bipolar voltage pulses at this voltage level. The PD activity is remarkably higher for Nytro 10XN in Figure 30 compared with the PD activity for Silicone oil in Figure 28, even though the pictures are taken at the same voltage level.

Considering the PD locations and the amount of picture numbers at the locations in Figure 28 and 30, it is clear that the rounded edge of the substrate is the most critical part of PD formation on the substrate. However, it is worth noting that some locations along the sides of the substrate have regular discharge activity. In the metal brazing process of the substrate, it is assumed that not all brazes are perfectly straight without any sharp tips. As a result, the discharges along the sides of the substrate are assumed to be caused by such sharp tips. The tips are assumed to partially behave like a needle-to-plane principle, as mentioned at the end of the introduction in Section 5.

5.6 Comparing the impact of various duty cycles on PD formation

By changing the duty cycle, one could get an indication of if and how the duty cycle impacts PD formation. Furthermore, negative unipolar pulses were used to determine how the PD occurred and if there was a difference in PD activity occurring during voltage turn-on and turn-off. Additionally, different duty cycles were analyzed to look at the possibility of getting a PD in the subsequent flank, given that a PD occurred in the prior flank.

With a duty cycle of 5 %, the voltage was high 5 % of the voltage period and low 95 % of the voltage period. This corresponds with the voltage being high for 1.7 milliseconds and low for 31.7 milliseconds for each voltage period with a system frequency of 30 Hz. The total duration

of each voltage period was approximately 33.3 milliseconds. The high and low voltage time was reversed with the 95 % duty cycle. Accordingly, the voltage was high for 31.7 milliseconds and low for 1.7 milliseconds within one voltage period.

Considering negative unipolar voltage pulses with the duty cycle of 5 % for Silicone oil and Nytro 10XN in Figure 32a and 32b, respectively, the probability of a PD occurring during voltage turn-on is much greater than PD occurring during voltage turn-off. This is the case for both liquids and is visual by considering the voltage turn-on, marked blue triangles $P(PD-)$, having a much higher PD probability than voltage turn-off, marked red triangles $P(PD+)$, at the same voltage level. Same as observed with a duty cycle of 5 %, the duty cycle of 95 % for Silicone oil and Nytro 10XN in Figure 33a and 33b, respectively, also indicate that the probability of a PD occurring during voltage turn-on is much greater than PD occurring during voltage turn-off.

Figure 32 and 33 indicate that the polarity of the voltage flank with different duty cycles affects the formation of PD in Silicone oil and Nytro 10XN. Figure 35 illustrates how negative unipolar voltage pulses, marked in blue, affect the discharge formation at the sharp tips along the edge of the substrate. As mentioned earlier, the sharp tips along the edge of the substrate surface can be comparable to the needle-to-plane principle. As the voltage turns on from zero to high, i.e., voltage turn-on, PDs will occur. The reason for the PD formation is due to the Laplacian field, illustrated as E_L in (1) in Figure 35, as earlier mentioned in Section 2.3. The space charge field, E_{SC}, will be very small during this period, almost equal to zero. The PDs occurring during this flank will result in the accumulation of charge, i.e., space charges. When the voltage is high, high plateau, the E_{SC} will distort the E_L and the total electrical field will be reduced. This can be seen in (2) in Figure 35. Regarding the voltage turn-off, marked (3) in Figure 35, the occurrence of PDs during this flank is attributed to the presence of space charges generated during the prior voltage plateau. The activity depends on whether the prior plateau's duration has been sufficient for the potential space charges present to have drifted away. Eventually, the electrical field is distorted due to the space charges, and the PDs will occur as a result of the absent E_L. Thus, the PDs occurring during voltage turn-off are due to the space charges [47]. The last part of (3) and part (4) in Figure 35 illustrates when the voltage is zero, low plateau, and no voltage is applied to the test object. At the start of the low plateau, the last part of (3), the present space charges will still affect the electrical field distribution. After some time of the low plateau, part (4) in Figure 35, the present space charges will have drifted away [21], and E_{SC} have decayed given that the off-time has been sufficient. Thus, the critical field, $E_{critical}$, results in becoming much higher than E_{SC}. As illustrated, the PD formation is highly dependent on the duration of the high plateau and the number of space charges, as it is here the space charge reduces the electrical field, thus resulting in PD formation during voltage turn-off [47]. This corresponds with the finding in Figure 32 and 33, as the PD activity is greater during voltage turn-on compared to voltage turn-off.

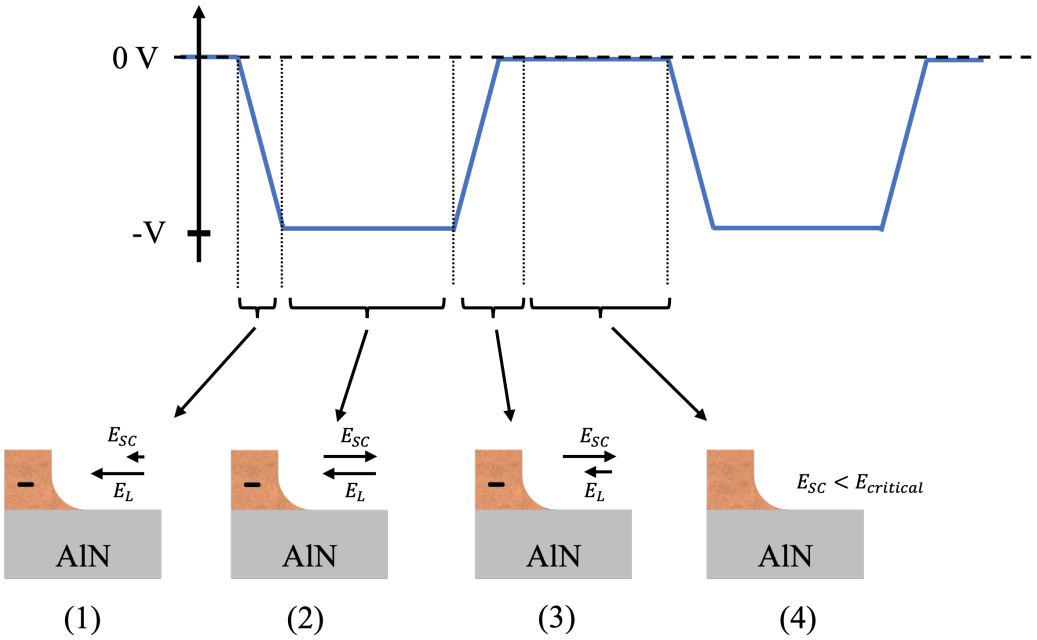

Figure 35: Illustration on how negative unipolar voltage pulses affect discharge formation at the sharp tips along the edge of the substrate, based on the needle-to-plane principle. The voltage signal is presented in blue and is divided into four parts: (1) voltage turn-on, (2) high plateau, (3) voltage turn-off, and (4) low plateau. The Laplacian field is denoted as E_L, the electrical field due to the space charges is denoted as E_{SC}, and the critical field as $E_{critical}$. The copper edge is marked in cobber color, and the AlN substrate is in grey. Illustrations are greatly inspired by [12, 21].

The results of Silicone oil with a duty cycle of 5 % and 95 %, Figure 32a and 33a, respectively, generally indicate more PD activity with a lower duty cycle than a higher. Comparing the PD probability for voltage turn-on, the progressions of the graphs are very similar. Also, this can be seen by the voltage turn-off, where the progressions of the graphs are alike but with more PD formation with a lower duty cycle. As the duration of the high plateau was relatively short, the space charges did not have enough time to drift away, leading to increased discharges. The overall results indicate a significant similarity despite the observation of increased PD activity with lower duty cycles. This suggests that there is not a substantial difference between the two duty cycles in terms of PD probability in Silicone oil, indicating that the duration of the high plateau does not lead to significant variations.

Furthermore, the findings for Nytro 10XN with a duty cycle of 5 % and 95 %, Figure 32b and 33b, respectively, are different compared with the findings for Silicone oil. Considering the voltage turn-on, the PD probability is higher at a lower duty cycle of 5 % than for 95 %. However, this is not the case for voltage turn-off, as there is more PD activity with a cycle of 95 % than 5 %. This indicates that the voltage turn-off is affected by space charges occurring due to the PD formation during the voltage turn-on. However, there are uncertainties regarding the impact of the high-field region, as the exact conductivity is unknown in a high-field region.

Figure 36 illustrates how dielectric liquids with different conductivity behave in a needle-to-plane principle with a negatively charged tip. The top part of Figure 36 illustrates the negative unipolar voltage pulse. The y-axis represents how the voltage, $V(x)$, differs along the x-axis. The middle part of Figure 36 shows how the charge magnitude, $Q(x)$, changes along the x-axis

for the two conductivities. Additionally, the high-field region is marked. While the bottom part of Figure 36 illustrates how the field strength curve for the liquids with different conductivity varies and how the field strength would be without the presence of space charges.

Considering the graph of the field strength at the bottom of Figure 36, it is observed that when the voltage is high, a liquid with low conductivity will make the space charges drift away relatively fast in the high-field region. In contrast, liquids with higher conductivity will hold longer on the present charges, i.e., the space charges will not drift away as fast as for a liquid with lower conductivity. The impact of conductivity on the discharge formation remains uncertain, especially in the high-field region where the conductivity of most dielectric liquids is expected to increase [48]. However, based on the graph for the field strength in Figure 36, it is illustrated that Silicone oil would make the discharges drift faster away compared with Nytro 10XN in the high-field region. This can also be observed in Figure 32 and 33, as there is overall more PD activity in Nytro 10XN than in Silicone oil. Additionally, the earlier presented results indicate a higher generation of space charges in Nytro 10XN during square voltage pulses, which consequently has a more significant impact on PD formation.

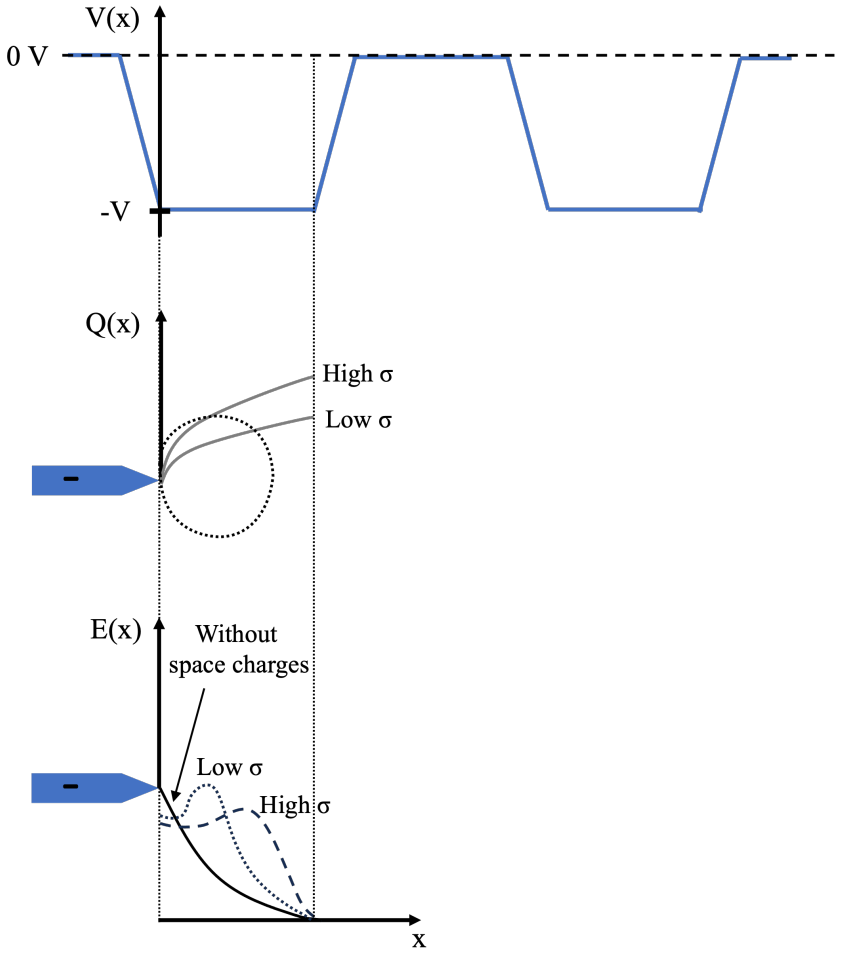

Figure 36: Illustration on how high and low conductivity dielectric liquids behave in a needle-to-plane principle with a negatively charged tip [46].

5.6.1 Influence of relaxation time with different duty cycles

Figure 32 and 33 show Nytro 10XN exhibits a higher PD probability than Silicone oil, regardless of the duty cycle. One factor affecting here is the relaxation time, which is affected by the conductivity and relative permittivity of the liquids. Additionally, other factors such as humidity and moisture in the liquid, and temperature differences, i.e., may affect the "performance" of the liquid properties. The relaxation time of Nytro 10XN was calculated to be approximately 32.01 seconds in Section 5.1, and the duration of one voltage period with a system frequency of 30 Hz is approximately 33.3 milliseconds. Whereas the relaxation time of the liquid is longer than the duration of one voltage period, one can not ignore that some PDs and space charges have affected the subsequent discharges. The same implies to Silicone oil, as the relaxation time was calculated to be a minimum of 3 minutes 41 seconds and a maximum of 3 minutes 50 seconds. Furthermore, the time duration of 15 minutes without applied voltage between the measurements for the different duty cycles was sufficient, as the time duration is longer than the relaxation time of both Silione oil and Nytro 10XN.

5.6.2 Influence of subsequent PDs due to PDs activity in the previous flank

As mentioned, the results indicate that the probability of a PD occurring during voltage turn-on is higher than during voltage turn-off. Furthermore, the same applies when considering PD formation, given that a PD has occurred during the prior voltage flank (with opposite polarity) in Figure 32 and 33. The probability of PD occurring during voltage turn-on, given that a PD occurred during the previous voltage turn-off, marked with a blue circle with the black center, denoted as $P(PD-|PD+_{n-1})$, is higher when comparing with the probability of PD occurrence during voltage turn-off, given that a PD occurred during the prior voltage turn-on, marked with the red circle with the black center, denoted as $P(PD+|PD-_{n-1})$, for both of the duty cycles. Interfacial polarization may have impacted the subsequent discharges by causing the charge to "attach" to the surface instead of drifting away.

5.6.3 Comparison of PDIVs for negative unipolar voltage pulses

Examining the average probability PD graph for negative unipolar voltage shown in Figure 27 indicates a significantly higher PDIV compared to the PDIV present in Figure 32 and 33. In Figure 32 and 33, the PDIV is approximately 4 $kV_{peak-to-peak}$, while PDIV for negative unipolar in Silicone oil and Nytro 10 XN in Figure 27 were 15 $kV_{peak-to-peak}$ and 10 $kV_{peak-to-peak}$, respectively. This contrast can be due to several factors. Firstly, the thresholds used for the two measurements, notably 300 pC for PD activity in Figure 32 and 33 and 500 pC for probability PD curve for negative unipolar voltage shown in Figure 27, were dissimilar. A 300 pC threshold detects discharges with smaller magnitudes than a 500 pC threshold. Thus, more discharges are detected. Furthermore, variations in the duty cycle and the positioning of the PMT inside the cabinet, without a light guide attached to its lens, contribute to these divergent results. When a light guide is utilized, it is expected that some light may be excluded compared to the PMT alone. This arises from the PMT lens being considerably wider in diameter than the lens of the light guide. The increased surface area of the larger lens collects light from a wider area of view, potentially resulting in higher light detection capabilities of the substrate surface. A visual representation of this difference in lens diameters can be seen in Figure 18 and 19.

5.7 Possible errors and limitations

There were multiple factors affecting the measurements and the presented result in this thesis that should be mentioned. One factor affecting all measurements is that PD is a stochastic phenomenon. The PD formation varies in magnitude and frequency from one voltage period to another. The phenomenon is affected by multiple factors, such as variations in the test object and the geometrical shape. Furthermore, the time delay between the initial acceleration of a free electron and the occurrence of an electron avalanche varies in each case [21]. Additionally, the dielectric properties of the insulation materials also influence the phenomenon due to factors such as particles, humidity, and temperature. Thus, even if two systems were identical, the stochastic nature of PD phenomena would result in a non-identical PD formation.

5.7.1 Test object

The test objects indicated a significant variability in terms of quality. Throughout the experimental work, variations in the substrate PD tolerance were observed, thus indicating variation in the quality. The results suggest that the edge of the substrate, due to the metal brazing, is a critical part that displays variation among the substrates. Therefore, this part of the substrate plays a crucial role in the PDs formation. Furthermore, it is noteworthy that the imperfections along the edge of the substrates contribute significantly to the overall PD formation variety observed throughout the different batches of substrates. Even though visual inspections of the substrates were conducted and removed from the measurements when necessary, it was not possible to detect, prior to measurements, substrates with internal damages, such as foreign particles inside the substrate, voids, or cracks.

5.7.2 Preparation of Silicone oil and Nytro 10XN

In order to provide a more accurate comparison between the two dielectric liquids, Silicone oil and Nytro 10XN, the liquids should undergo approximately the same preparation. The potential impact of liquid contamination should be addressed, as the presence of particles and other contaminants in the liquids may not be visible to the naked eye. Potentially contamination in the liquid may affect the formation of PDs and space charges. The environmental conditions surrounding the test object could also influence the PD formation. Factors such as moisture or humidity in the atmospheric air could affect the properties of the liquids. Furthermore, the optimal temperature for the best insulation properties for the two liquids was not considered, potentially impacting the PD formation.

Another factor that should be considered is the preparation of the liquids. The filling processes for Silicone oil and Nytro 10XN, described in Section 3.4.1 and 3.4.2, respectively, were carried out differently. Therefore, one could question if the preparation of the liquids was sufficient enough to compare the liquids. Specifically, the filling procedure of Nytro 10XN was conducted by hand, exposing the liquid to atmospheric air, which could introduce dust, air bubbles, and other particles into the liquid. Additionally, the efficiency of one hour of degassing in a vacuum to remove air bubbles may be questioned. In contrast, the filling process and degassing of the Silicone oil were done in a vacuum, hence not that exposed to contamination from the atmospheric air.

5.7.3 Experimental setups and measuring procedure

The experimental setups and measuring procedures were influenced by limitations in the components and equipment used. Despite using the same PMT for all experimental setups, to try to provide an identical condition as possible, it is essential to acknowledge that the PMT was a limitation for the measurements. The PMT is heavily affected by its surroundings, especially considering the sensitivity to light from its surroundings. Although efforts were made to minimize light during the measurements by turning off all lights in the room and reducing possible light sources, there somehow could be light emissions from the surroundings affecting the PMT and resulting in the detection of "fake" PDs. Additionally, PMT cooling is often used to prevent dark currents. However, it was not included in the experimental setups for sinusoidal and square voltage. The implementation of cooling equipment could have prevented the occurrence of dark currents.

Furthermore, the constant noise floor caused by the dark currents affected the results. Even though the threshold was set to remove the noise floor, it also resulted in filtering out the PDs with the same magnitude and below the noise floor. Consequently, only PDs with high magnitudes were detected, indicating the threshold setting was a limitation in the measurements. Additionally, as only one PMT was used during the experimental setup, it was impossible to distinguish between actual PDs and dark currents. Another PMT should be included in the experimental setup to reduce this limitation. This would allow separation between actual PD and dark currents, as actual PDs would be present in both PMTs, while dark currents would only be present in one PMT. Additionally, electrical measurements should be included in the square voltage setup to contribute to more reliable results, as PD occurring inside the substrate would be included.

Another limitation was placing the PMT outside the cabinet and using a light guide. Although this setup provided a somewhat identical setup for sinusoidal and square voltage setups, the sensitivity of the measurements would increase with the PMT placed inside the cabinet. Such a setup would result in higher light detection capabilities of the substrate surface, as mentioned in Section 5.6.3.

As the experimental square voltage setup had some limitations, it was not possible to start the measurements at a sufficiently low start voltage value. The graphs in Figure 26 and 27 suggest that the start voltage value may have been too high in some measurements, resulting in a high PD probability at the start of the measurement before stabilizing during increased ramping. It is essential to acknowledge that these discharges occurring during the start of the measurements could have influenced the degradation of the material, thus possibly affecting further PD formation.

6 Conclusion

The objective of the thesis was to contribute to the ongoing research on the Partial Discharge (PD) formation and space charge phenomenon of the ceramic substrate inside Insulated Gate Bipolar Transistor (IGBT) power modules. The primary focus was to determine how different applied voltage pulses would affect Aluminum Nitride (AlN) ceramic substrate and how the PD formation would vary for the two dielectric liquids, Silicone oil and Nytro 10XN.

The PDIV results indicate that different voltage pulses significantly affect the PD and space charge formation on the substrate. The PD activity increases when the substrates are exposed to square voltage pulses, compared with sinusoidal voltage pulses, regardless of liquids. This indicates that the rise time of the voltage pulses is the critical factor for the PD formation of the substrates. Furthermore, the presence of space charges heavily influences the field strength along the edge of the substrate. Additionally, when comparing the behavior of Silicone oil and Nytro 10XN, it becomes evident that Nytro 10XN shows a relatively more negative response to square voltage pulses than Silicone oil. This is evident when considering that the Nytro 10XN has a higher PDIV than Silicone oil when exposed to sinusoidal voltage pulses. However, the positions are reversed when exposed to square voltage pulses. Therefore, a reasonable assumption for this case is that Nytro 10XN is more exposed to charges being injected from the sharp edges of the substrate during the flanks than compared with Silicone oil. As a result, there are overall more space charges present in the volume of Nytro 10XN, which increases the probability of PDs.

Implementing the ultra-fast gated intensified high-speed camera provided valuable insight into the PD formation along the edge of the substrate. The findings indicate that even though PDs occur sporadically along the edge, the rounded corners of the substrates are the most critical part of the substrate. The results also indicate that sharp tips along the edge due to the metal brazes heavily affect the PD probability. Moreover, the high-speed camera revealed that the PDs occur during the flanks of the bipolar voltage pulses. However, the results are affected by space charges, as seen by PD activity during the voltage plateau. The space charges are further contributing to discharges at the subsequent voltage flanks. In addition to the findings in the prior section, the implementation of the high-speed camera also revealed that Nytro 10XN is much more prone to PDs and space charges than Silicone oil during bipolar voltage pulses. Thus, it suggests that the accumulation of space charges may be one of the main reasons for the observed difference in the PD behavior between the two liquids.

Nytro 10XN exhibits a higher PD probability during square voltage pulses compared to Silicone oil, which is also evident during the duty cycle variations. The findings from the variations of the duty cycles reveal that, with negative unipolar voltage pulses, the flank corresponding to the voltage turn-on plays the most dominant role in PD formation during one voltage period. Therefore, the probability of getting a PD is higher during the voltage turn-on than the turn-off. Additionally, the PD occurring during the voltage turn-off is solely due to the space charges accumulated during the voltage turn-on. Furthermore, considering turn-off, it is visible that Silicone oil is not significantly affected by the different duty cycles. However, Nytro 10XN exhibits more PD activity with a longer duration of the high plateau. Consequently, a change in a higher duty cycle results in more PD and space charge formation in Nytro 10XN.

The results suggest that optical measurements can be used to detect PDs with higher magnitudes. However, the addition of electrical measurement should be implemented to provide more reliable measurements, as PD formation inside the substrates would also be included. The findings would then better represent the actual impact of the voltage pulses on insulation properties and material degradation of the substrate.

7 Further work

This thesis aimed to contribute to further understanding and research on partial discharge (PD) formation on an Aluminium Nitride (AlN) ceramic substrate exposed to sinusoidal and square voltage pulses. The thesis also aimed to provide insights into how PD formation varied in two dielectric liquids, Silicone oil and Nytro 10XN. In order to contribute to further research and understanding of PD formation and the space charge phenomenon in a substrate, the following suggestions are presented:

- Implementation of electrical measurement for the square voltage experimental setup: To get more reliable results and a better understanding of how the square voltage pulses affect the substrates, it would be of interest to implement electrical measurements in addition to the optical measurement. In such a way, PDs occurring inside the voids of the substrates would also be detected.

- Analyze the PD formation along the surface and light intensity of the discharges: To understand better how the energy accumulation and intensity of the emitted light occurs and behaves, further configurations and triggering of the ultra-fast gated intensified high-speed camera should be implemented. As mentioned in the thesis, the variations in the light intensity can be seen in Appendix A. Further application and development of the custom code provided by SINTEF would be beneficial in better understanding the PD formation along the surface of the substrate. Another valuable addition would be the implementation of trigging the high-speed camera to capture pictures with known voltage polarity. In such a way, the picture with discharge and its corresponding voltage polarity could be found and contribute to further understanding of the PD phenomenon.

- Further research on the effect of different voltage pulses: Measurements with different square voltage pulses should be conducted to see how bipolar and unipolar voltage pulses affect the PD formation along and within the substrate. The purpose of further investigation will be to determine if the substrates are more exposed under specific voltage pulses. As the results in this thesis only consisted of five substrates in each voltage pulse form, reproducing the measurements with more substrates would be beneficial to get a more reliable result.

- Further research on the effect of different duty cycles: It would be valuable for further understanding the PD formation along and inside the ceramic substrates to research the impact of different duty cycles of the applied square voltage pulses. While the measurements conducted during this thesis were with Silicone oil, an earlier study reveals that there is no to very little difference in the PD formation between Silicone gel and Silicone liquid [49]. Thus, investigating the PD formation in Silicone oil with different duty cycles would be valuable for Insulated Gate Bipolar Transistors (IGBTs) development. The duty cycle results presented in this thesis initiate no significant change in the PD activity with the duty cycles of 5 % and 95 % in Silicone oil. However, variations were observed in Nytro 10XN. Therefore, further measurements and experiments using lower duty cycles than 5 % and higher duty cycles than 95 % to observe if more extreme cases of duty cycles would impact the PD formation in Silicone oil.

- Evaluate the geometrical shape of the ceramic substrate: The result in this thesis indicates that the rounded corners are the most critical part of PD formation on the substrate. Even though the test object was of simplified geometrical formation as compared with actual ceramic substrates used in IGBTs, the results indicate that the geometrical form of the

substrate is critical. Hence, further development for a more optimal geometrical shape of the substrate should be prioritized to reduce PD formation.

References

[1] SINTEF, "FastTrans - Påkjenning på elektrisk isolasjon fra raske transiente spenninger fra høyspennings konvertere."

[2] M. Ghassemi, "Pd measurements, failure analysis, and control in high-power igbt modules," *High Voltage*, vol. 3, no. 3, pp. 170–178, 2018.

[3] I. Smisethjell, "Analysis of partial discharge formation in ceramic substrates under ac voltage stresses," project report in TET4510 - Electrical Energy and Power Systems, Specialisation Project, Department of Electric Energy, NTNU – Norwegian University of Science and Technology, December 2022.

[4] B. Zhang, Z. Yang, K. Li, X. Jiang, X. Li, G. Chang, and M. Ghassemi, "Electrical properties of silicone gel for wbg-based power module packaging at high temperatures," *IEEE Transactions on Dielectrics and Electrical Insulation*, vol. 30, no. 2, pp. 852–861, 2023.

[5] J.-H. Fabian, S. Hartmann, and A. Hamidi, "Analysis of insulation failure modes in high power igbt modules," in *Fourtieth IAS Annual Meeting. Conference Record of the 2005 Industry Applications Conference, 2005.*, vol. 2, pp. 799–805 Vol. 2, 2005.

[6] U.S. Department of Energy, "Power electronics research and development program plan," 2011.

[7] C. Qian, A. M. Gheitaghy, J. Fan, H. Tang, B. Sun, H. Ye, and G. Zhang, "Thermal management on igbt power electronic devices and modules," *IEEE Access*, vol. 6, pp. 12868–12884, 2018.

[8] Z. Valdez-Nava, D. Kenfaui, M.-L. Locatelli, L. Laudebat, and S. Guillemet, "Ceramic substrates for high voltage power electronics: past, present and future," in *2019 IEEE International Workshop on Integrated Power Packaging (IWIPP)*, pp. 91–96, 2019.

[9] B. Zhang, M. Ghassemi, and Y. Zhang, "Insulation materials and systems for power electronics modules: A review identifying challenges and future research needs," *IEEE Transactions on Dielectrics and Electrical Insulation*, vol. 28, no. 1, pp. 290–302, 2021.

[10] L. Lundgaard, *Teknisk rapport - PARTIELLE UTLADNINGER*. EFI SINTEF GRUPPEN, 1996.

[11] M. Do, J.-L. Auge, and O. Lesaint, "Optical measurement of partial discharges in silicone gel under repetitive pulse voltage," in *Proceedings of 2005 International Symposium on Electrical Insulating Materials, 2005. (ISEIM 2005).*, vol. 2, pp. 360–363 Vol. 2, 2005.

[12] I. Semenov, I. F. Gunheim, K. Niayesh, H. K. H. Meyer, and L. Lundgaard, "Investigation of partial discharges in aln substrates under fast transient voltages," *IEEE Transactions on Dielectrics and Electrical Insulation*, vol. 29, no. 2, pp. 745–752, 2022.

[13] P. Wang, A. Cavallini, and G. C. Montanari, "Characteristics of pd under square wave voltages and their influence on motor insulation endurance," *IEEE Transactions on Dielectrics and Electrical Insulation*, vol. 22, no. 6, pp. 3079–3086, 2015.

[14] W. J. K. Raymond, H. Illias, A. Bakar, and H. Mokhlis, "Partial discharge classifications: Review of recent progress," *Measurement*, vol. 68, pp. 164–181, 2015.

[15] T. Grav, "PD measurements at fast transients," *SINTEF Energy Research - Project memo*, vol. 1, pp. 1–28, 2013.

[16] F. Skirbekk, "Transformer insulation stressed by power converters," *Master's thesis in Energy and Environmental Engineering*, vol. 1, pp. 1–129, 2021.

[17] B. Fagerli, "AC voltage stress on transformer insulation materials," *Specialisation project in TET4510 Electrical Energy*, vol. 1, pp. 1–49, 2022.

[18] H. Illias, G. Chen, and P. L. Lewin, "Partial discharge behavior within a spherical cavity in a solid dielectric material as a function of frequency and amplitude of the applied voltage," *IEEE Transactions on Dielectrics and Electrical Insulation*, vol. 18, no. 2, pp. 432–443, 2011.

[19] I. Semenov, I. G. Folkestad, K. Niayesh, and L. Lundgaard, "Characterization of defects in aluminum nitride substrates through partial discharge measurements," in *2022 IEEE 4th International Conference on Dielectrics (ICD)*, pp. 380–384, 2022.

[20] A. Küchler, *High Voltage Engineering*. Springer Nature, 2018.

[21] I. G. Folkestad, "Investigation of PD behavior in ceramic substrates under fast repetitive square voltage pulses," *Master's thesis in Energy and Environmental Engineering*, vol. 1, pp. 1–98, 2022.

[22] L. Sevgi, "A review of discrete solutions of poisson, laplace, and wave equations," *IEEE Antennas and Propagation Magazine*, vol. 50, no. 1, pp. 246–254, 2008.

[23] E. Ildstad, *TET4160 Insulating Materials for High Voltage Applications*. NTNU, 2021.

[24] B. Fagerli, "Converter stress on transformer insulation materials," *Master's thesis in Energy and Environmental Engineering*, vol. 1, pp. 1–64, 2022.

[25] G. Chen and A. E. Davies, "Electric stress computation - a needle-plane electrode system with space charge effects," *COMPEL - The international journal for computation and mathematics in electrical and electronic engineering*, vol. 15, no. 1, pp. 40–56, 1996.

[26] NTNU, *TET4160 High Voltage Insulation Materials - Preparation exercise for HVIM1*. NTNU, 2021.

[27] L. Lundgaard. (From private conversation and discussion with Lars Lundgaard, Chief Scientist at SINTEF Energy Research, Department Electric Power Technology), December 2022.

[28] K. Preis, "Numerical computation of transient quasistatic electric fields," in *The Fourth International Conference on Computation in Electromagnetics, 2002. CEM 2002 (Ref. No. 2002/063)*, pp. 2 pp.–, 2002.

[29] A. Namboodiri and H. S. Wani, "Unipolar and bipolar pwm inverter," *International Journal for Innovative Research in Science & Technology*, vol. 1, no. 7, pp. 237–243, 2014.

[30] E. Tutorials, "Insulated gate bipolar transistor." https://www.electronics-tutorials.ws/power/insulated-gate-bipolar-transistor.html. [Online; accessed: 19.04.2023].

[31] M. H. Rashid, *POWER ELECTRONICS HANDBOOK Third Edition*. Butterworth-Heinemann, 2011.

[32] C. D. Systems, "Pulse width modulation characteristics and the effects of frequency and duty cycle." https://resources.pcb.cadence.com/blog/2020-pulse-width-modulation-characteristics-and-the-effects-of-frequency-and-duty-cycle. [Online; accessed: 19.04.2023].

[33] FLUKE, "What is duty cycle?." https://www.fluke.com/en-us/learn/blog/electrical/what-is-duty-cycle, 2023. [Online; accessed: 19.04.2023].

[34] EDN, "Slew rate vs. rise time: Not quite the same." https://www.edn.com/slew-rate-and-rise-time-not-quite-the-same/, 2019. [Online; accessed: 20.04.2023].

[35] KEB, "How pulse width modulation in a vfd works." https://www.kebamerica.com/blog/pulse-width-modulation-in-vfds/, 2021. [Online; accessed: 20.04.2023].

[36] M. M. Tousi and M. Ghassemi, "The effect of type of voltage (sinusoidal and square waveform) and the frequency on the performance of nonlinear field-dependent conductivity coatings for electric field control in power electronic modules," pp. 552–555, 2019.

[37] I. G. Folkestad, "A physical interpretation of various defects and related PRPD patterns," *Specialisation project in TET4510 Electrical Energy*, vol. 1, pp. 1–61, 2021.

[38] RCA, *Photomultiplier Manual*. RCA, Electronic Components, pp. 1-193, 1970.

[39] HAMAMATSU, *PHOTOMULTIPLIER TUBES*. version 3, pp. 1-323, 2007.

[40] L. Lundgaard and S. Kyrkjeeide, "Evaluation of dielectric liquids by measurement of their partial discharge characteristics," in *Proceedings of IEEE Conference on Electrical Insulation and Dielectric Phenomena - (CEIDP'94)*, pp. 901–909, 1994.

[41] SINTEF, "High speed cameras." https://www.sintef.no/projectweb/elpowerlab/lab_facilities/high-speed-cameras/, 2023. [Online; accessed: 12.04.2023].

[42] H. K. H. Meyer, "AC resonant voltage source for PD-measurements," *SINTEF Energy Research - Project memo*, vol. 1, pp. 1–12, 2020.

[43] D. Linhjell, "High voltage pulse source 65 kV," *SINTEF Energy Research - Project memo*, vol. Rev 2.0, pp. 1–27, 2023.

[44] R. Bartnikas, *Engineering Dielectrics Volume III Electrical Insulating Liquids*. ASTM, 1994.

[45] T. Grav and L. E. Lundgaard, "Currents in ac stressed liquid insulated needle plane gap," in *2014 IEEE 18th International Conference on Dielectric Liquids (ICDL)*, pp. 1–5, 2014.

[46] L. Lundgaard. (From private conversation and discussion with Lars Lundgaard, Chief Scientist at SINTEF Energy Research, Department Electric Power Technology), May 2023.

[47] A. A. Abdelmalik, A. Nysveen, and L. E. Lundgaard, "Partial discharges in liquid embedded power electronics: Effects of pressure and liquid nature under negative pulse voltage stress," *IEEE Transactions on Dielectrics and Electrical Insulation*, vol. 23, no. 2, pp. 1119–1125, 2016.

[48] O. L. Hestad, D. Linhjell, L. E. Lundgaard, J. Samseth, and M. Unge, "Field dependent conductivity of n-pentane," in *2017 IEEE 19th International Conference on Dielectric Liquids (ICDL)*, pp. 1–4, 2017.

[49] J.-L. Auge, O. Lesaint, and A. V. Thi, "Partial discharges in ceramic substrates embedded in liquids and gels," *IEEE Transactions on Dielectrics and Electrical Insulation*, vol. 20, no. 1, pp. 262–274, 2013.

Appendix

A Appendix - PD detected with the high-speed camera

In order to gain a better understanding of the formation of PDs and the variation in light intensity, Figure 37 and 38 shows two different pictures captured by the high-speed camera.

Figure 37 is a picture of the substrate surface with bipolar voltage at 11 kV_{peak} in Silicone oil with a camera frequency of 60 Hz. The one white dot in the picture is a PD in the form of light emission. This specific picture corresponds to one of the detected PDs displayed in Figure 28. Referring to the top left rounded corner of Figure 28, Figure 37 corresponds to picture number 29 in Figure 28.

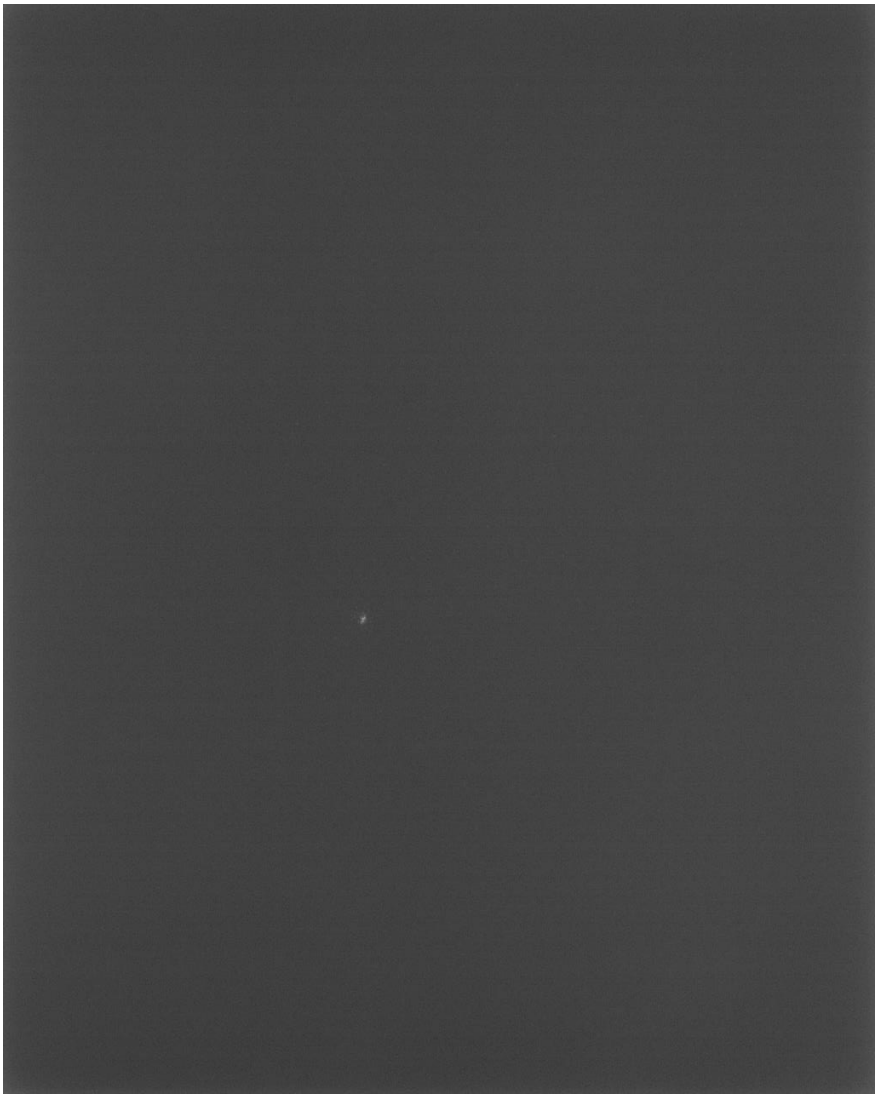

Figure 37: Picture of the substrate surface with bipolar voltage at 11 kV_{peak} in Silicone oil with a camera frequency of 60 Hz: Picture number 29 (in Figure 28).

Figure 38 is a picture of the substrate surface with bipolar voltage at 11 kV_{peak} in Nytro 10XN with a camera frequency of 480 Hz. The four white dots/streamers in the picture are PDs in the

form of light emission. This specific picture corresponds to four of the detected PDs displayed in Figure 30. Referring to all four of the rounded corners of the substrate in Figure 30, Figure 38 corresponds to picture number 7 in Figure 30.

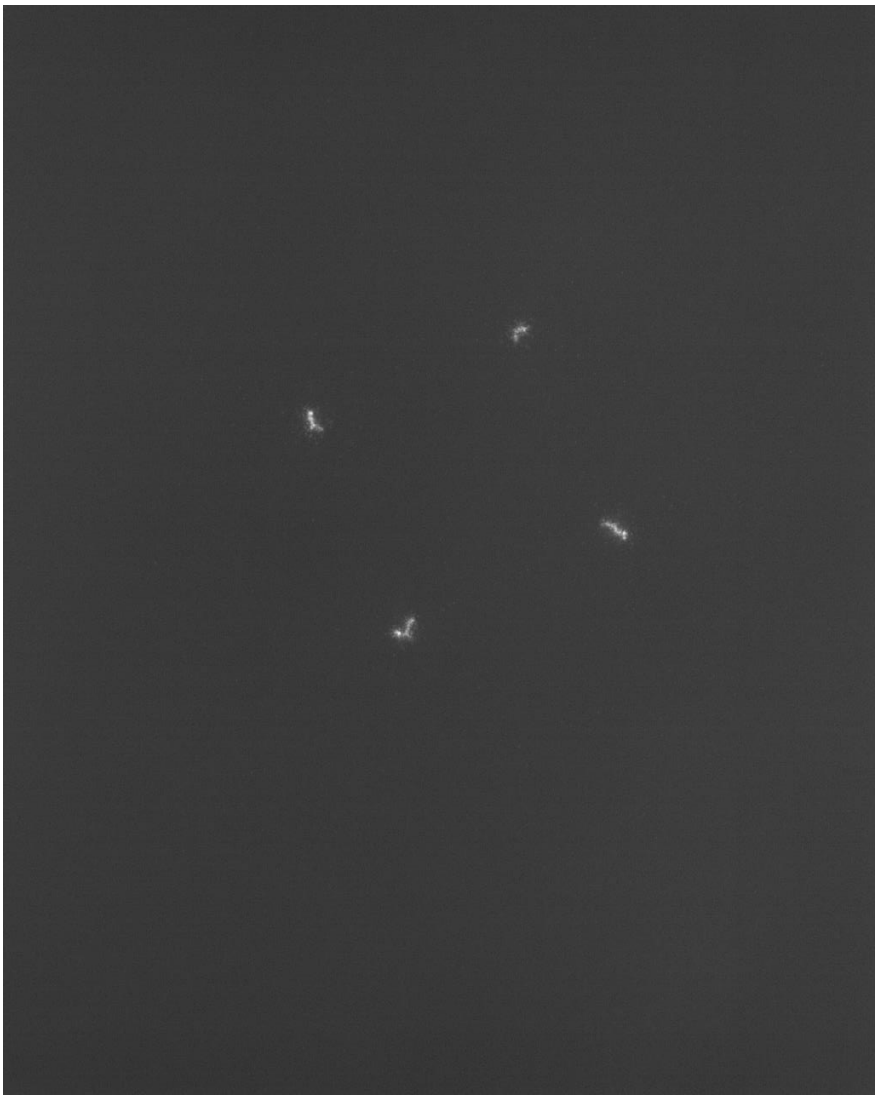

Figure 38: Picture of the substrate surface with bipolar voltage at 11 kV_{peak} in Nytro 10XN with a camera frequency of 480 Hz: Picture number 7 (in Figure 30).

B Appendix - High-speed camera with camera frequency of 480 Hz and implementation of $n = 1$ and $n = 8$

The picture sequence principle of the high-speed camera with a camera frequency of 480 Hz, with the implementation of $n = 1$ and $n = 8$, is presented in Figure 39.

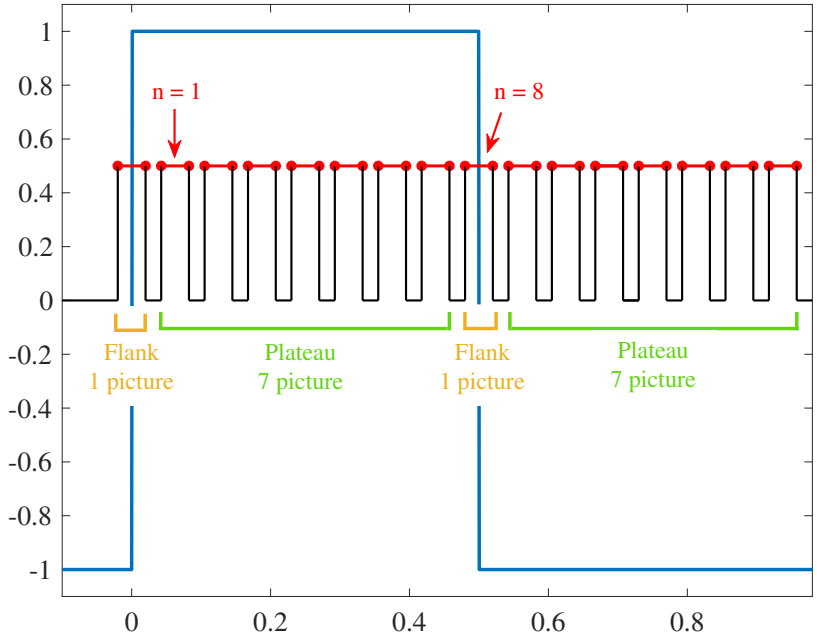

Figure 39: The picture sequence principles for the high-speed camera for square voltage setup, with a camera frequency of 480 Hz, with the implementation of $n = 1$ and $n = 8$. The x- and y-axis are defined per unit (PU). The voltage signal is marked in blue.

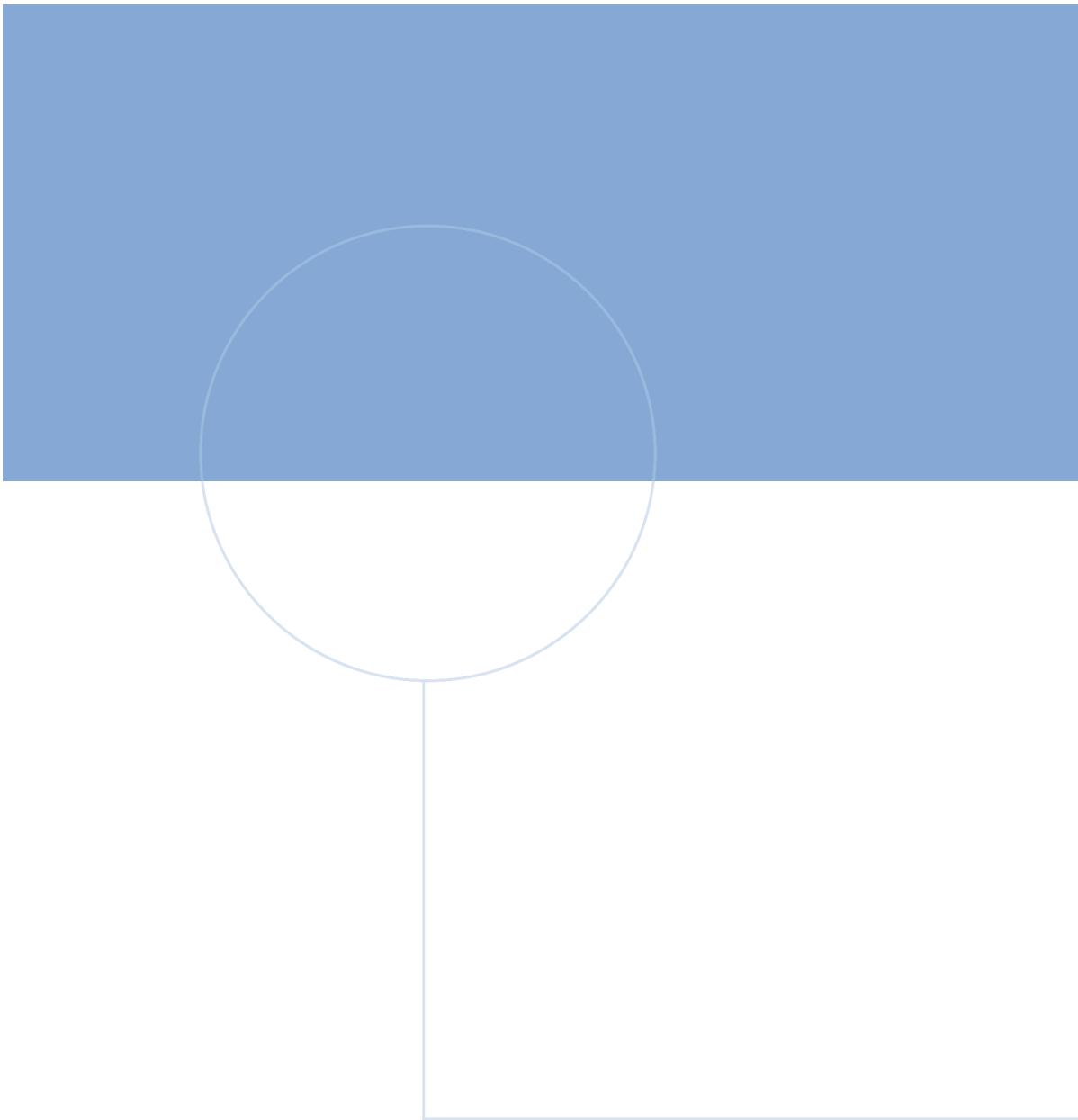

NTNU

Norwegian University of
Science and Technology